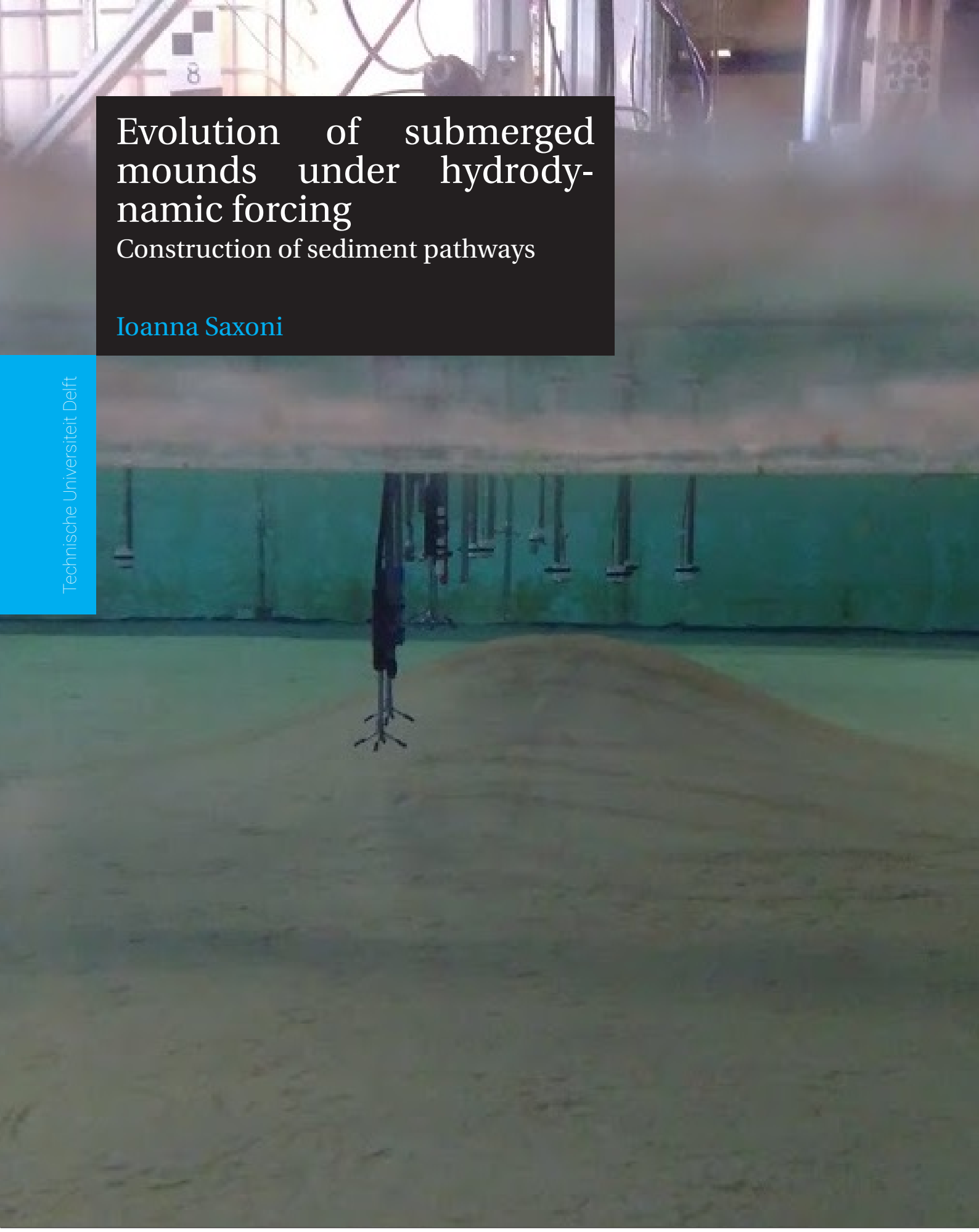

Evolution of submerged mounds under hydrodynamic forcing

Construction of sediment pathways

Ioanna Saxoni

Technische Universiteit Delft

TU Delft Delft University of Technology

Challenge the future

Evolution of submerged mounds under hydrodynamic forcing

Construction of sediment pathways

by

Ioanna Saxoni

in partial fulfilment of the requirements for the degree of

Master of Science

in Hydraulic Engineering

at the Delft University of Technology,

to be defended publicly on Wednesday December 19, 2018 at 16:00 PM.

Supervisor:	Dr. ir. J. A. Hopkins,	TU Delft
Thesis committee:	Prof. dr. ir. S. G. J. Aarninkhof,	TU Delft
	Dr. ir. M. A. de Schipper,	TU Delft
	Dr. ir. M. E. Wengrove,	OSU
	Dr. ir. B. C. van Prooijen,	TU Delft

An electronic version of this thesis is available at http://repository.tudelft.nl/.

TU Delft Delft University of Technology

Preface

This thesis is the final product of my master degree in Hydraulic Engineering at the Delft University of Technology. It has been an exciting and challenging nine months, and I couldn't have done it without the support and guidance of all the people that contributed to this project.

First off, I would like to express my deepest appreciation to my supervisor, Julia Hopkins, for her continuous support and encouragement (on academic and personal matters). I am impressed by your endless energy, and unlimited enthusiasm. You have significantly shaped the direction of my work, while always giving me the freedom to develop my own ideas.

I would like to acknowledge my committee members Stefan Aarninkhof, Matthieu de Schipper, Meagan Wengrove, and Bram van Prooijen for their involvement and insightful feedback. Special thanks are offered to Matthieu de Schipper and Meagan Wengrove, for their intellectual input and help over the duration of my thesis. Matthieu, I am grateful for this amazing opportunity to be part of MODEX, through which I have been able to grow as researcher and make a scientific contribution. Meagan, your mentoring and advice have truly been enlightening, I have learned a lot from you.

I would to acknowledge the staff members of TES at University of Hull, Stuart McLelland, and Brendan Murphy for their invaluable contribution to the organisation and handling of all necessary to complete MODEX.

My master thesis could not have been completed without the funding from Hydralab+ EU Project for the execution of MODEX.

Finally, I am very grateful to Thom Olsthoorn for being always by my side from the beginning of this thesis. Thom, I couldn't have done this without you, thank you.

Ioanna Saxoni
Delft, December 2018

Contents

List of Figures

List of Tables

List of symbols and abbreviations

List of symbols

Sign	Description	Unit
A	mound footprint area	m^2
C	friction factor	-
E	flow energy	$N \cdot m$
g	gravitational acceleration	m/s^2
H	wave height	m
H_m	mound height	m
K	friction coefficient	s^2/m
Q	flow dischange	l/s
s	ρ_s/ρ	-
S	total sediment transport rate	m^2/s
S_y	cross-flume component of sediment transport rate	m^2/s
T	wave period	s
u	mean free stream flow velocity	m/s
U	total free stream flow velocity	m/s
U_0	energetics model total velocity vector	m/s
$\tilde{U_0}$	energetics model orbital velocity vector	m/s
W_0	sediment fall velocity	m/s
x	along-flume distance	m
y	cross-flume distance	m
ϵ	efficiency factor	-
θ	Shields parameter	-
ρ	water specific density	kg/m^3
ρ_s	sediment specific density	kg/m^3
ϕ	angular difference between current ans wave directions	°
Ψ	nondimensional sediment transport rate	-

Subscript	Description
b	refers to value associated with bedload transport
c	refers to value associated with current
crit	refers to critical value
max	refers to maximum value
orbital	refers to value associated with orbital motion
rms	refers to room mean square value
s	refers to value associated with suspended load transport
total	refers to component summation resultant value
w	refers to value associated with waves
wc	refers to value associated with combined flow
x	refers to value in the along-flume direction
y	refers to value in the cross-flume direction

List of abbreviations

ABS	Acoustic Backscatter Sonar
ADV	Acoustic Doppler Velocimeter
AVT	Antonyan Vardan Transform
EEFF	Extended Energetics Friction Factor model
MODEX	MOrphological Diffusivity EXperiment
RPS	Ripple Profiling Scanner
TES	Total Environmental Simulator
URS	Ultrasonic Ranging System

Abstract

Coastal regions are more and more affected by changes in water levels, storm patterns etc. owing to climate change. Nourishments and other human interventions constitute common practice in order to maintain and secure these areas. However, many aspects, especially the hydrodynamics, are not yet fully understood due to the complexity of the acting processes. This study investigates the evolution of submerged sand mounds under wave, current, and combined flow conditions, and examines the relation between the observed morphodynamic response, and the imposed hydrodynamic forcing. It aims to provide insight towards a better understanding of the hydrodynamics and morphodynamics that will lead to more efficient design, and accurate behaviour prediction of the nourishments.

A physical experiment (MODEX) provided a reference dataset of hydrodynamic and morphodynamic measurements (wave height, flow velocity, bathymetry). The extent to which the dataset covers the full spectrum of acting processes was examined via a literature study of the documented mechanisms under wave, current, and combined flow conditions. It was found that the data do not capture slope effects, flow separation, and ripple influence on flow velocity.

The analysis of the data resulted in the quantification of the flow types effect on several geometrical aspects (mound height, footprint area and shape, ripple pattern), and the position of the mound. In order to examine the extent to which the measured velocities are responsible for the observed response, sediment transport rates were estimated using an energetics model that depends on total, and orbital velocity. The results provided evidence that the observed response can not be fully explained using mean and orbital velocities. For this reason the study suggests an interpretation of the sediment pathways under the various flow types. Nevertheless these are on based on reasoning, and thus are not considered to be proven.

Moreover, the results revealed a relation between aspects of the morphological response and $\overline{Umax}^2$ (which relates to the instantaneous maximum flow energy). The mound height reduction rate (dH_m/dt), and migration rate (dx/dt) scale linearly with $\overline{Umax}^2$, while the mound footprint length/width ratio displays an inverse linear relation. Lastly, the relation between mound area change rate (dA/dt), and flow energy is linear for non-oscillatory, and combined flow, and a parabolic for oscillatory flow.

Finally, despite the limitations and omissions, this study provides significant insight on the evolution of submerged mounds. It is first step in the direction of more accurate prediction of morphological change, and more efficient design of nourishments.

1 Introduction

1.1. Motivation and problem statement

Coastal regions are among the most densely populated areas worldwide and hold great economic, social and environmental value. They are typically dynamic regions ever affected by human interventions and climate change, resulting in potential changes in sediment transport, water levels, and storm patterns. Thus, the need for measures to maintain and secure those areas arises.

There are many possible soft and hard measures for protection against erosion, among which nourishments are ever gaining popularity. A nourishment is a volume of sand placed at the backshore or the foreshore (beach or shoreface) (Figure 1.1), which artificially replaces a deficit in sediment budget over a stretch of coast (VLIZ, 2008). It promises to be a sustainable and natural solution that doesn't intervene greatly with the natural environment but rather collaborates with it.

From the various nourishment types, shoreface nourishments are of particular interest. "A shoreface nourishment is the supply of sand to the outer part of the coastal profile, typically on the seaside of a bar" (VLIZ, 2008). Despite its wide application, many aspects, especially the hydrodynamics, are not fully understood due to the complexity of the processes. Some examples are the diffusion and sediment distribution mechanism, the interaction with the existing morphological features (e.g. sandbars, ripples), the extent of the shelter area, and the timescale to reach an equilibrium. Thus, the behaviour of such a measure cannot always be predicted correctly.

From the above it is clear that a better understanding of the hydrodynamics and morphodynamics is crucial, opening the way towards more efficient nourishment design and more accurate behavior prediction in an effort to better adapt to climate change. In this framework, the EU launched the Hydralab+ Project, as a sequence of HydralabIV EU Project, with a horizon of September 2015 to August 2019. It comprises of a number of large scale physical experiments that provide insight into various processes and simultaneously circumvents the limitations of numerical models and field measurements.

MODEX (MOrphological Diffusivity EXperiment), conducted in the framework of Hydralab+ Project, looks into the overall evolution of a submerged sand mound under various hydrodynamic conditions, with the aim to specify the main drivers of morphological diffusivity in the nearshore.

This master thesis relates to MODEX under the hypothesis that the examined submerged mound can teach us about the processes acting on a shoreface nourishment. By analysing part of the MODEX observations, this study will look into the influence of waves and currents on the mound

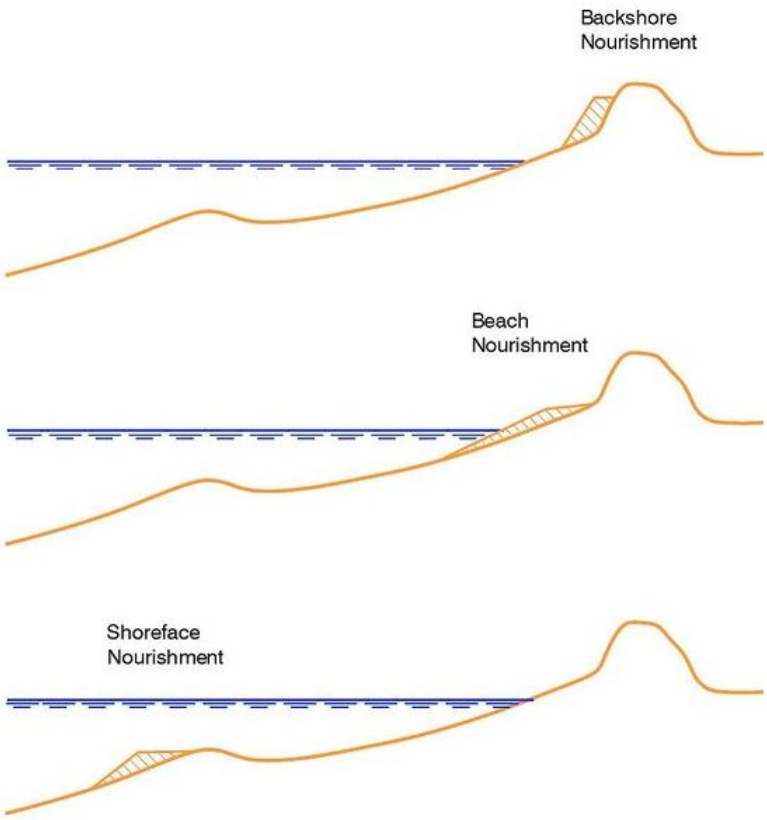

Figure 1.1: Nourishment types (VLIZ, 2008).

morphological development, and determine the sediment pathways. The conclusions are related to nourishment placement in the foreshore due to the similarities between mound and measure.

1.2. Background information

A study similar to the one proposed here was conducted by Garcia-Hermoza (2008), where the morhodynamic response of sand mounds under unidirectional steady (current) flow and reversing (tidal) flow was investigated, by means of flume experiments. In all cases the results showed the creation of a wake and a recirculation bubble on the lee side of the mound, significant velocity deficit downstream of the mound, ripple formation around and on the mound, lowering of the peak, and overall diffusion with the mound becoming more elongated and narrower with time. Especially under steady flow, significant mound migration was observed while its shape evolved into a barchan dune (Figure 1.2). However, no wave conditions were tested, nor were steps taken to relate the measurements to a sediment transport rate.

Another study in a flume (Smith et al., 2017) placed a mound of dredged sand on a sloping movable bed and subjected it to breaking waves of the spilling breaker type. The results showed an overall flattening and lateral diffusion of the mound, but no significant migration in the cross-shore direction. Even though this study looked into accretion and erosion evolution in the mound area, there is no clarification of the processes responsible for this sediment movement or the sediment pathways in the mound vicinity.

More studies have looked into submerged sand mounds. Lloyd and Stansby (1997) performed experiments of sand mounds under steady flows, investigating the recirculating wake flows occurring

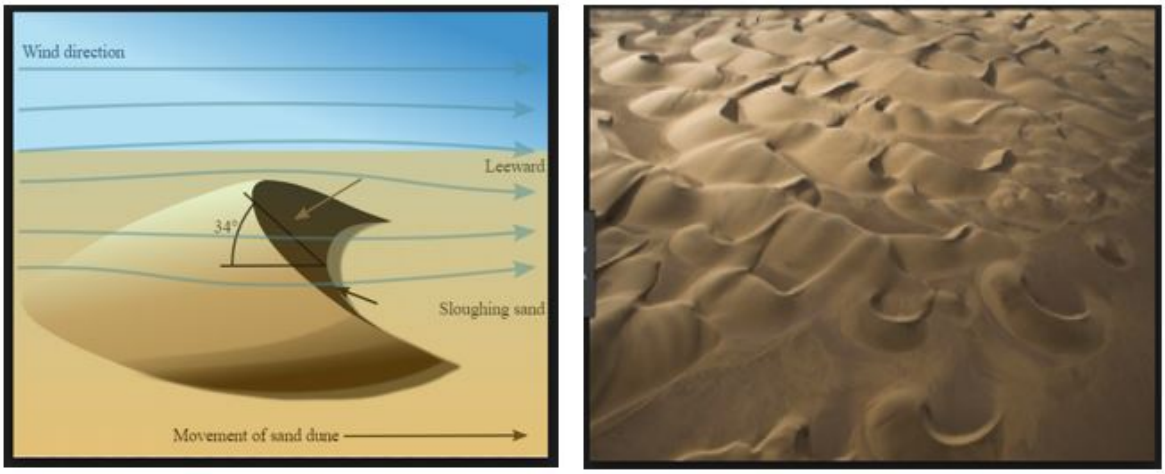

Figure 1.2: Barchan dune geometry (left). Barchan dune ripple pattern (right).

downdrift the model. They tested models of different side slopes and height/depth ratios, and established detailed flow patterns and their evolution. However, only steady flow and only the wake evolution were analysed. Berkhoff et al. (1982) applied numerical modelling on shoals to investigate the skill of several models in simulating short - wave refraction and diffraction. The resulting wave heights were compared with measurements. Again, important information on the refraction - diffraction patterns, and the skill of the different models were introduced, but the overall evolution was not investigated.

Behaviour similar to that seen in Smith et al. (2017) was observed during the field measurements on a foreshore nourishment by van Duin et al. (2004), where the nourishment slightly flattened but no migration occurred in the cross-shore during the first 2 years. Instead, the sediment fed the existent bars which grew in height and migrated onshore at first. However, this behaviour was unexpected and attributed possibly to the nourishment dimensions (height and length) which appear too large for it to start diffusing right away. In addition, the study doesn't explain why the bars migrated onshore or what changed after the first two years that led the system back towards its initial state (since the nourishment had altered very slightly).

Moulton et al. (2014) inferred a morphological diffusivity estimation from the measured bathymetric evolution of excavated holes. They found that downslope transport contributes to sediment diffusion and is proportional to a morphological diffusivity (κ) that scales with the three halves power of shear stress, for bedload transport. However, this is not a uniform law, as in cases where suspended sediment is important (as in breaking waves) the above proportion is expected to differ. Moreover, they considered symmetric flow and Gaussian shaped bathymetry with a fixed centre point, which is different from the situation in shoreface nourishments.

1.3. Research description

1.3.1. Research objective

The objective of this thesis is to investigate the effect of various hydrodynamic conditions on the general shape of a submerged sand mound and explore the link between morphodynamic response and hydrodynamic forcing.

In particular the focus of this thesis is on:

- investigation of the mound response to different hydrodynamics conditions (oscillatory flow, non-oscillatory flow, combined flows with various wave - current contributions)
- understanding of sediment movement, and construction of the sediment pathways that follow from result interpretation
- investigation of possible links between morphodynamics and hydrodynamics

1.3.2. Research questions

The problem statement in combination with the literature review lead to the main research question and sub-questions. The main research question is:

How does a submerged sand mound evolve under wave, current and combined flow conditions?

In order to answer the above question, the following sub-questions are specified in an attempt to cover its various aspects:

1. Which hydrodynamic processes in the mound vicinity are captured by the measurements?
2. How do waves, current and combined flow affect the mound geometry and position?
3. How can the morphodynamic response be related to hydrodynamics?

The posed research questions cover a wide sector of the field, and can be answered in various levels of detail which aren't always within the scope of this study. For this reason, they are translated into hypotheses which are tested in the current thesis.

- Hypothesis 1: The observed sedimentation - erosion pattern can be explained using mean and orbital velocities.
- Hypothesis 2: The morphodynamic response under all flow condition types scales with flow energy.

1.3.3. Scope

This master thesis is limited by the experimental setup and the flume capabilities within the MODEX experiment. The along-flume flow is in the cross-shore direction with reference to the beach, and as such no longshore current or alongshore sediment transport can be simulated. Moreover, only regular waves are generated, but the expected shoaling and skewness over the mound is believed to lead to satisfactory simulation of the actual phenomena. Finally, no return flow (undertow) occurs due to the absence of wave set up.

Regarding the mound response, the direction and spreading of the sediment, as well as the general mound shape and bathymetry evolution are going to be investigated. However, the mound diffusivity isn't quantified. Also, although bedload conditions are assumed, a detailed analysis of sediment transport within the boundary layer is outside the limits of this research.

1.3.4. Research approach

The literature review shows that the general subject of diffusion in the nearshore includes many 3D processes, covers several research fields (nourishments, ripples, bottom roughness, near-bed sediment transport) and entails many unsolved problems (mechanism of ripple formation, good bottom roughness approximation method). All the above hinder the accurate prediction and modelling of the response of a nourishment to hydrodynamic forcing. Therefore, the core of the experiment was to obtain accurate observations of flow velocity, bathymetry, free surface elevation and

suspended sediment concentration, that will provide the necessary insight in the knowledge gaps and will comprise a reference dataset to use for modelling purposes.

This thesis can be broken down to the following phases:

- Phase 1: Literature review
- Phase 2: MODEX: experimental setup, flume measurements, and observations
- Phase 3: Data processing, and analysis

The research sub-questions are answered during the above phases as indicated in Table 1.1 below.

Research Method	Research Questions	Content
Literature review	Q1 & Q2	Q1: Expected processes at the mound Q2: Previous findings of experimental work
Experimental setup	Q1	Experiment limitations, simplifications and omissions
Flume measurements & observations	Q1 & Q2	Q1: Verification of the captured processes Q2: Differences in mound evolution under the various hydrodynamic conditions
Data processing	-	Clarification of quality and range of collected data Better understanding of the data
Data analysis	Q1, Q2 & Q3	Q1: Verification of the captured processes Q2: Support, and explanation of observed response Q3: Exploration, and analysis of underlying relations

Table 1.1: Thesis research approach.

1.4. Reading guide

The report is divided into three parts in accordance to the phases in which the thesis was conducted:

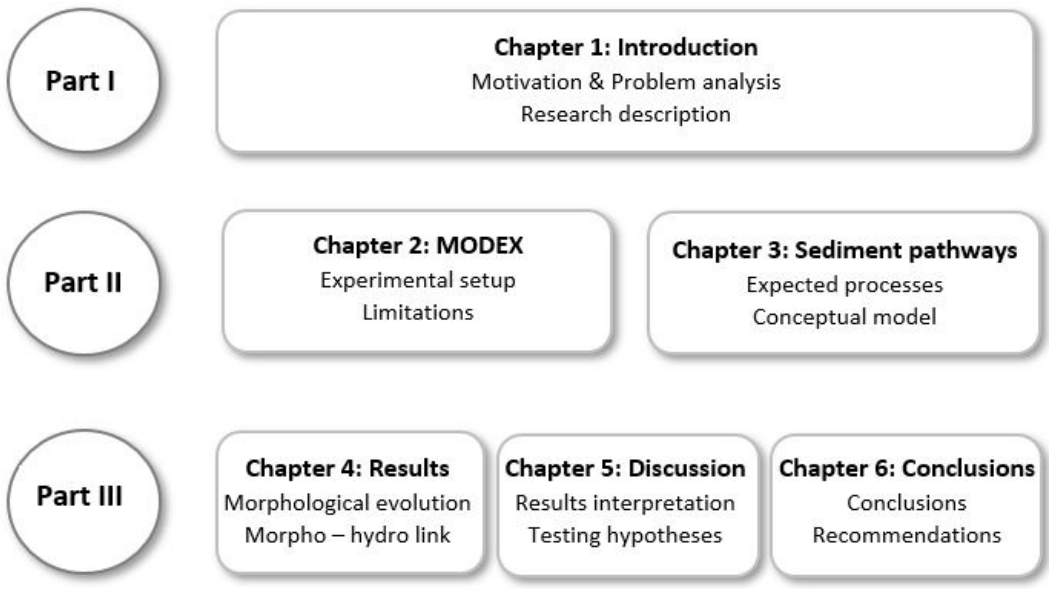

Chapter 2 describes in detail the experimental setup: the assumptions made, the instrumentation, the tested scenarios. It provides enough information for the reader to understand later references to instruments and scenarios, and gives some insight on the limitations of the experiment.

Chapter 3 discusses a conceptual model for the derivation of the sediment transport pathways. It describes the main parts of the model (acting processes, sediment transport rate, and pathway determination approach) and clarifies the processes that are going to be further investigated in the current analysis.

Chapter 4 presents the MODEX results on the morphological evolution, and sediment movement at the mound in the various scenarios. In addition, results including morphological aspects of the mound response in all scenarios are discussed. They detect trends in, and explore the relation of the observed response with hydrodynamics.

Chapter 5 reflects critically on the results of the study, and provides the answers to the suggested hypotheses. Moreover, it provides an interpretation of the sediment pathways under different flow types.

Finally, chapter 6 summarises the conclusions of this study and provides the answers to the research questions. In addition, it discusses aspects of the study that were not (fully) treated, as well as some recommendations for future research.

2

MODEX description

This chapter discusses the basic concept of MODEX (Morphological Diffusivity Experiment) and the logistics of the experiment. Section 2.1 highlights the hypotheses behind MODEX design and the questions it aims to answer. In section 2.2 the experimental setup is briefly presented. Finally in section 2.3 the limitations of the physical model are explained.

2.1. Basic concept

MODEX comprised of 9 experiments that investigate the morphological evolution of a submerged sand mound under waves, currents, and combined wave-current forcing, with the aim to determine the physical processes that drive morphological diffusivity in the nearshore. Since the lack of data is one of the main obstacles in understanding and quantifying morphological diffusivity (MODEX, 2018) the experiment will provide insight in the hydro- and morphodynamic physical processes responsible for the mound's evolution through a unique reference dataset.

The physical model is designed based on the following hypotheses:

- The investigated sand mound bears similarity with sand berms and shoreface nourishments, hence the acquired knowledge can be used for better predictions and design of nourishments.
- Morphological diffusivity in the nearshore is connected to the behavior of sand banks and nourishments, features that migrate mostly in the cross-shore direction. Hence, the focus lies on diffusivity owing to cross-shore processes.
- Intermittent flow is similar to continuous flow with reference to mound evolution.

2.2. Experimental Setup

MODEX was conducted in UK at the Total Environment Simulator (TES) of Hull University. During every experiment (9 in total), a circular mound of 1.5 m in diameter and 0.2 m in peak height was constructed and placed in the centre of the 12 x 6 m flume basin of the facility (Figure 2.1). The mound laid on a movable sand bed 0.1 m thick. The grain size of the sand used for the construction of both the mound and the sand bed was 215 μm. The water depth in the basin was at 0.4 m.

A total of 39 instruments were deployed in the flume to measure bathymetry, flow velocity, sediment concentration and wave height. Most of them were mounted on a gantry above the flume while others were placed on constructed frames updrift and downdrift of the mound, as shown in Figure 2.2. The majority of the instruments (37 out of 39) sampled during running flow while others

required no flow or dry bed. This resulted in the experiments being conducted intermittently, with the duration of each run depending on the severity of the imposed hydrodynamic conditions.

The sampling frequency values of all the deployed instruments are presented in Table 2.1. These values were during running flow and were kept constant during MODEX.

Instrument type	Sampling frequency (Hz)
Wave rod	29
Vectrino profiler	50
ADV	25
URS	1
ABS	128
GoPro	1/30 or 1/5

Table 2.1: Sampling frequency of deployed instruments per instrument type.

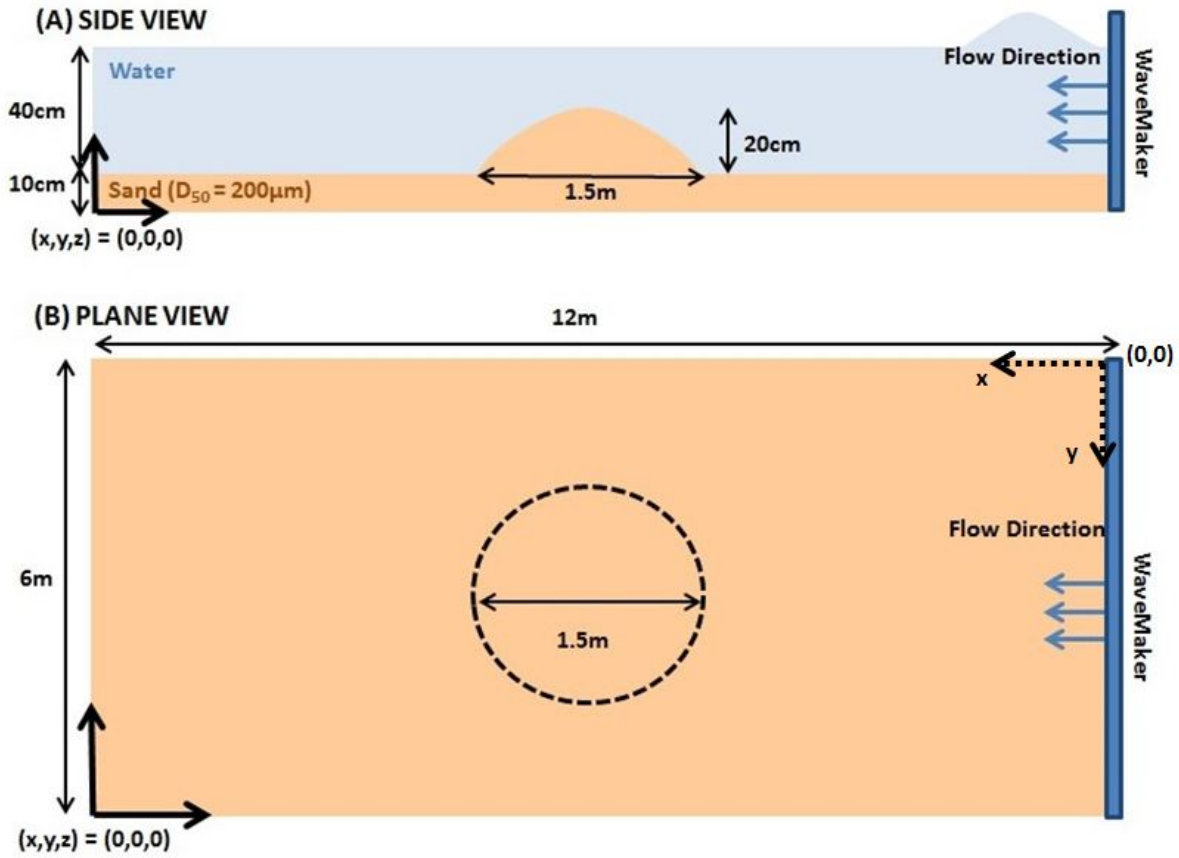

Figure 2.1: Side view (A) and plane view (B) of the initial mound bathymetry. Flow and waves move from right to left, with the waves being generated by wave paddles at the side of the basin, and the currents by recirculating flow via a double pump system.. The origin of the coordinate system is defined as the lower left hand corner of the flume (in plane view, B) and the bottom of the sand bed (in side view, A) (MODEX, 2018). Exceptions to this coordinate system are the laser scanner and the RPSs. Their coordinate system has its origin at the top right corner (dashed arrows in plane view, B) and the bottom of the sand bed (in side view, A).

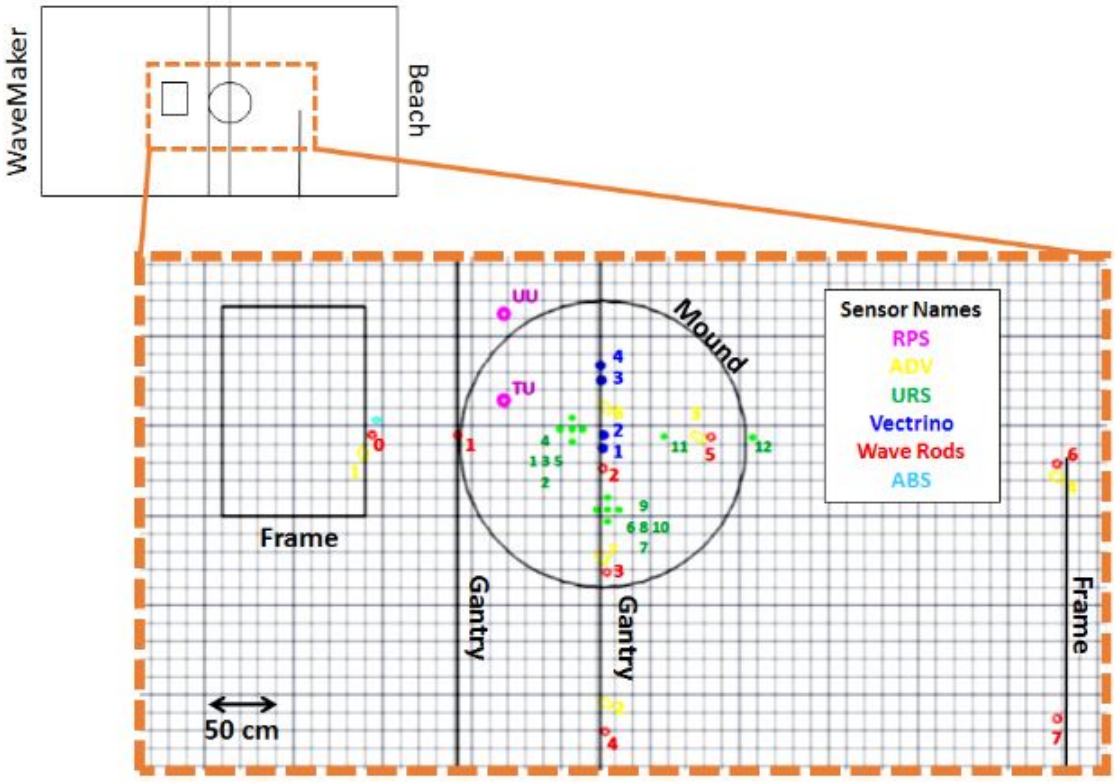

Figure 2.2: Schematic of instrument deployment for the experiment. Instruments measuring the flow field are placed before (Vectrinos, blue), around (wave rods, red) and above (ADVs, yellow) the mound. The position of the RPSs (magenta) in this schematic is not one of the actual measuring positions. The LiDAR and the GoPro cameras used are not included in this schematic (MODEX, 2018).

Flow velocities were measured with 6 acoustic Doppler velocimeters (ADVs, Figure 2.3) and 4 profiling acoustic Doppler velocimeters (Vectrino profilers, Figure 2.4a). Out of the 6 ADVs, 4 were down-facing (Figure 2.3a) and 2 were side-facing (Figure 2.3b).

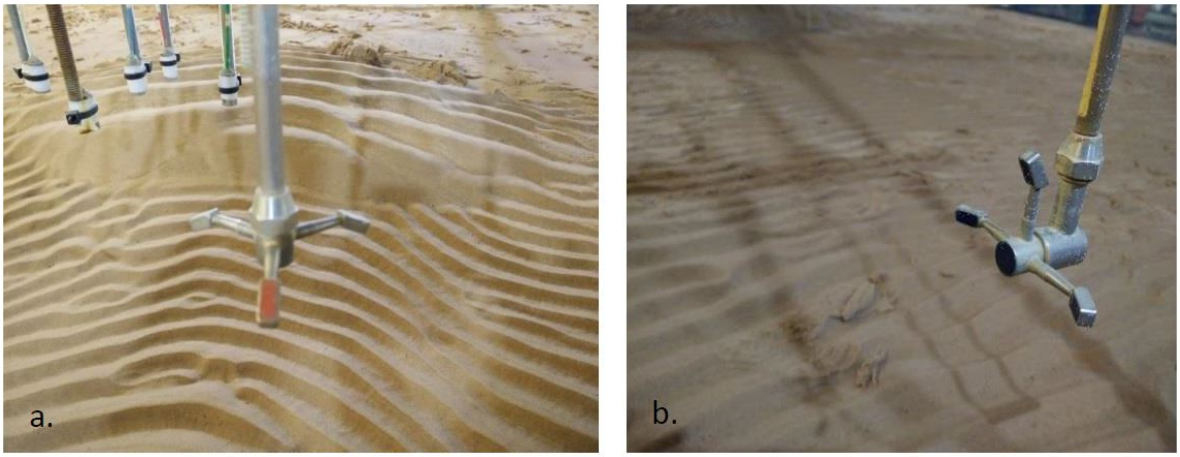

Figure 2.3: ADV probes. (a) Down-facing probe. The red marker is in the direction of the flow and facing the beach in the flume. (b) Side-facing probe.

The Vectrinos measure over a distance in the water column as shown in Figure 4b, hence they allow the measurement of the boundary layer shape and evolution during flow.

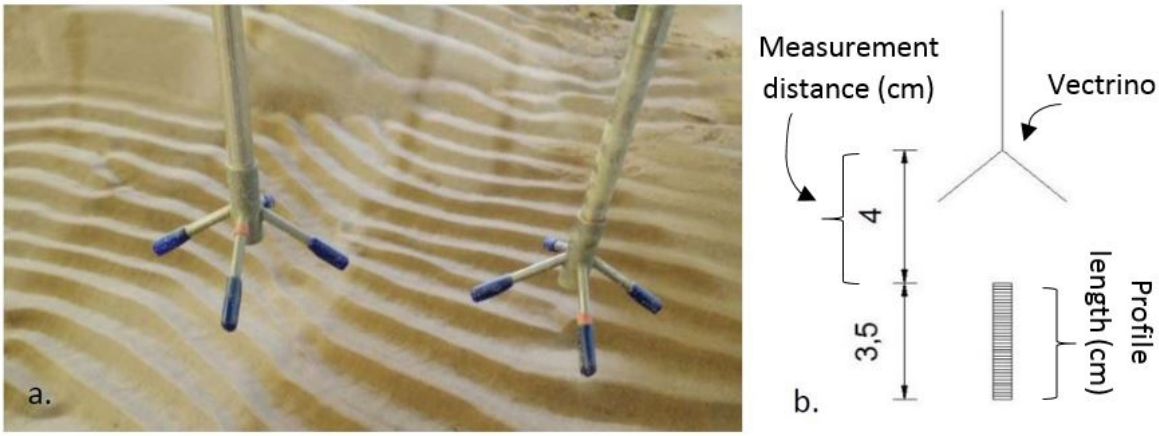

Figure 2.4: (a) Vectrino profilers. The red marker is in the direction of the flow and facing the beach in the flume. (b) Measurement distance and profile length of Vectrino profilers.

In order to have synchronised measurements, the Vectrinos were paired. Each pair had a “master” and a “slave” instrument. In a "master" - "slave" configuration, the "slave" instrument is synchronised with the "master" meaning that it emits pulses only when the “master” is active and at the moments that the last dictates (i.e. the moments that the “master” itself is sending pulses). In this setting the "slave" instrument cannot detect the bed. Moreover, the paired instruments were set at specific distances to one another (Figure 2.5), to capture as much of the velocity profile as possible.

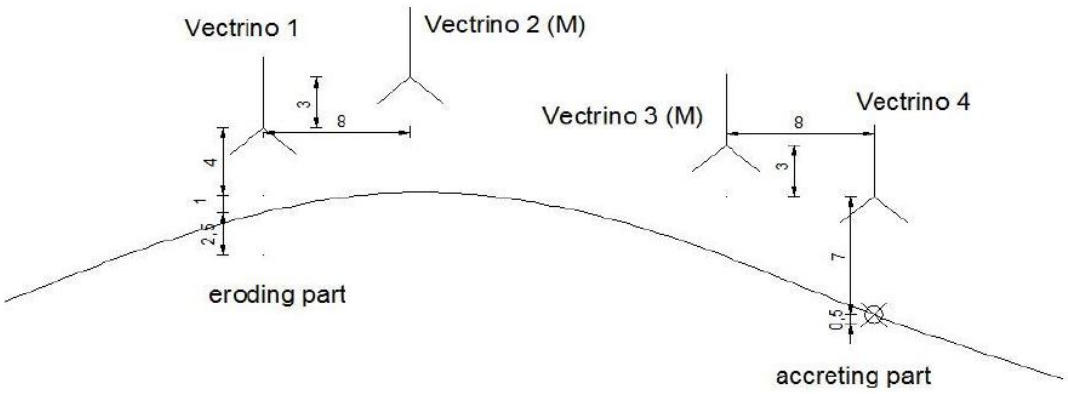

Figure 2.5: Vectrino profilers deployment around the mound: the “masters” are placed 3 cm higher than the “slaves” with the last being partly in the bed (part of the profile is in the bed) accounting for the expected erosion/accretion of the bed locally. However, in the last experiments this configuration was no longer maintained.

Bed level was measured with 12 altimeters (URSs, Figure 2.6a) and 2 Vectrino profilers (the 2 “masters”) during running flow. In order to capture ripples, altimeters were deployed in a cross configuration with small distances in between devises (URS cross, Figure 2.6b). Two such crosses were deployed, one over the mound upslope and the other over the mound sideslope, while the remaining two URSs were placed downstream of the mound and along the flow direction.

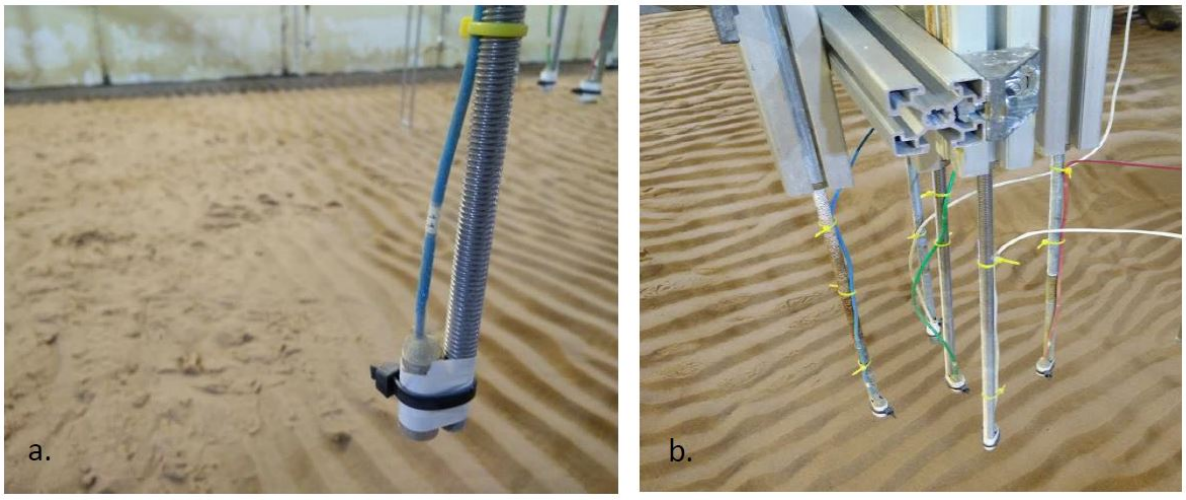

Figure 2.6: (a) URS probe. (b) URS cross configuration.

The bathymetry (bedforms, footprint) in the mound vicinity was acquired with 2 ripple profiling scanners (RPSs) with approximately 1m footprint. The objective was to closely monitor the morphological evolution. Since the RPSs would disturb significantly the hydrodynamics if they measured while waves and currents were running, the flow was frequently stopped (every 5, 10 or 15 minutes, depending on the strength of the flow). During the no-flow intervals, the instruments were lowered into the water and moved along the length of the flume to cover the whole mound footprint (Figure 2.7).

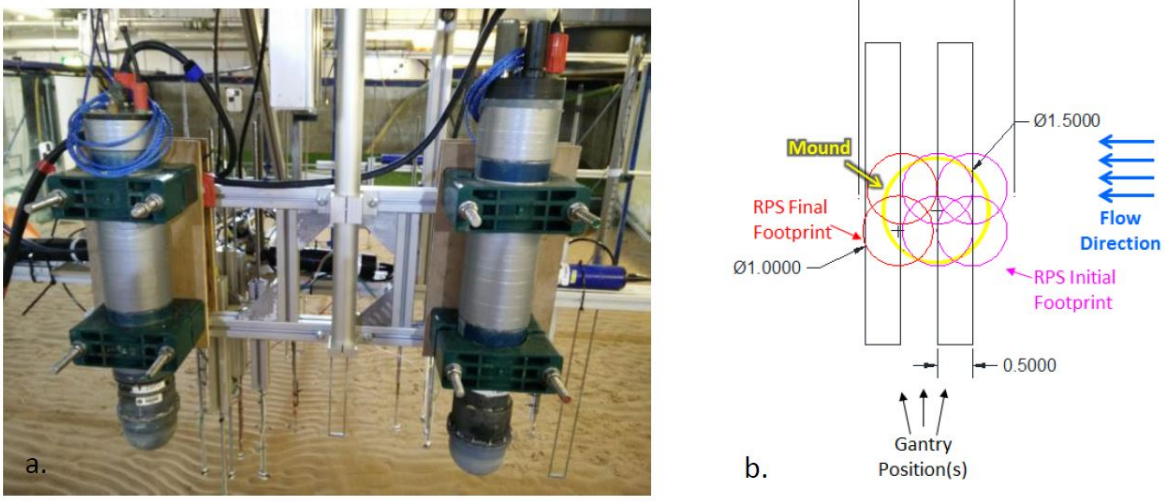

Figure 2.7: (a) RPS configuration: the two scanners were set 0.7m apart. (b) Footprint of the RPS scans. The instruments moved 0.5m along the length of the flume between scans to achieve full coverage of the mound as it evolved (MODEX, 2018).

Wave heights were sampled with 7 wave rods (Figure 2.8a). An acoustic backscatter sonar (ABS) measured the concentration of suspended sediment in the water column (Figure 2.8b). The overall bathymetry of the flume, before and after an experiment, was acquired with laser scanner (LiDAR) measurements which were performed on dry bed (Figure 2.9a). Finally, GoPro cameras, 2 downfacing over the mound (Figure 2.9b), 1 submerged sidefacing, and 2 overhead downfacing over the

flume, captured time lapses of the flow and the morphological evolution.

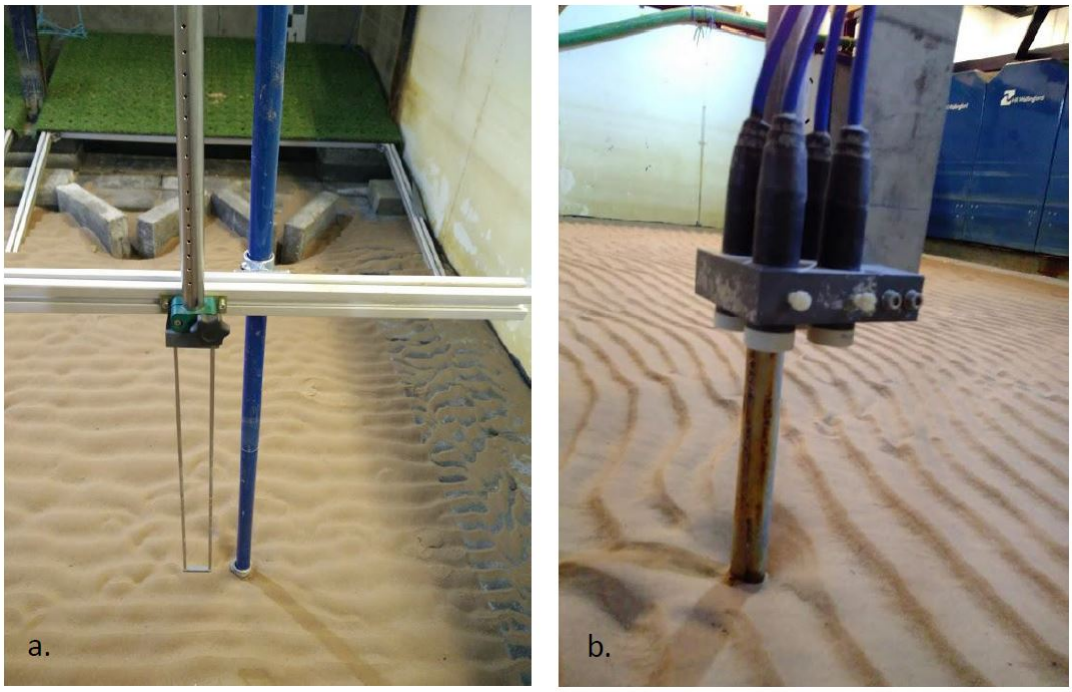

Figure 2.8: (a) Wave rod (or wave gauge). (b) ABS probe.

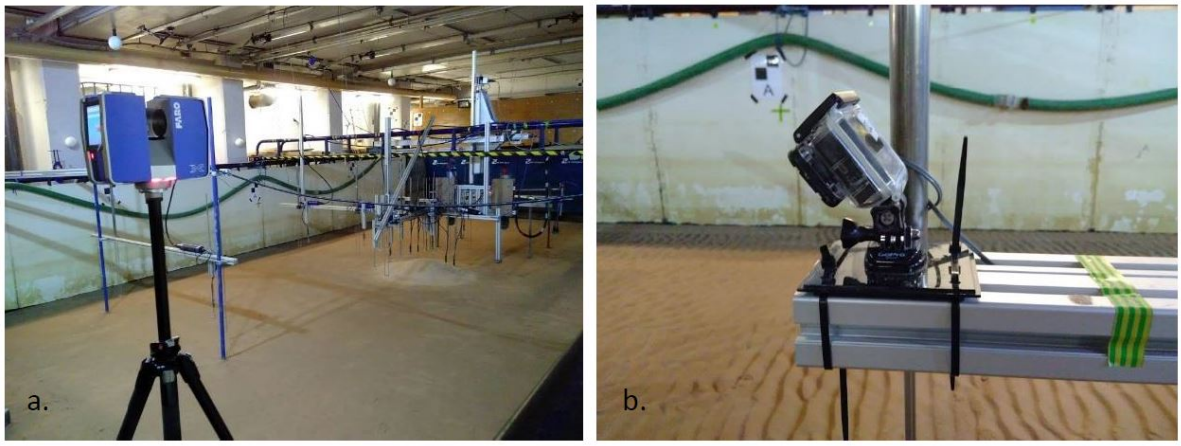

Figure 2.9: (a) LiDAR scanning the dry bed before an experiment. (b) Downfacing over the mound GoPro camera.

To investigate the response of the mound under wave, current, and wave-current attack, nine scenarios (Table 2.2) were run. For each scenario the Shields parameter (Θ) was estimated as an indication of the non-dimensional shear stress. For scenarios with the same flow type (e.g. only waves or only current) the Shields parameter was incrementally increased while for the combined wave-current scenarios, the Shields parameter was kept approximately stable with varying energy contributions from the individual conditions. The priority order in Table 2.2 also indicates the order in which the scenarios were run. The run duration refers to the approximate interval when flow or waves were running. The table gives the value of the first runs which is kept constant in most cases. Scenarios 1 is an exception as the run duration increased towards the end of the experiment.

Feature	θ_c	θ_w	θ_{wc}	Q (l/s)	H (m) (input to WM) Observed	T (s)	Priority	Run Duration (min)	Nr. of runs
Waves only low	-	0.22	-	0	(0.11) 0.098	1.0	1	15	10
Waves only medium	-	0.27	-	0	(0.14) 0.12	1.2	2	10	9
Waves only high	-	0.3	-	0	(0.16) 0.12	1.3	3	5	9
Currents only high	0.6	-	-	900	-	0.0	4	5	6
Currents only low	0.45	-	-	700	-	0.0	5	5	8
Combined low energy	0.18	0.17	0.30	400	(0.07) 0.055	0.8	6	5	10
Combined $E_w = E_c$	0.27	0.27	0.47	500	(0.14) 0.12	1.2	7	5	9
Combined $E_c > E_w$	0.35	0.22	0.49	580	(0.11) 0.098	1.0	8	5	10
Combined $E_w > E_c$	0.22	0.32	0.47	420	(0.16) 0.12	1.3	9	5	9

Table 2.2: Sequence of mound experiments.Θ is the Shields parameters owing to currents (c) or waves (w). Q is the discharge for the flow (based on the pump rate), H the incident wave height on the mound, and T the incident wave period (MODEX, 2018).

The above scenarios are based on the following assumptions and hypotheses:

- Monochromatic unidirectional waves are sufficient to explore sediment transport processes.
- "The current Shields parameter (θ_c) was calculated by means of observations using the momentum integral method (Medhi et al. 2014, Wengrove et al. 2018).
- The wave Shields parameter (θ_w) was calculated as $\theta_{2.5}$ using the bed shear stress formulation proposed by Nielsen (1992) with the friction factor proposed by Swart (1974).
- The combined flow Shields parameter (θ_{wc}) was computed as

$$\theta_{wc} = \sqrt{\theta_c^2 + \theta_w^2 + \theta_c \theta_w \cos\phi}$$

  where ϕ is the angular difference between the current and wave directions (0 in this case) as proposed from Lacy et al. (2007)." (MODEX, 2018)

2.3. Experiment limitations

No experiment can simulate the full real environment. In addition, the scaling effects, the various introduced errors, and the encountered physical limitations pose fundamental differences which need to be identified in order to compare situations and use correctly the obtained knowledge.

In MODEX no alongshore current was imposed and the generated waves were unidirectional and regular, both of which contradict the environments of sand banks or nourishments. Also, it wasn't

possible to measure the sediment transport over the bed, hence all derived shear stresses and sediment fluxes are the result of computations. The wavemaker had an upper limit of 1.3 s inputted wave period, while the generated wave height proved to be lower than the inputted one.

In terms of errors, some limitations of the wave panels and the basin introduced subharmonics and some small wave angle with respect to the length of the flume. Also, some reflection from the flume side walls and the downdrift beach occurred although the setup was such that most of it was eliminated. Finally, the instrument setup may have caused flow obstruction over the mound and local scour holes (especially in the stronger flow scenarios).

3

Sediment pathways conceptual model

The term sediment pathways refers to the direction of sediment movement in an area as a response to hydrodynamic forcing. Therefore, knowledge of the hydrodynamic processes provides a good indication of the sediment pathways.

However, in three-dimensional situations identifying the effect of these processes is no easy task. The complex bed morphology creates gradients (e.g. in velocity) and gives rise to secondary effects (e.g. vortex shedding, flow separation over ripples etc.), thus creating the need for careful examination of all possible ways sediment might move due to the hydrodynamics. A useful tool to facilitate such an analysis is a conceptual model, as it identifies the key elements and establishes the interconnections driving the evolution of the bed.

Since MODEX has complex three-dimensional bathymetry, a conceptual model is used to guide the identification of the sediment pathways. However, the suggested model is a qualitative method for determining the sediment pathways, giving hypotheses of the driving processes. It should be verified with measurements, as is demonstrated in Chapter 5.

The chapter is structured in a top-down manner with the conceptual model discussed in section 3.1 and its most important components described in the following sections. Section 3.2 highlights the hydraulic processes that occur upstream, on top, downstream and on the sides of a submerged sand mound, with a focus on the bathymetry induced flow velocity changes. In section 3.3 the connection is made between flow velocity, shear stress and initiation of sediment movement. Finally, section 3.4 elaborates on the logic behind the identification of the sediment pathways key components (erosion - deposition areas, and direction of movement) by the model.

3.1. Model setup

The starting point of the model is the identification of the hydraulic processes taking place around the mound for the x- and y-direction. This step is maybe the most important over the whole procedure as it provides the basis for the next steps of the model as well as the later comparison with the data, so all possible mechanisms should be taken into account. These, in combination with the initial bathymetry, provide the velocity field, which is subsequently transformed into a near-bottom shear stress field.

The next step is to identify the locations where the initiation of motion threshold is exceeded, which is achieved by comparing the shear stress field with the critical shear stress. These locations mark

the onset of sediment pathways. Then, the direction of movement is determined by looking into the locally dominant processes. Finally, the locations where the transported sediment settles are identified.

All the above refer to a time span in which the considered bathymetry doesn't change dramatically. When the bathymetry changes significantly over the simulated period, the described procedure should be conducted iteratively in smaller time steps until the desired time period is completed or the system has reached an equilibrium. The structure of the developed conceptual model as described above is presented in Figure 3.1.

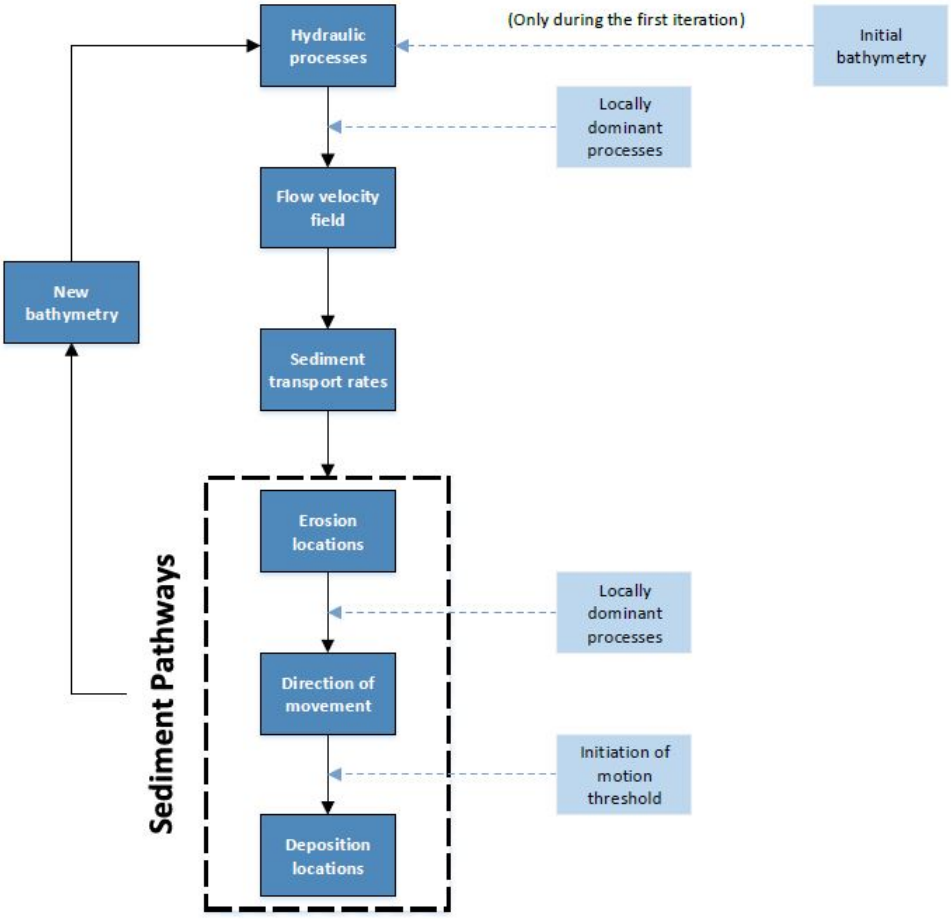

Figure 3.1: Sediment pathways conceptual model.

It's important to note that the determination of locally dominant processes is not always straightforward. In cases of opposingly acting mechanisms it isn't always clear which direction the sediment will move and it is in such cases that data may provide valuable insight. Therefore, a feedback mechanism between the theoretical pathways and the collected data is crucial to get an accurate representation of the sediment pathways.

3.2. Hydraulic processes in the vicinity of a mound

The current section describes the hydraulic processes taking place in the mound vicinity. In 3.2.1 all the occurring processes and their effect on flow velocity are described, while 3.2.2 distinguishes

between the situation under waves, current and combined flow. In addition 3.2.2 discusses the weak spots of the conceptual model.

3.2.1. General processes

Figure 3.2 provides an overview of the main hydraulic processes occurring during waves, current, and combined wave – current flow, followed by a brief explanation of the driving mechanism, the location of occurrence and the effect on flow velocity and sediment transport for each one. In general, the mound bears similarity with shoals, from which a large part of the list of processes is obtained.

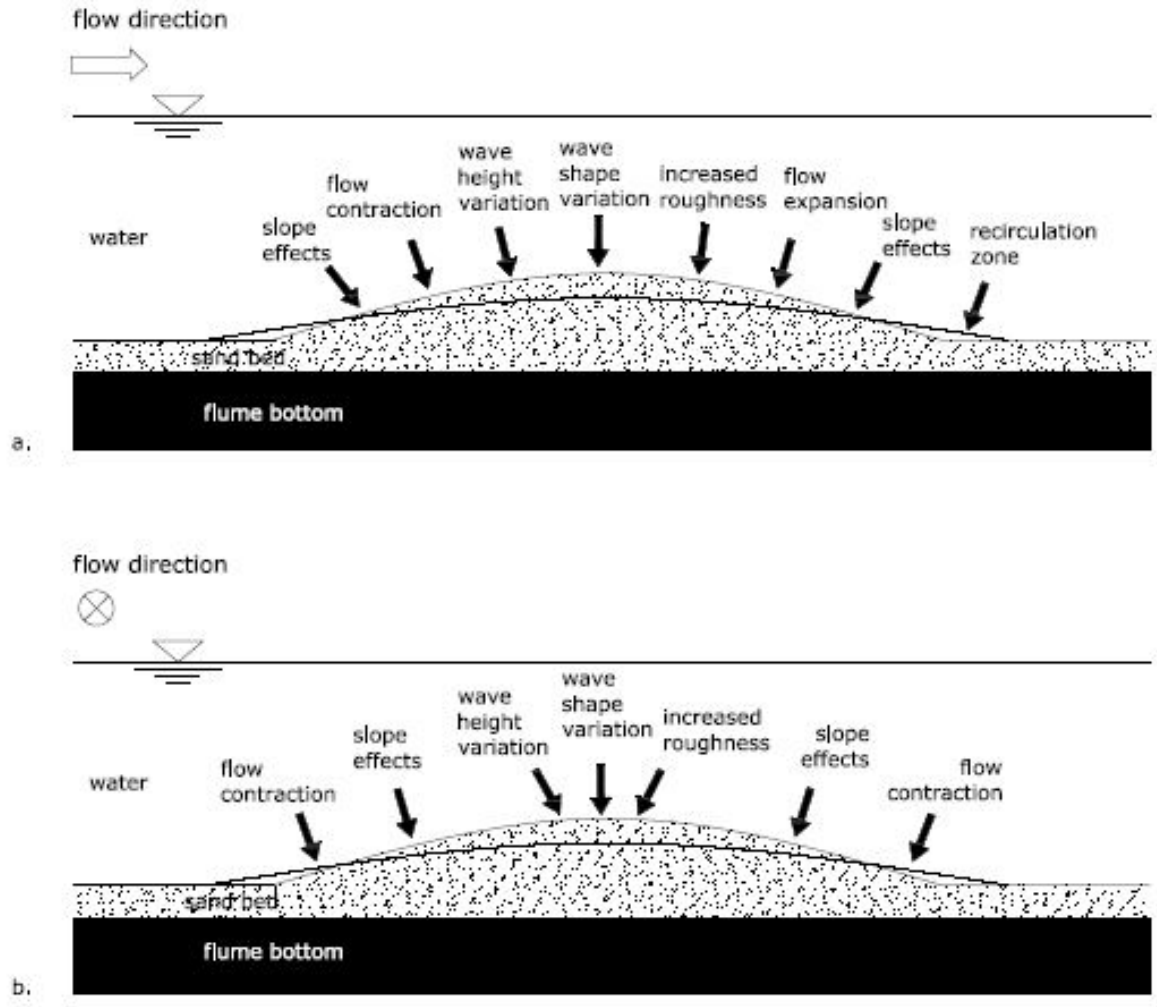

Figure 3.2: Main hydraulic processes in the mound vicinity in the (a) along-flume and (b) cross – flume direction.

Flow contraction - expansion - separation

Flow contraction is expected to occur all around the first half of the mound volume for the case of non-oscillatory flow (steady current) as a reaction to the mound obstructing the flow. No significant energy losses are assumed, thus flow contraction causes an increase in flow velocity.

Since the cross-section width varies over depth, there are velocity gradients in both the along- and cross-flume direction, with the lower velocities at the toe of mound, the higher over the mound peak, and the stream lines converging over the mound shape. The strongest flow contraction (or maximum convergence) occurs at the widest cross-section along the x axis, at the peak of the mound over depth.

Expansion of flow is expected at the second half of the mound volume and may also reach the down-drift of the mound area of the flume, depending on the flow strength. It is the opposite mechanism of flow contraction, hence it causes a decrease in flow velocity along with increased turbulence.

Expansion is often accompanied by flow separation, which occurs when the streamlines are unable to follow the shape of an obstacle. Whether there is actually going to be flow separation depends on the geometry and roughness of the obstacle, as well as the Reynolds number of the flow (Munson et al., 2009, Schiereck, 2012). In case flow separation occurs, the turbulent structures dissipate energy, resulting in a flow velocity lower than the initial.

In the case of oscillatory flow (waves) shoaling and deshoaling cause the orbital velocity to increase and decrease respectively.

Wave height variation

According to the linear wave theory (Holthuijsen, 2007) in shallow and intermediate water, as water depth decreases (assuming a progressive decrease) the wave celerity, wave height, and wave length evolve as shown in Figure 3.3. This energy flux of a non-breaking wave remains constant (neglecting bottom friction and white-capping). As can be seen in Figure 3.3 the orbital velocity behaves inverse of the wave height: an increase in one leads to a decrease in the other. This process is called shoaling and is expected to occur along the upslope of the mound.

In addition to shoaling, refraction is also expected over the mound. Refraction occurs owing to changes in bathymetry. Here, as waves pass over the mound they propagate more and more slowly until they reach the mound peak, a process described by the dispersion relation. However, the part of the waves that propagates over the bed maintains its original celerity, since it experiences no depth changes. As a result a gradient perpendicular to the propagation direction is formed, which causes the waves to curve towards the slower part. The streamlines will curve towards the peak of the mound causing a focus of energy which contributes to a wave height increase.

While the waves pass over the top of the mound, the opposite mechanisms takes place. The waves adjust again to the larger water depth, altering once more their wave height and speed. This mechanism is called deshoaling. Moreover, due to the physics as described by Snell's law, the streamlines turn away from the mound causing a decrease of the wave height.

Wave shape variation

The process of shoaling causes changes in wave height and in wave shape due to non-linear effects. The waves gradually become skewed and asymmetric, which also affects the orbital velocities.

Skewness refers to a change in shape relative to the horizontal axis: the crests become sharper and more peaked, while the troughs become flatter and wider (Holthuijsen, 2007,Bosboom and Stive,

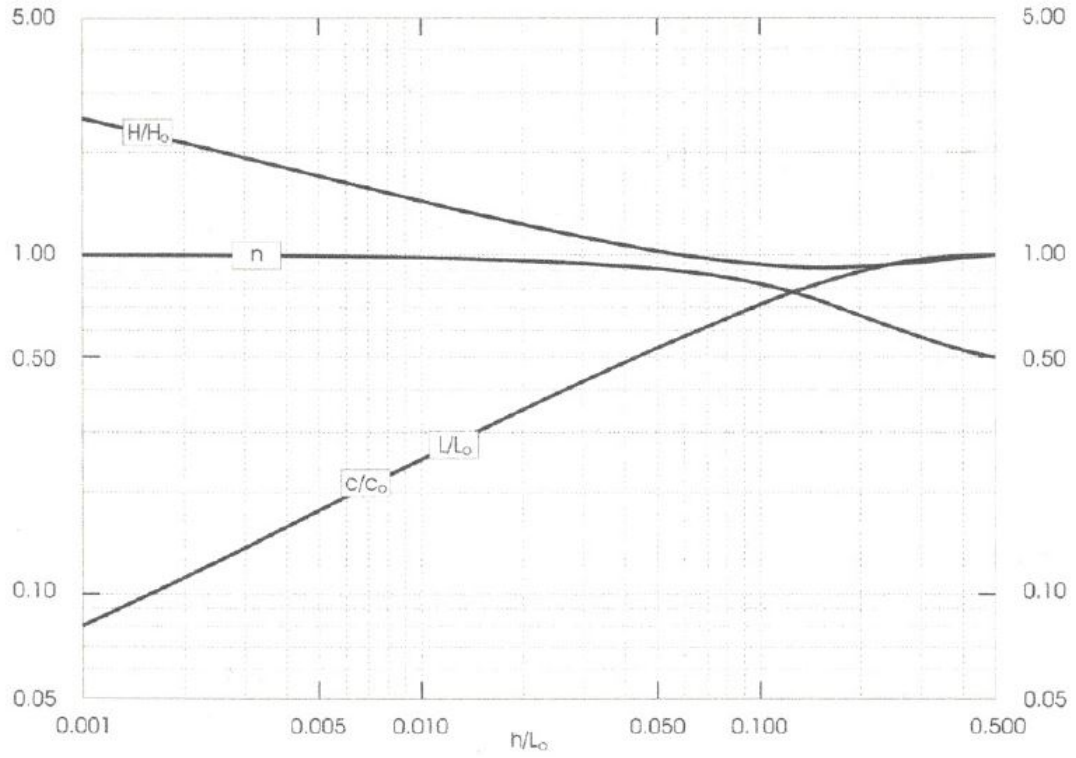

Figure 3.3: Wave celerity and wave height variation with depth (Bosboom and Stive, 2015). All the magnitudes in the graph are dimensionless. Depending on the water regime that the wave is in, namely intermediate or shallow water, the orbital velocity will increase or decrease respectively, accompanied by the correspondent wave height variation.

2015). The resulting wave is called a Stokes wave and its shape is depicted in Figure 3.4.

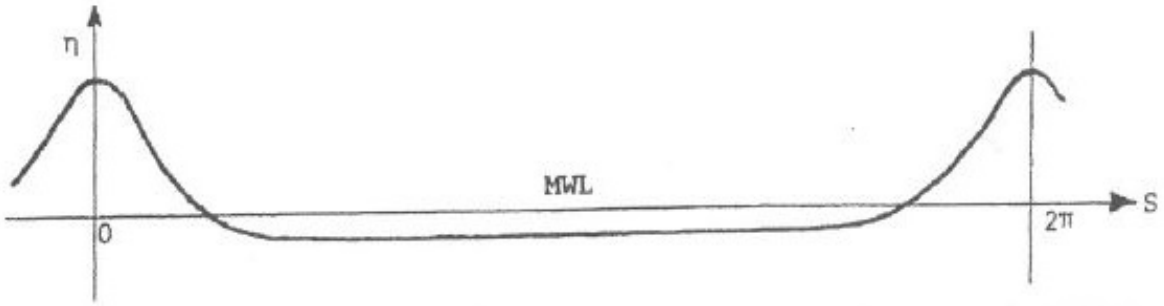

Figure 3.4: Skewed waves (Bosboom and Stive, 2015).

The effect of this change in shape is reflected in the orbital velocities profile, which also becomes skewed. The positive, onshore directed velocities become higher and shorter in duration, in contrast to the negative, offshore directed orbital velocities which become smaller and longer in duration. The skewness of the velocity profile can be seen by computing its time-averaged cube $\langle u_0^3 \rangle$, which is positive for shallow water waves (in contrast to deep water water for which it is zero).

This quantity is related to the sediment transport rate (S) in the case of bedload (Bosboom and Stive, 2015, p.296), as $S \sim \langle u_0^3 \rangle$. Hence, sediment transport occurs in shallow water due to shoaling (S>0) whereas this is not the case in deep water (S=0).

Asymmetry refers to a change in shape relative to the vertical axis, caused by the difference in speed between the wave crest and wave trough. The result is a sawtooth wave shape with a pitched forward crest and a steep face, as shown in Figure 3.5. It's been observed that, in waves propagating from deep to shallow water, the wave shape is initially more skewned than asymmetric, while later on skewness decreases and asymmetry becomes more pronounced due to a phase shift between harmonics.

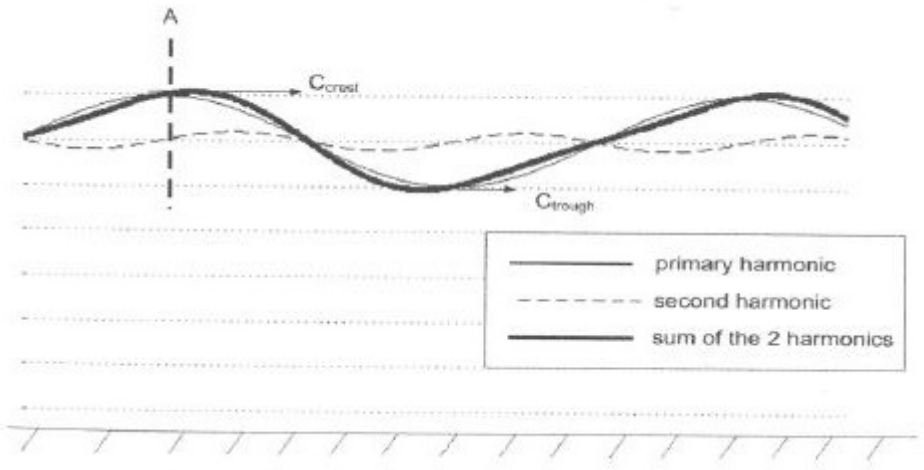

Figure 3.5: Asymmetric waves (Bosboom and Stive, 2015).

Due to the steeper wave face, the positive onshore directed orbital velocities accelerate faster than the negative offshore directed velocities. This causes a greater near-bed shear stress and thus sediment mobilisation. In combination, the flow velocity is larger under the crest of shoaling waves and mobilises more sediment due to its steep gradient.

In reality, shoaling waves become at first skewed without demonstrating great asymmetry, and later on, closer to the surfzone, asymmetry increases while skewness decreases. Asymmetry is characteristic of breaking waves. During MODEX there was no breaking, but both skewness and asymmetry where observed during the measurements. Therefore, their effects on the orbital velocities will be considered together as part of the shoaling process.

Slope effects

A sloping bed introduces a downslope gravitational force component which acts on the grains along the slope (in addition to the flow induced drag force). This affects the sediment transport direction which is influenced by the angle of the bed slope with the flow direction (Kovacs and Parker, 1994) and therefore isn't always streamwise.

In our case, the situations when the slope of the bed is parallel (0°or 180°angle) or perpendicular (90°angle) to the flow direction are of interest. The forces acting on these cases are depicted in Figure 3.6.

Slope effects result in decreased sediment stability leading to more mobile grains which tend to move, in most cases, downslope in response to this added force (Moulton et al., 2014). In general, this is a diffusive process as it tends to smoothen out the bed (Moulton et al., 2014,Garnier et al., 2008). Moreover, since the forcing component is unidirectional, it creates a constant sediment transport flux which isn't zero over a wave cycle (Moulton et al., 2014) and thus can be locally dominant and can even maintain equilibrium as shown by Garnier et al. (2008).

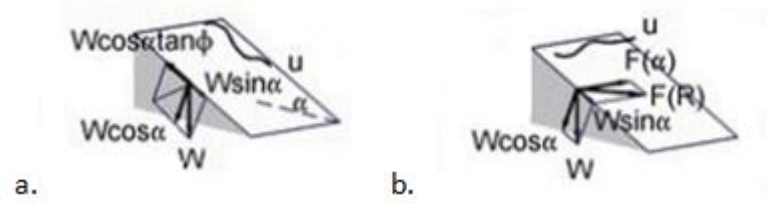

Figure 3.6: Forces acting on a slope in the cases of a) a slope parallel to the flow and b) a transverse slope (Schiereck, 2012). The situation of a slope parallel to the flow can be distinguished in an upslope (180°) and a downslope (0°). In both cases the downslope component of the gravitational force acts in the same direction as the drag force, however in an upslope it opposes to the flow force while on a downslope it enhances it (Kovacs and Parker, 1994). In the case of a traverse slope, the downslope component of the gravitational force acts perpendicular to the flow direction therefore the sediment grains are expected to move in the general direction of the combined force (F(R)).

Increased bed roughness

In order to be able to predict morphodynamic evolution, physical bed roughness (k_b) must be quantified. This parameter expresses the distance in the water column to which the bed affects the flow. It mainly consists of two elements, skin friction and form drag (Drake and Cacchione, 1992). For a plane bed k_b is related to grain size, whereas in the case of a rippled bed it depends on the bedforms' dimensions (Grant and Madsen, 1982).

Ripples are of particular interest as they develop in bedload regimes (as in the case of MODEX). These features, once formed, persist and grow until they reach an equilibrium steepness, unless high-energy conditions wash them out (Wilberg and Harris, 1994). There can be wave- and current-generated ripples. The first are usually symmetric, and can depend on orbital diameter (orbital ripples), grain size (anorbital ripples) or both (suborbital ripples) (Wilberg and Harris, 1994) (classification as described by Clifton (1976)). These may or may not cause flow separation (vortex ripples and rolling grain ripples, respectively) (Bagnold, 1946).

The second are mostly asymmetrical, with a steep lee side and gentle stoss side.They may yield strongly three-dimensional patterns. Linguoid and lunate ripples are characteristic shapes of current-generated ripples where the crest moves faster or more slowly than the wings, respectively (van Rijn, 2007). They are usually much smaller than the water depth but rise higher than the boundary layer. As a result, they induce increased form drag over their crest which results in flow separation and vortex shedding, increasing flow turbulence and sediment transport.

3.2.2. Scenarios

Depending on the type of flow, a different subgroup of the aforementioned processes occurs. It is important to be aware of the phenomena taking place in the mound vicinity since they are the basis for the sediment pathways derivation. Table 3.1 summarises the situation for each of the examined flow conditions.

With an understanding of which processes are likely important for each examined flow condition, the next step is determining locally dominant mechanisms. However, in locations where two (or more) processes cause opposing effects or lead to different directions, data is needed to distinguish these effects.

Processes \Flow type	**Oscillatory flow (waves)**	**Non-oscillatory flow (current)**	**Combined flow (wave+current)**
Flow contraction - expansion	X	✓	✓
Shoaling - Deshoaling	✓	X	✓
Refraction	✓	X	✓
Flow separation	X	✓	✓
Skewness - Asymmetry	✓	X	✓
Slope effects	✓	✓	✓
Increased bed roughness	✓	✓	✓

Table 3.1: Occurring processes in examined flow conditions.

Some examples of such cases are:

- At the mound upslope, slope effects lead to downward sediment transport which is opposite the flow direction.
- The mechanisms of shoaling and refraction may have the same effect for waves in shallow water or the opposite effect for waves in intermediate water.
- Flow separation results in settling at the back of the mound, while flow streaming tends to move sediment further.

Unfortunately, the available dataset doesn't cover the full spectrum of presented processes. As a result, the following processes aren't directly treated in this thesis:

- Slope effects investigation requires an array of instruments measuring near bed velocity and shear stress along the mound slopes. In the case of MODEX there were no direct shear stress measurements. In addition, the profiling instruments which could capture the near bed velocities were deployed in an array that wasn't dense enough, since the focus was the general evolution of the mound.
- The effect of ripples is often coupled to turbulent velocities. In our case, the instrument frequency isn't high enough to capture them in detail.
- The velocity data may give indications of flow separation. However, there are very few instruments in the area which might not be able to catch it, as separation bubbles have been observed to move downstream as the mound lowers.

3.3. Sediment transport rate

Sediment transport rate (S) formulations are related to mean and orbital flow velocities (U). Most transport formulations distinguish between bed and suspended load such that:

- $S \sim U^3$ for bedload transport
- $S \sim U^{4to5}$ for suspended load transport

In this study an Extended Energetics Friction Factor (EEFF) model proposed by Hsu et al. (2006) is used for the derivation of the sediment transport rate at the locations of the deployed instruments. In the EEFF model sediment transport is given by

$$S = K_w[\frac{\epsilon_b}{\tan\phi}\langle|\vec{\tilde{U}_0}|^2\tilde{U}_0\rangle + \frac{\epsilon_s}{W_0}\langle|\vec{\tilde{U}_0}|^3\tilde{U}_0\rangle] + K_c[\frac{\epsilon_b}{\tan\phi}\langle|\vec{U_0}|^2\overline{U_0}\rangle + \frac{\epsilon_s}{W_0}\langle|\vec{U_0}|^3\overline{U_0}\rangle] \tag{3.1}$$

where

$$K_w = \frac{C_w}{(s-1)g} \text{ and } K_c = \frac{C_c}{(s-1)g} \tag{3.2}$$

with

K_w	friction coefficient for waves (s^2/m)
K_c	friction coefficient for current (s^2/m)
ϵ_b	efficiency factor for bedload transport (-)
ϵ_s	efficiency factor for suspended load transport (-)
ϕ	angle of repose (°)
W_0	sediment fall velocity (m/s)
$\lvert\overrightarrow{\tilde{U}_0}\rvert$	magnitude of orbital velocity vector (m/s)
$\lvert\overrightarrow{U_0}\rvert$	magnitude of the total (orbital and mean) velocity vector (m/s)
C_w	friction factor for waves (-)
C_c	friction factor for current (-)
s	ρ_s/ρ (-)

The model was developed under the assumption that sediment transport occurs near the bed and is in phase with the bottom shear stress. It is a two-dimensional vertical (2DV) model that depends on free-stream velocity skewness and differentiates between the friction caused by the oscillatory and mean velocity component. This distinction was motivated by Hsu et al. (2006) findings where even in cases of weak mean current, the cubed total velocity varied significantly from the cubed orbital component and the sediment transport gradients resulting from the first weren't consistent with the observations.

The model skips shear stress calculations and goes directly from flow velocity to sediment transport rate. However, the connection between the two is formed by relating the free-stream velocity to bottom shear stress via a boundary layer turbulence model, and through this to sediment transport via a Meyer-Peter-Muller power law given by

$$\Psi = 11^{\theta}_{|\theta|}[|\theta| - 0.05]^{1.65} \tag{3.3}$$

Equation 3.3 incorporates implicitly a threshold of motion of $\theta_crit = 0.05$, a value which is equal to the critical Shields parameter for a flat bed, since the energetics models of Hsu et al. (2006) was developed for sheet flow conditions. However, Wengrove (2018) showed that this model can be used for bedload transport in the ripple regime, provided that the friction coefficients K_w and K_c are adapted to fit the bedform migration conditions.

The model can be used for waves only, current only and combined flows, thus making the results of different conditions comparable. This is not the case when it comes to shear stress estimation, as different formulations are used for different types of flow. Therefore the presented method was chosen over a direct estimation of the shear stress due to its uniform applicability,

3.4. Estimating sediment pathways

This section elaborates on the method and model criteria used to determine the sediment pathways from the hydrodynamic data, and equations 3.1 and 3.2.

Erosion locations

Erosion occurs at the locations where the critical shear stress is exceeded, and in cases when there is convergence of sediment transport vectors. In the first instance, the energetics model results in a transport rate value which indicates that the flow is strong enough to mobilise the sediment. In the

second instance, whether or not sediment transport gradients are present and what their sign is can be determined by linking bathymetry with sediment transport rate, and observing its profile along a direction.

Direction of movement

After an erosion location has been specified, the focus lies on the locally acting processes. First, the effect of all on stream velocity is taken into account, and then the locally dominant one is determined. This is achieved by looking into the data and checking which mechanism they comply with in terms of direction and magnitude. This dictates the direction of movement as it has the strongest effect on the mobilised sediment of this area.

In some cases, there might be more than one possible direction due to either gradients in several directions or inconclusive indications of which mechanism is the locally dominant.

Deposition locations

Finally, after tracking the initiation areas and direction of sediment movement as dictated from the various mechanisms along and across the flume, the focus returns to the sediment transport rates. Deposition occurs at those locations where the bottom shear stress is lower than the critical shear stress, and in cases when there is divergence of sediment transport vectors. The first criterion is once again determined by the energetics model which returns zero values when the implicit threshold for initiation of motion (θ_cr) is not satisfied. The second is determined by following the same method as for the detection of the erosion areas.

3.4.1. Theoretical response

Following the methodology described above the expected mound response under waves, current, and combined flow as dictated by the literature and the conceptual model, is presented in Figures 3.7, 3.8, and 3.9, respectively.

3.4.2. Parameter definition

In order to implement the conceptual model in practice, the flow velocities, and sediment transport gradients are key components according to the methodology described above. Representative values for the components need to be estimated from the measurements, which will form the basis of the analysis.

Flow velocity

A statistically representative velocity measure for waves is the root mean square velocity (U_{rms}). In its general form it is described as

$$U_{rms} = \sqrt{\overline{(U-\overline{u})^2}} \tag{3.4}$$

where

- U is the total velocity vector (m/s)
- $\overline{u}$ is the average (over a run duration) flow velocity (m/s)

In case of combined or pure oscillatory flow (where $\overline{u} = 0$), equation 3.4 gives the orbital velocity. If the total velocity is separated in velocity components in x- and y- direction, the U_{rms} is estimated as

$$U_{rms,total} = \sqrt{\overline{(U_x - \overline{u_x})^2 + (U_y - \overline{u_y})^2}} \tag{3.5}$$

where

U_x is the velocity vector in x-direction (m/s)
$\overline{u_x}$ is the average (over a run duration) velocity in x-direction (m/s)
U_y is the velocity vector in y-direction (m/s)
$\overline{u_y}$ is the average (over a run duration) velocity in y-direction (m/s)

Sediment transport gradients

The estimated gradients are averaged in time, and computed between instruments in space. A distinction between along- and cross-flume direction is made, as different velocity components are of importance in each direction. The domain comprises the whole flume. The along-flume gradients are estimated from the wavemaker to the beach, while the cross-flume gradients are computed from the top of the mound to the side walls of the flume.

The along-flume sediment transport gradient between two instruments is computed based on the total transport at each location, and is given by

$$dS = \frac{d\overline{S_2} - d\overline{S_1}}{dx} \tag{3.6}$$

where

dS_1 is the averaged (over the scenario duration) sediment transport rate of the first instrument (m^2/s)
dS_2 is the averaged (over the scenario duration) sediment transport rate of the consecutive instrument (m^2/s)
dx is the distance along the x-axis between the two instruments

The cross-flume sediment transport gradient between two instruments is computed based on the transport due to the y velocity component only, and is given by

$$dS = \frac{d\overline{S_2, y} - d\overline{S_1, y}}{dy} \tag{3.7}$$

where

dS_1, y is the averaged (over the scenario duration) cross-flume sediment transport rate of the first instrument (m^2/s
dS_2, y is the averaged (over the scenario duration) cross-flume sediment transport rate of the consecutive instrume
dy is the distance along the y-axis between the two instruments

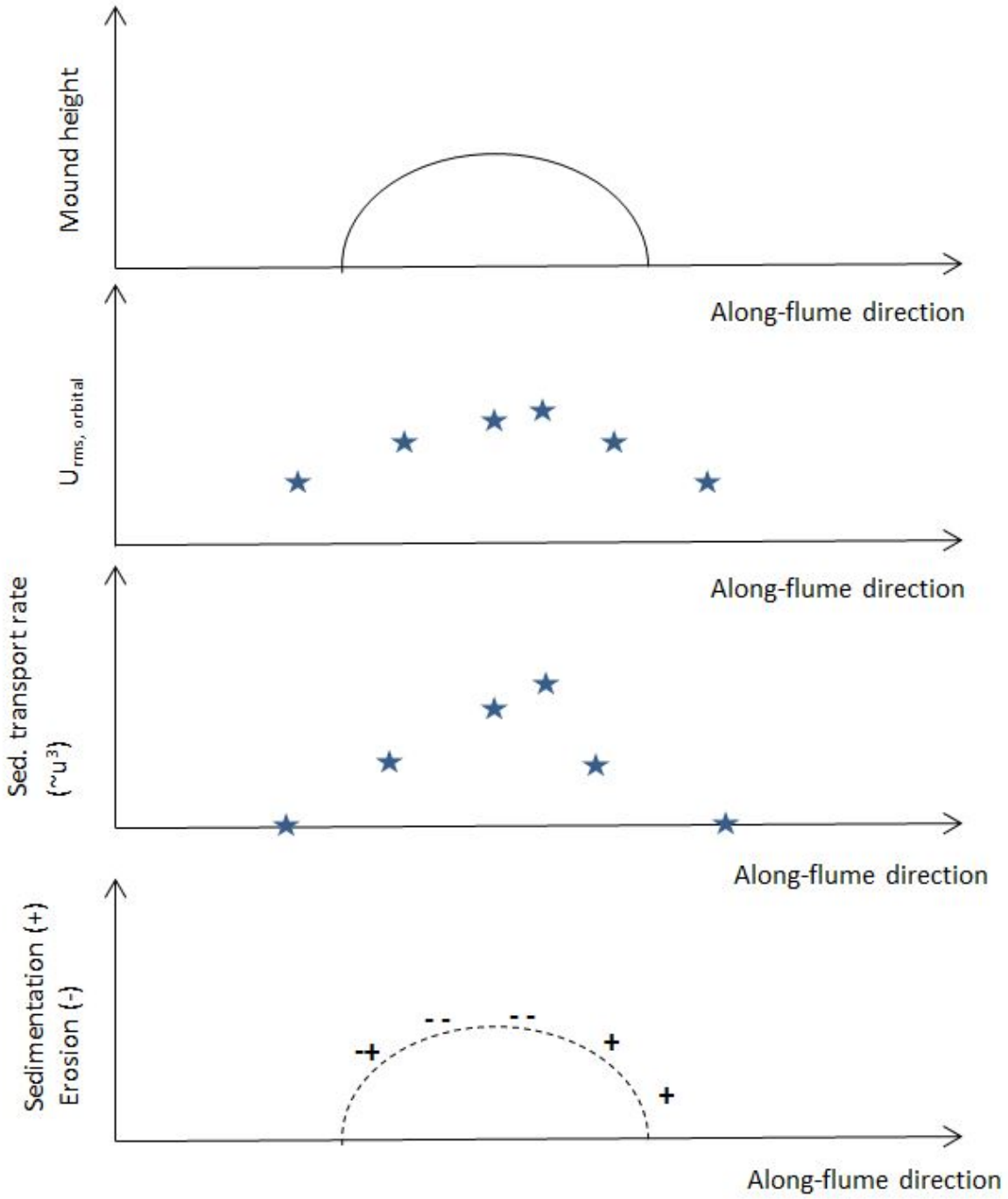

Figure 3.7: Theoretical mound response under oscillatory flow. This plot translates the expected variations in flow velocity due to the acting theoretically mechanisms (second panel), to fluctuations of the sediment transport rate along the mound length (third panel), and finally to the expected sedimentation - erosion pattern at the mound (last panel).

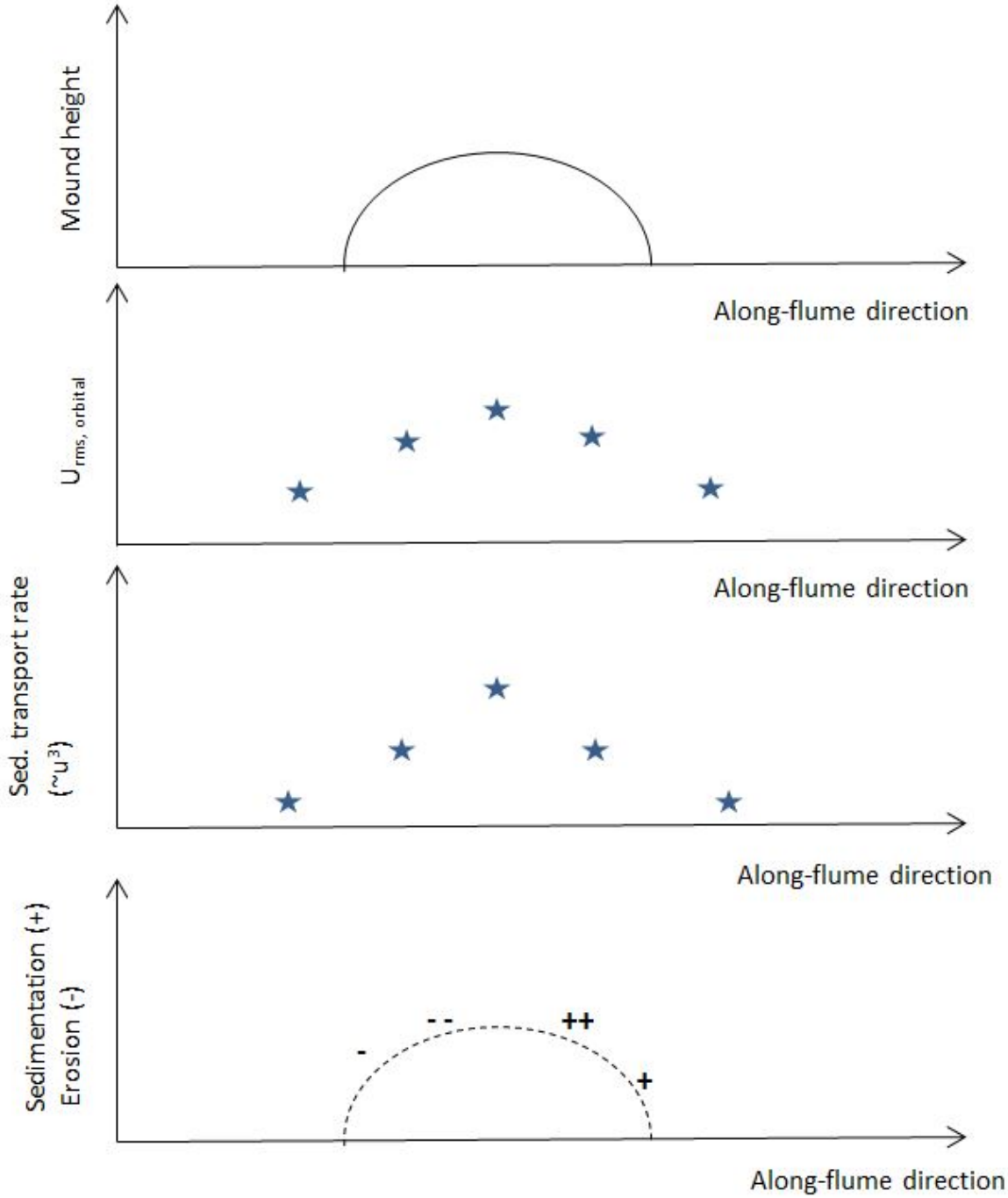

Figure 3.8: Theoretical mound response under non-oscillatory flow. This plot translates the expected variations in flow velocity due to the theoretically acting mechanisms (second panel), to fluctuations of the sediment transport rate along the mound length (third panel), and finally to expected sedimentation - erosion pattern at the mound (last panel).

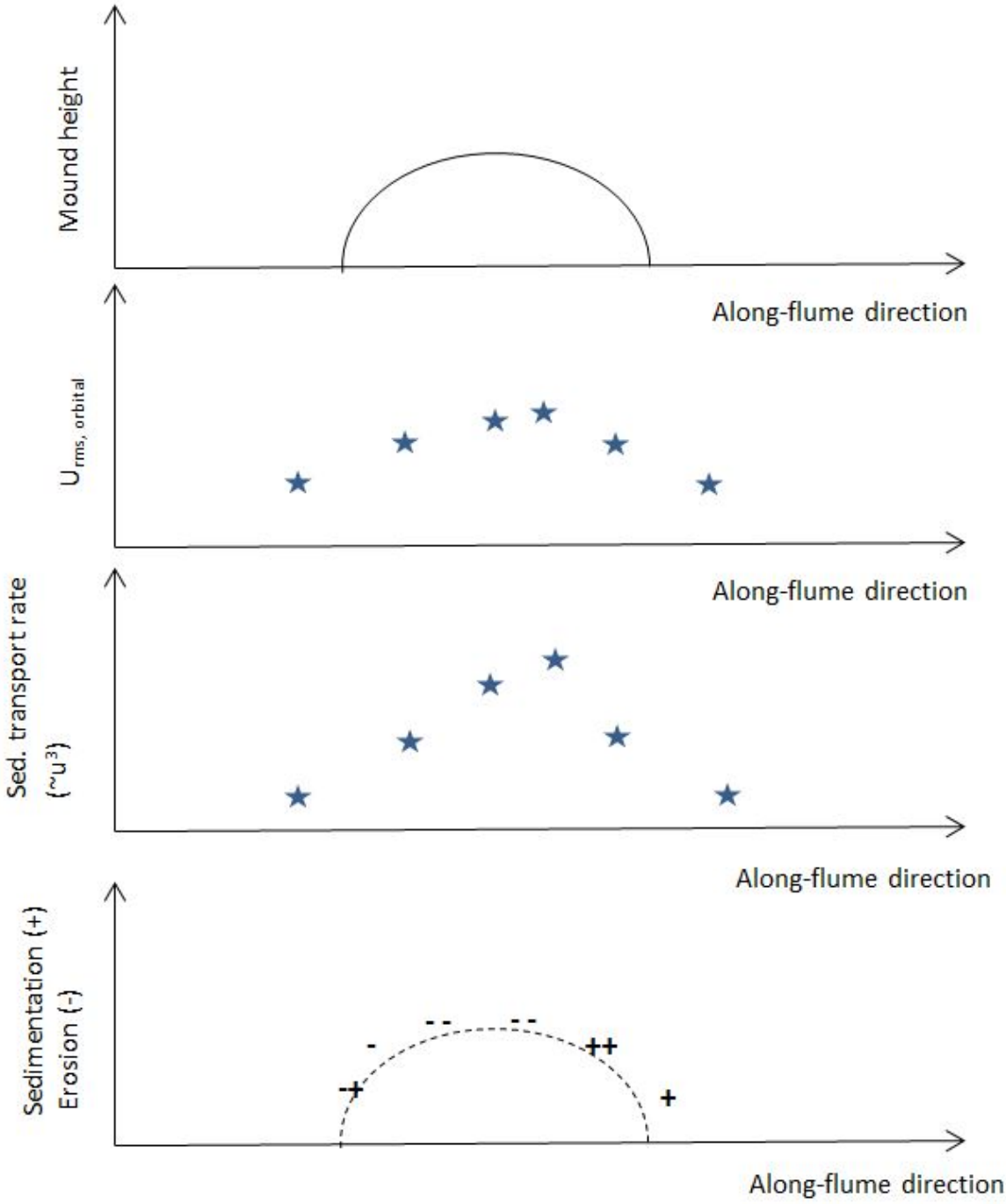

Figure 3.9: Theoretical mound response under combined flow. This plot translates the expected variations in flow velocity due to the acting theoretically mechanisms (second panel), to fluctuations of the sediment transport rate along the mound length (third panel), and finally to expected sedimentation - erosion pattern at the mound (last panel).

4

Results

In this chapter the results of MODEX (mound bathymetry, morphological evolution, and sediment transport rate) are presented for each flow type. Section 4.1 discusses the mound evolution under oscillatory flow (waves), section 4.2 focuses on non-oscillatory flow (current), and section 4.3 reviews combined flow. Finally, in section 4.4 results combining all the scenarios are presented.

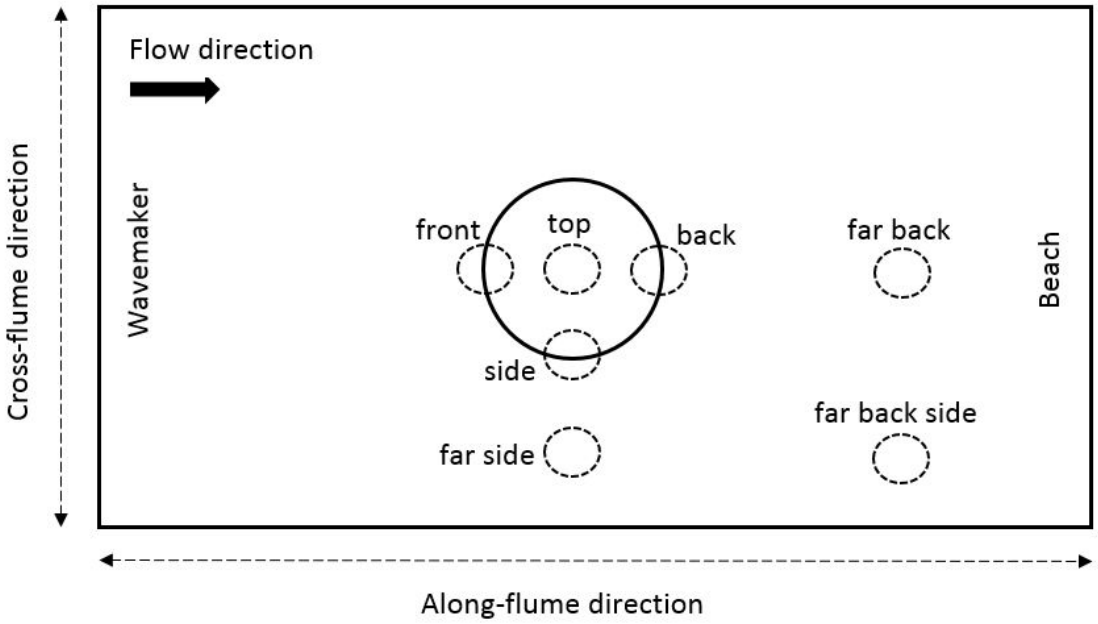

Figure 4.1: Frame of reference for directions and mound areas in result description.

When describing and analysing results a clear frame of reference for the terminology used is vital. Figure 4.1 provides the frame of reference regarding the terms that are going to be used from this point on in this study, for the results description and discussion.

4.1. Oscillatory flow cases

Three experiments with pure oscillatory flow were conducted ranging from low (scenario 1) to high (scenario 3) waves. In this section the case of low waves is going to be discussed in detail because it clearly shows the effect of the flow on the mound as it didn't interact with the surrounding bed. The remaining two wave cases show similar overall behaviour as scenario 1. Their differences and similarities are assessed at the end of the section, while their results can be found in Appendix B.

4.1.1. Low waves

Morphological evolution

The mound footprint remains mostly confined to the initial area, which is indicated by the before and after laser scan in Figure 4.2. Sediment is eroded from the top of the mound, there is accretion at the sideslopes (as indicated by the colour scale) and there is a linear ripple pattern covering the whole mound (Figure 4.3). According to the underwater GoPro footage these initiated from the top of the mound and spread uniformly downslope in all directions. The largest bedforms are spotted on the mound top, while the front and back toe are smooth which indicates sediment deposition (in accordance with Figure 4.2). Around the mound base the bedforms show changes in crest angle: the ripples at the right half are directed towards the front of the mound (right toe in Figure 4.3) while the ripples at the left half are directed towards the back of the mound (left toe in Figure 4.3). Lastly, at the back of the mound appear two arms extending on either side of the centerline.

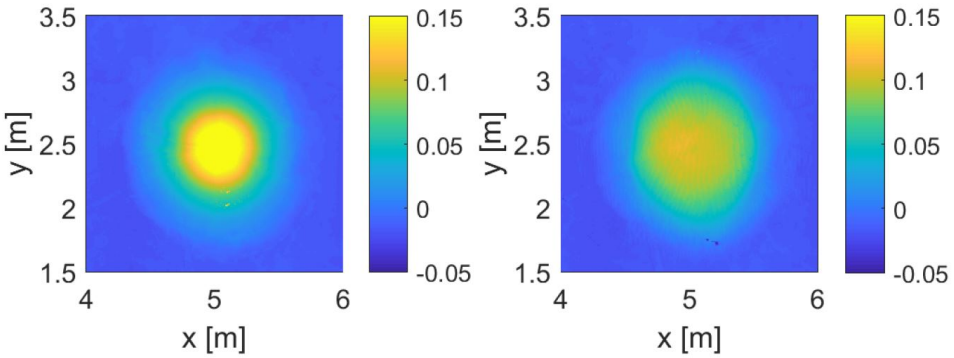

Figure 4.2: Mound morphology before (left) and after (right) scenario 1 (low waves), as captured by the laser scanner. x- and y-axes are in the along-flume and cross-flume direction, respectively. The flow direction is from left to right. The colorbar represents elevation (in m) with regard to flat bed level.

Figure 4.3: Mound morphology after the end of scenario 1 (low waves). The flow direction is from right to left.

When looking more closely to the evolution of the bed level during the experiment, the results are in accordance with Figure 4.2. The top of the mound (Figure 4.4, top panel) erodes with a decreasing rate until run 8 from which point the bed level stabilises. At this point the total bed depression of the top (URS5) is 5.1 cm. Although all experiments were run until the mound height reduced to about half the initial, this scenario ended earlier (mound height of 14 cm) as the bed was considered to have stabilised during the last runs. The bed at the side slope of the mound (Figure 4.4, middle panel) shows constant accretion, with the bed having raised about 3 cm by the end of the experiment. From run 2 and on migrating ripples are visible which grow in wavelength over time. The bottom panel shows a constant bed level with possible accretion under URS11 during the last run.

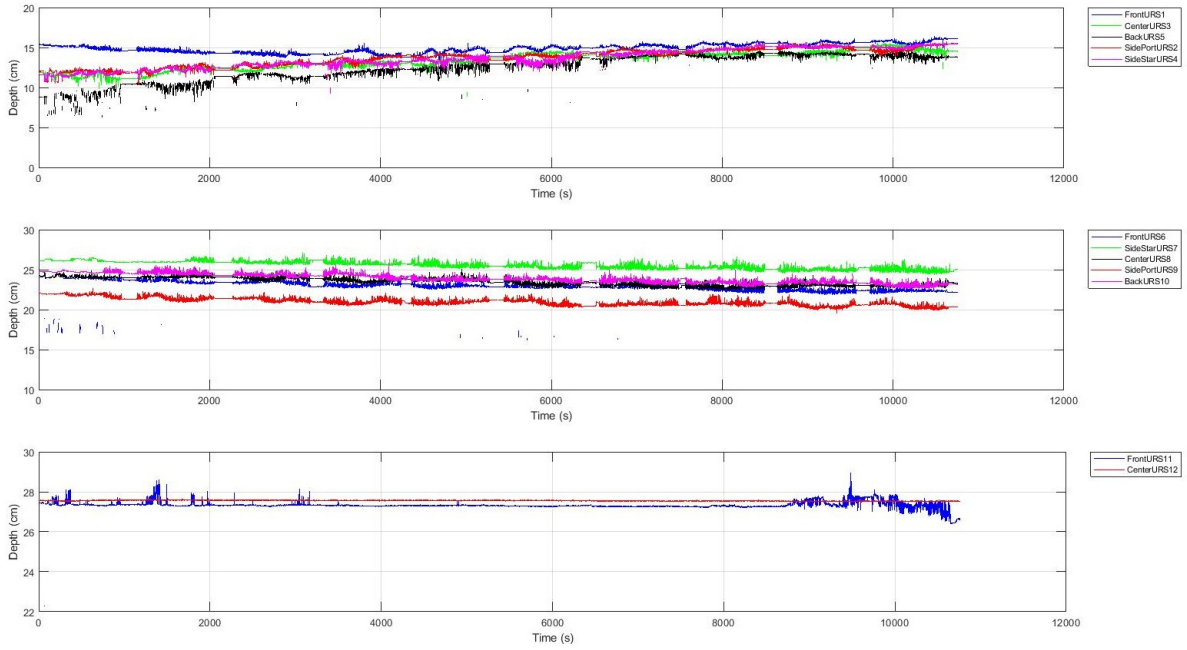

Figure 4.4: Cumulative plot of bed level change evolution during scenario 1 (low waves). The top panel depicts the measurements of the URS cluster located on the side of the peak (URSs 1-5). The middle panel depicts the measurements of the URS cluster just downdrift the mound over the downslope (URSs 6-10). The bottom panel depicts the measurements of the URSs on the back of the mound (URSs 11-12). The horizontal axis is the duration (in seconds) of the measuring period for the depicted scenario, and the vertical axis is the distance (in cm) of the bed from the probe.

Sediment movement

The overall sedimentation-erosion pattern of the mound (Figure 4.5, left panel), confirms previous statements regarding the footprint shape changes. The final footprint is wider towards the back of the mound and not entirely symmetrical (the top right side extends all the way to the 0 m contour, in contrast to the bottom right side). Moreover, accretion occurs at both mound toes in the along-flume direction. The cross-flume asymmetry indicates a slightly oblique wave incidence, which was also observed during the experiment.

However, the sedimentation - erosion pattern that results from the sediment transport vector gradients (Figure 4.5, right panel) is different since it shows that sediment erodes mostly from the upslope at the front of the mound and less from the top. In addition, even though it shows sedimentation both at the sideslopes and at the back of the mound (which is in accordance with Figure 4.5, left panel), the accretion at the back downslope (near the toe) is far more than that of the sideslopes which is not reflected in the overall sedimentation-erosion pattern.

Finally, regarding the sediment transport rate evolution across the flume, the strongest sediment transport occurs at the back of the mound where both its magnitude and direction remain unchanged throughout the experiment. At the other locations a gradual increase of the sediment transport rate is evident. At all locations the transport shows a general angle, which could be related to flume operation or instrument alignment. Looking at the relative angles between the arrows in front and on top of the mound, it can be noticed that the angles of the left (from the centerline) part of the mound show a gradual turning and decreasing of transport. The top of the mound displays the strongest change in direction and magnitude throughout the experiment.

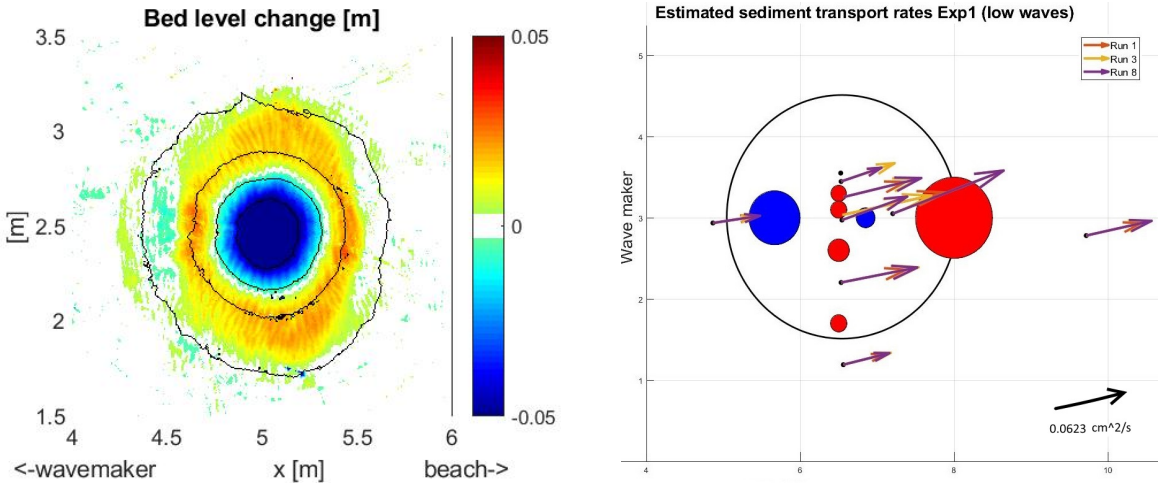

Figure 4.5: Left panel: Sedimentation - erosion pattern at the mound at the end of scenario 1 (low waves) as captured by the laser scanner. The colorbar indicates the height (in m) of accretion (positive values) and erosion (negative values). Right panel: Estimated sediment transport rates at the instrument locations across the flume, and resulting sedimentation - erosion pattern at the mound during scenario 1 (low waves). The arrows represent sediment transport rates (S). Their direction and size correspond to the model estimated values. At the bottom right corner is a scale for magnitude reference, and is equal in size to the most right purple arrow. All circles are estimated based on sediment transport gradients (dS) and are scaled according to gradient magnitude. The blue circles indicate erosion (dS>0), while the red circles show accretion (dS<0). In both panels, the flow is from left to right, and x and y axes are in the along-flume and cross-flume direction, respectively.

4.1.2. Comparison between wave cases

All three wave cases show similar behaviour. However, there are some differences that are worth to mention.

Morphological evolution

The stronger the flow conditions the larger the final footprint area according to Figures 4.2, B.4 and B.11. In scenarios 2 and 3 the footprint is no longer confined in the initial area. Sediment is deposited in the whole area between the 0 m and 0.05 m contour, and the footprint shape is more circular.

The formed ripples are in all cases linear, with growing dimensions as wave height increases. However, in scenario 2 a checkered ripple pattern occurs (Figure B.5). This is the only case that such a pattern was observed. In scenario 3 the ripple pattern is linear with small irregularities on the mound (Figure B.12). In all cases the front and back toe are smoother than the rest of the area.

While the flow increases in strength the bed on top of the mound erodes with a faster rate, and more accretion is observed at the back of the mound (URS11) (Figures 4.4, B.6, and B.13). In all cases, the

URS cluster over the sideslope shows slight accretion.

Sediment movement

The sedimentation - erosion pattern captured by the laser scanner is the same (Figures 4.5, B.7 and B.14, left panels), with increasing flow intensity leading to stronger erosion of the mound top and accretion of the sideslopes (at all directions). However, the flow velocity inferred sediment movement pattern (Figures 4.5, B.7 and B.14, right panels) differs strongly between scenario 1 and the rest wave only cases. Although, all cases show the strongest erosion at the front of the mound (instead of the top), scenarios 2 and 3 show that sediment is deposited mostly at the back of the mound between peak and mid-height, while there is also some accretion at the sideslopes near the peak, and the back toe.

4.2. Non-oscillatory flow cases

In this section the results of scenario 5 are going to be presented by describing the observed morphological evolution and sediment movement.

Morphological evolution

The general shape of the mound changes from Gaussian to barchan (Figure 4.6) with a mild sloping stoss side and a steep lee side (Figure 4.7). Its footprint expands outside the initial area and goes from circular to horseshoe-like (Figure 4.6). The mound top is transformed into a wider plateau of similar elevation with its centre shifted towards the back of the mound. An irregular three-dimensional ripple pattern is formed over the whole flume. The ripples are asymmetric with a milder upslope and a steep front according to the flow direction. The largest and most irregular ripples are on top of the mound. Some local regularity in the ripple pattern is encountered over the lee side, where the ripples are small in dimensions, linear, and curving towards the centerline of the mound (Figure 4.7, rectangulars).

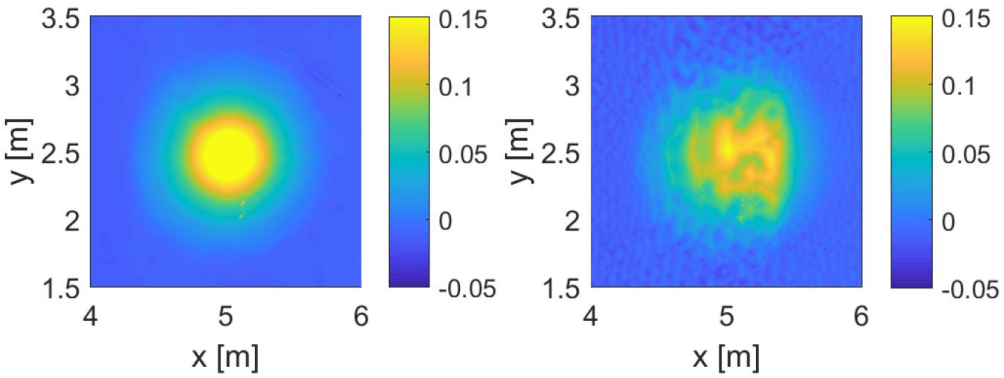

Figure 4.6: Mound morphology before (left) and after (right) scenario 5 (current only), as captured by the laser scanner. x- and y-axes are in the along-flume and cross-flume direction, respectively. The flow direction is from left to right. The colorbar represents elevation (in m) with regard to flat bed level.

The bed near the mound peak (Figure 4.8, top panel) erodes, with the final mound height decreasing by 7 cm by the end of the experiment.The sideslope of the mound (Figure 4.8, middle panel) accretes towards the back of the mound (URSs 8,9,10) and erodes at the front (URS 6). Migrating ripples of large dimensions are apparent in the record over the whole mound. The bed level downdrift of the

mound (Figure 4.8, bottom panel) remains constant. No ripples are apparent in the record in this area.

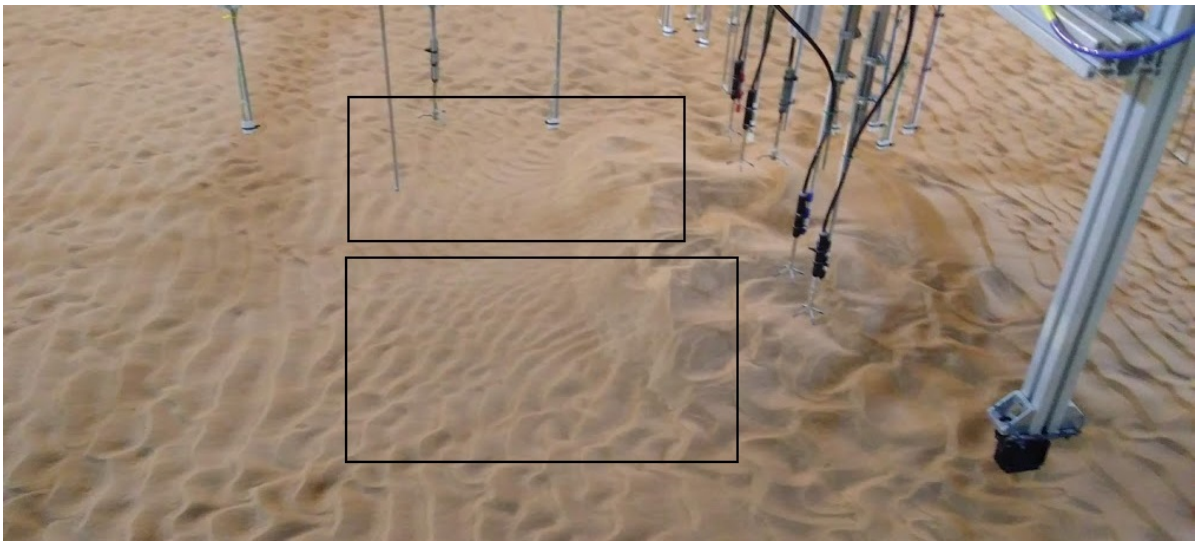

Figure 4.7: Mound morphology after the end of scenario 5 (current only). The flow direction is from right to left. The rectangulars show the curving towards the centerline ripples at the back of the mound.

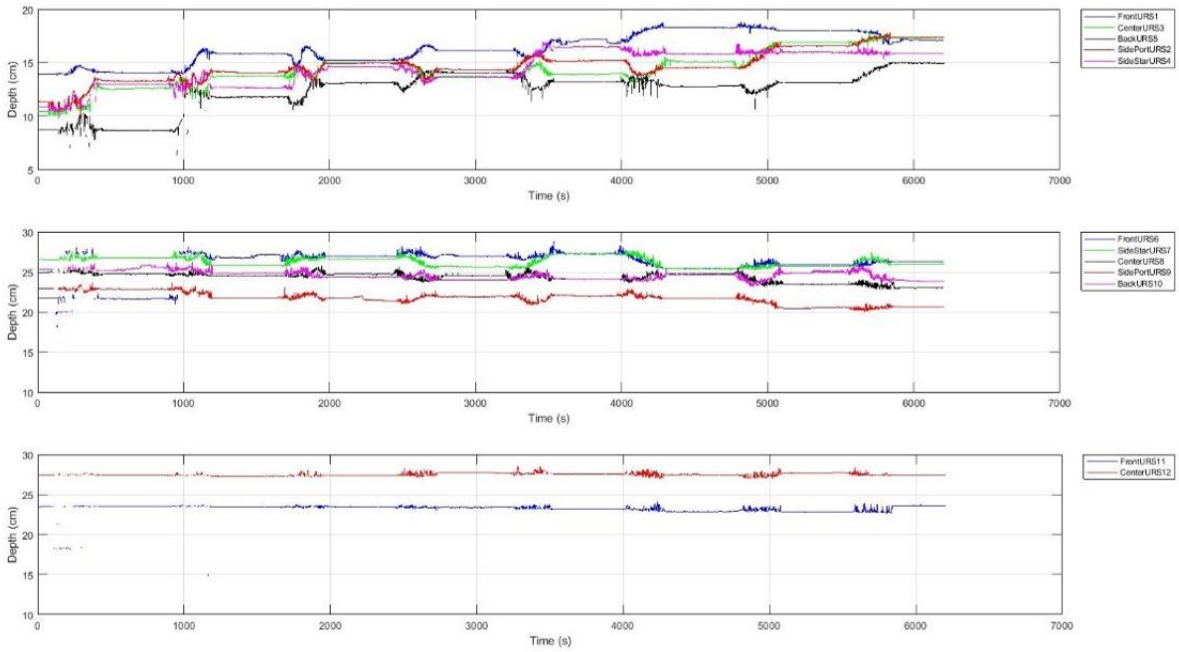

Figure 4.8: Cumulative plot of bed level change evolution during scenario 5 (current only). The top panel depicts the measurements of the URS cluster located on the side of the peak (URSs 1-5). The middle panel depicts the measurements of the URS cluster just downdrift the mound over the downslope (URSs 6-10). The bottom panel depicts the measurements of the URSs on the back of the mound (URSs 11-12). The horizontal axis is the duration (in seconds) of the measuring period for the depicted scenario, and the vertical axis is the distance (in cm) of the bed from the probe.

Sediment movement

The overall sedimentation-erosion pattern of Figure 4.9 (left panel) confirms the observed change in shape. Sediment is eroded from the top half of the mound around the peak, as is indicated by the dark blue colour in the area inside the 0.1 m height contour, and is deposited at the downdrift downslope (dark red area), creating the barchan shape. The mound peak migrates downstream, although the mound footprint doesn't migrate. On the spot sediment compaction measurements confirm the deposition at the back of the mound, where the sediment was found to be loosely packed. Finally, no sediment deposition at the front toe of the mound, although the compaction measurements showed some relaxation of the sand.

The sedimentation-erosion pattern derived from the measured velocities (Figure 4.9, right panel) is in accordance with the laser scanner pattern as it shows erosion of the peak and deposition at the back of the mound. The only difference is that is shows deposition at the upper half of the mound sideslope, and the erosion at the side toe.

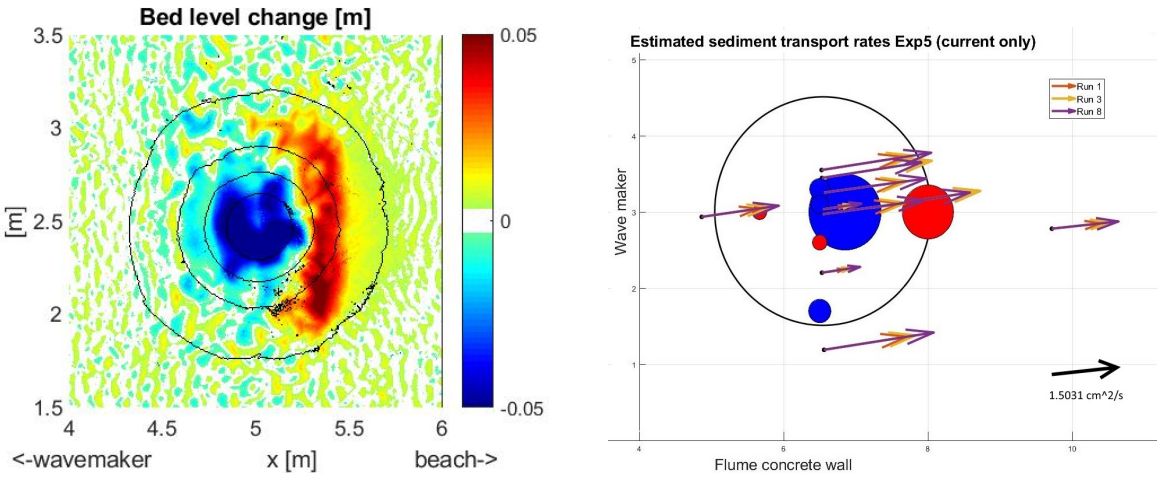

Figure 4.9: Left panel: Sedimentation - erosion pattern at the mound at the end of scenario 5 (current only) as captured by the laser scanner. The colorbar indicates the height (in m) of accretion (positive values) and erosion (negative values). Right panel: Estimated sediment transport rates at the instrument locations across the flume, and resulting sedimentation - erosion pattern at the mound during scenario 5 (current only).The arrows represent sediment transport rates (S). Their direction and size correspond to the model estimated values. At the bottom right corner is a scale for magnitude reference, and is equal in size to the most right purple arrow. All circles are estimated based on sediment transport gradients (dS) and are scaled according to gradient magnitude. The blue circles indicate erosion (dS>0), while the red circles show accretion (dS<0). In both panels, the flow is from left to right, and x and y axes are in the along-flume and cross-flume direction, respectively.

4.3. Combined flow cases

Three experiments with combined flow (scenarios 7 - 9) were conducted with different ratio of wave and current contributions. In this section the case of equal wave and current contributions (scenario 7) is going to be discussed in detail as it considered the most representative to investigate the mound response under the combined effect of waves and current. The remaining two combined flow cases show similar behaviour as scenario 7. Their differences and similarities are assessed at the end of the section, while their results can be found in Appendix B.

4.3.1. Equal wave - current contributions

Morphological evolution

The general shape of the mound bears similarities to both the previously observed responses. The mound footprint spreads outside the initial area but remains circular. It forms a mild sloping stoss side and a steep lee side. The mound peak migrates downstream (Figure 4.10) and forms a plateau of uniform elevation, similar to Figure 4.6. The ripple pattern comprises linear asymmetric ripples all over the flume bed, with the largest at the mound (Figure 4.11). As we move from the front toe towards the back of the mound, the ripples become larger and three-dimensional, and appear to converge towards the mound centerline.

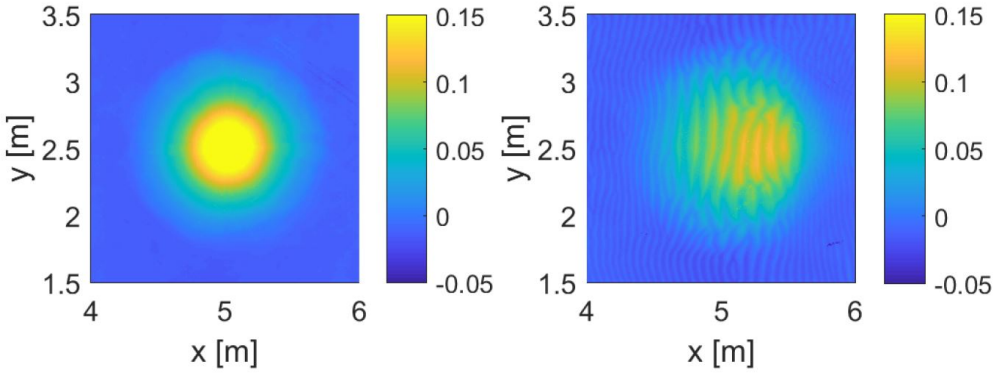

Figure 4.10: Mound morphology before (left) and after (right) scenario 7 (combined, equal contributions), as captured by the laser scanner. x- and y-axes are in the along-flume and cross-flume direction, respectively. The flow direction is from left to right. The colorbar represents elevation (in m) with regard to flat bed level.

The bed at the top of the mound erodes with a decreasing rate without stabilising until the end of the experiment (Figure 4.12, top panel). The total mound height decrease is 9 cm. The sideslope overall shows some accretion although the five instruments display varying behaviour (Figure 4.12, middle panel). Migrating ripples are apparent in the record over the whole mound. The bed right downdrift of the mound (Figure 4.12, bottom panel) accretes constantly between runs 3 and 8, sign of mound migration.

Figure 4.11: Mound morphology after the end of scenario 7 (combined, equal contributions). The flow direction is from right to left.

Sediment movement

The overall sedimentation-erosion pattern of Figure 4.13 (left panel) confirms the observed change in shape. Sediment is eroded from the first half of the mound, mostly from the upper upslope and peak. Sediment is deposited all over the back of the mound, reaching and outgrowing the back toe. The sedimentation-erosion pattern derived from the measured velocities (Figure 4.13, right panel) follows the same main lines as the laser scanner pattern, as it shows erosion of the peak and deposition at the back of the mound. However, it shows slight accretion at the upslope and of the mound which are not observed in the overall sedimentation - erosion pattern. In addition, some erosion appears at the sideslope. This may be positioned anywhere in the distance between the two surrounding arrows so it can be or not in contradiction to the laser scanner pattern.

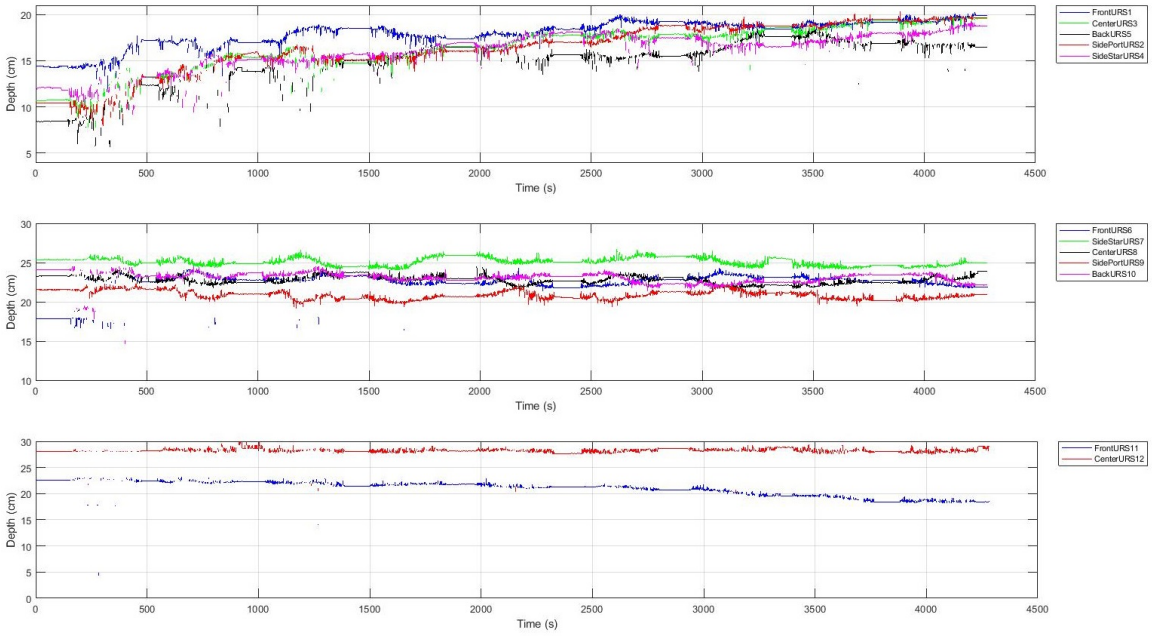

Figure 4.12: Cumulative plot of bed level change evolution during scenario 7 (combined, equal contributions). The top panel depicts the measurements of the URS cluster located on the side of the peak (URSs 1-5). The middle panel depicts the measurements of the URS cluster just downdrift the mound over the downslope (URSs 6-10). The bottom panel depicts the measurements of the URSs on the back of the mound (URSs 11-12). The horizontal axis is the duration (in seconds) of the measuring period for the depicted scenario, and the vertical axis is the distance (in cm) of the bed from the probe.

4.3.2. Comparison of combined flow cases

Morphological evolution

In all three cases the footprint appears rather circular. A more extensive examination is presented in section 4.4.

In the wave-dominant case (scenario 9) the formed ripples are more linear and with smaller wavelengths, in contrast to the current-dominant case (scenario 8) where the ripple pattern is more irregular, with bedforms of larger dimensions.

The mound also migrates in scenario 8 (Figure B.25, bottom panel), while this is not the case in scenario 9 (according to the bottom panel of Figure B.30). Besides that, the bathymetry evolution is the similar in all three cases.

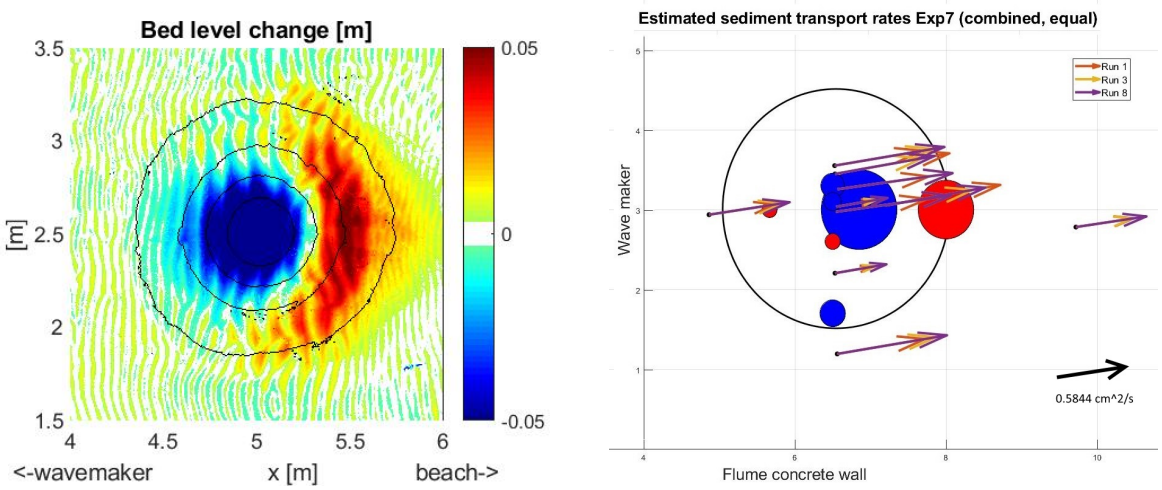

Figure 4.13: Left panel: Sedimentation - erosion pattern at the mound at the end of scenario 7 (combined, equal contributions) as captured by the laser scanner. The colorbar indicates the height (in m) of accretion (positive values) and erosion (negative values). Right panel: Estimated sediment transport rates at the instrument locations across the flume, and resulting sedimentation - erosion pattern at the mound during scenario 7 (combined, equal contributions).The arrows represent sediment transport rates (S). Their direction and size correspond to the model estimated values. At the bottom right corner is a scale for magnitude reference, and is equal in size to the most right purple arrow. All circles are estimated based on sediment transport gradients (dS) and are scaled according to gradient magnitude. The blue circles indicate erosion (dS>0), while the red circles show accretion (dS<0). In both panels, the flow is from left to right, and x and y axes are in the along-flume and cross-flume direction, respectively.

Sediment movement

During the combined flow with equal wave and current contributions, the erosion and accretion zones were the most intense in comparison to the other two cases (Figures 4.13, B.26 and B.31, left panels). As waves grow stronger and current weaker, the sediment movement becomes more restrained into the initial footprint area.

In all cases, the sediment transport rate derived panels show the same areas of accretion and erosion in the mound vicinity. The agreement of these with the laser scanner sedimentation-erosion patterns has been discussed earlier in the section and will not be repeated here.

4.4. Morphological aspect comparison

In this section results linking the observed morphodynamic response with the imposed hydrodynamic forcing for all scenarios are presented.

First of all, the mound height reduction and the timescale of this change under the various conditions is an interesting aspect of the mound response. The mound peak eroded constantly with a decreasing rate in time in all scenarios. High waves and all types of combined flow resulted in a peak erosion magnitude of about 9 cm after 50 min of flow, as shows Figure 4.14. In these cases the desired amount of erosion (about half the initial mound height) was achieved. Differences are observed for low (Exp1) and medium waves (Exp2), as well as pure current (Exp5). In these scenarios, although the mound height reduction criterion was not fulfilled, the experiments were stopped as the mound was considered to be close to equilibrium based on the URS measurements. Regarding the wave cases, as the wave height increased the mound top eroded more, and with a faster rate. Under oscillatory flow the mound initially behaved in the same way as for experiments 3, and 7 - 9. However an accreting period appeared midways the experiment owing to growing and migrating ripples, which resulted in a smaller reduction of the mound height (8 cm).

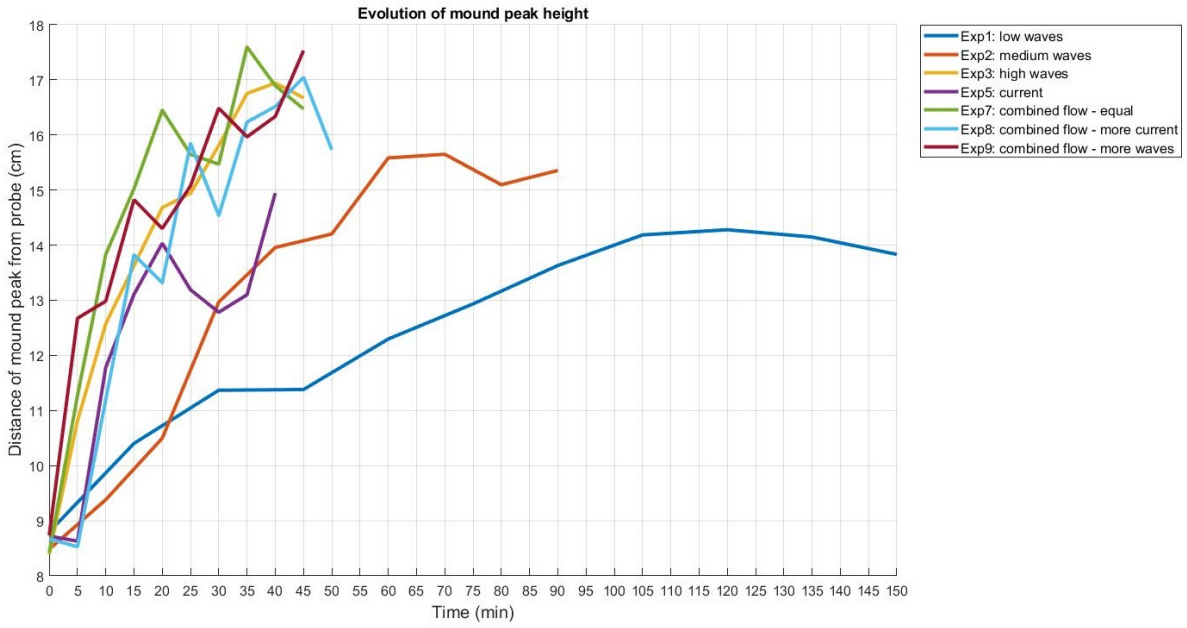

Figure 4.14: Bed level change evolution at the mound peak during all scenarios. The curves are based on the bed level measurements of URS5, which is located over the mound peak, at the beginning and at the end of each run for every scenario.

In order to examine how the observed morhodynamic response relates to the imposed hydrodynamics, measures of the mound geometry and position are plotted against hydrodynamic aspects. U_{rms}, $\overline{U_{max}}$, and $\overline{U_{max}^2}$ were used, from which $\overline{U_{max}}$, and $\overline{U_{max}^2}$ showed the best agreement with the results. Since $\overline{U_{max}^2}$ also has an important physical meaning as it relates to flow energy, it was the one chosen to be used in the analysis of the results.

The aforementioned morphodynamic aspects are:

1. The mound height reduction rate (dH_m/dt).
2. The footprint area change rate (dA/dt).
3. The footprint length/width ratio, which reflects the footprint shape.
4. The migration rate of the mound (dx/dt).

The above rates are estimated over the duration of the fully developed flow in each scenario.

In Figure 4.15 a linear relation is observed between dH_m/dt and flow energy. The pure oscillatory flow cases are the least energetic, as they are located at the bottom left corner of the graph. However, they are scattered which implies not a strict compliance to the relation. The combined flow cases are located at the top right corner. They are the most energetic, with little difference between the scenarios, which signifies little influence of the flow dominant contribution on the height reduction rate. Finally, the current only scenario can be found in between the two groups, and slightly lower than the imaginary line connecting the scenarios.

A closer look at the subgroups of Figure 4.15 reveals two separate relations, a parabolic between the wave only scenarios, and a linear with less scatter between the current only and combined flow scenarios.

Focusing on the mound footprint, area and shape changes are worth examining. Figure 4.16 shows dA/dt for all scenarios against flow energy. The footprint area increased in all cases. No uniform relation between the two can be observed. The same also holds for the other hydrodynamic aspects

that were used (U_{rms} and $\overline{U_{max}}$).

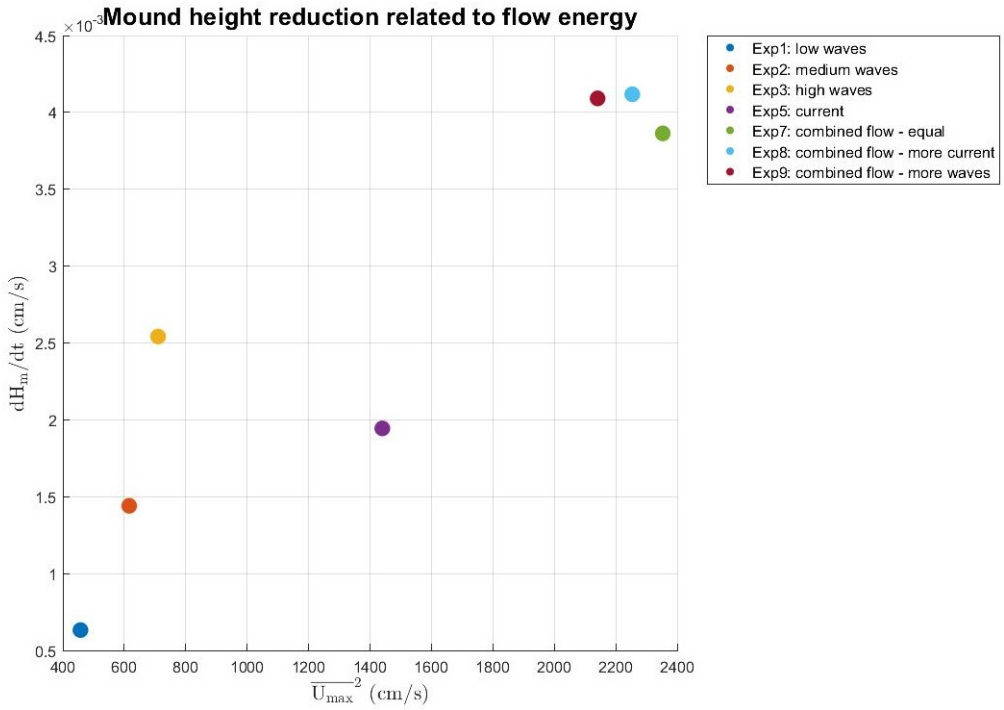

Figure 4.15: Mound height reduction rate (dH_m/dt) plotted against the second power of the average maximum free stream velocity ($\overline{U_{max}}^2$) for all scenarios.

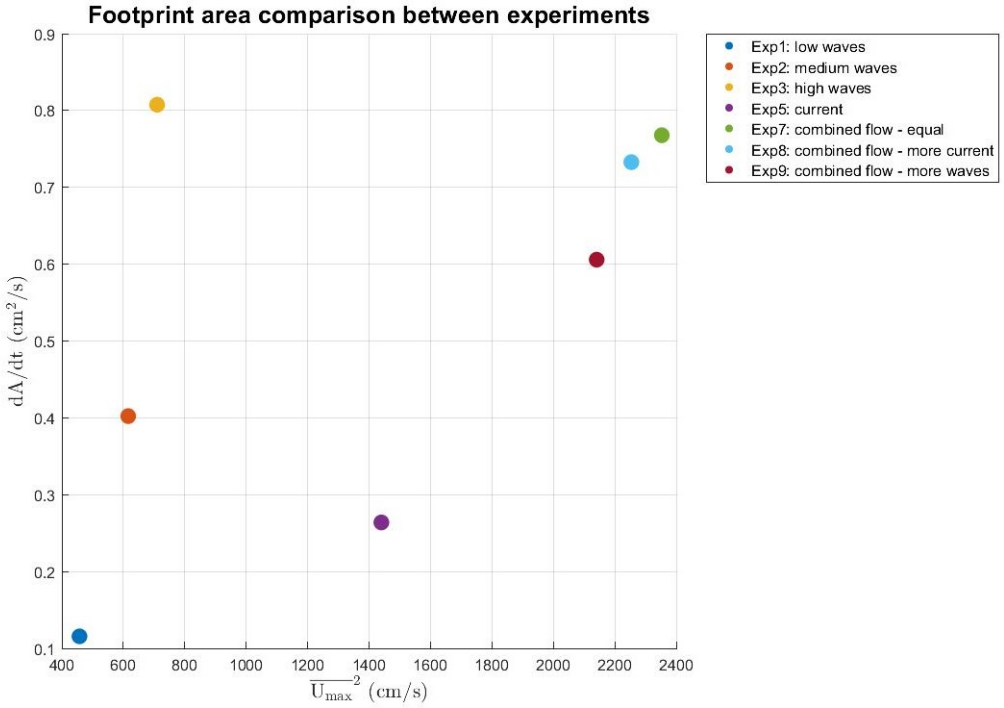

Figure 4.16: Rate of change of mound footprint area (dA/dt) plotted against the second power of the average maximum free stream velocity ($\overline{U_{max}}^2$) for all scenarios. The footprint detection is based on the laser scanner data. The measured footprint corresponds to an elevation of 0.01 m from the sand bed.

However, the two previously mentioned relations with reference to the subgroups can also be spotted here. The graph can be separated in two regions. The first is on the left side, where the wave only scenarios display a parabolic increase of the rate with increasing flow energy. The second comprises the central and right side of the graph, where the current only and combined flow scenarios appear to have a linear relation. In this diagram the combined flow cases are not clustered but in line, with cases 7 and 8 being close together, and scenario 9 further.

The footprint shape evolution is presented in Figure 4.17. Even though the constructed mounds were not in all cases circular (ratio = 1), the final shape seems to follow an inverse linear relation wit flow energy. In almost all scenarios the footprint tends to become more ellipsoidal, with the exception of scenario 5 where it becomes more circular, and scenario 7 where it remains exactly the same.

In all diagrams the order of the scenarios, in terms of flow energy, is the same. The combined flow cases are of particular interest as it appears that a greater wave contribution results in a weaker flow than a greater current contribution. The strongest flow results when the two contributions are equal.

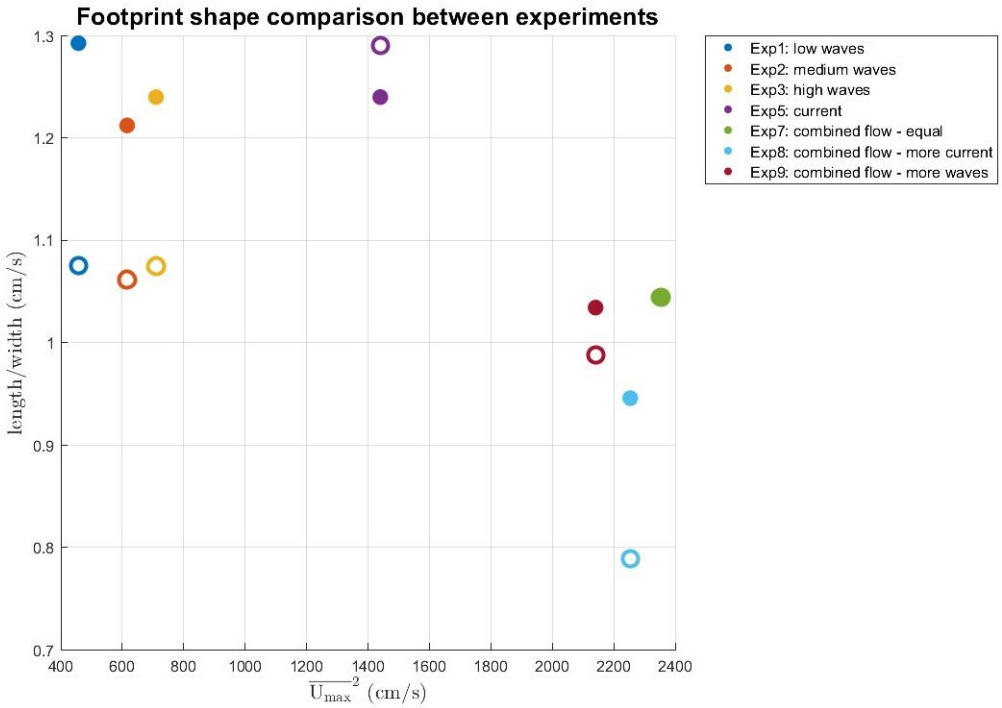

Figure 4.17: Length/width ratio of mound footprint shape plotted against the second power of the average maximum free stream velocity ($\overline{U_{max}}^2$) for all scenarios. The footprint detection is based on the laser scanner data. The measured footprint corresponds to an elevation of 0.01 m from the sand bed. The hollow markers represent the footprint ratio at the beginning of a scenario. The filled markers represent the footprint ratio at the end of a scenario. A ratio equal to 1 signifies a circular shape.

Finally, the migration of the mound is another important aspect of its morphological evolution that is investigated. Under oscillatory flow, the mound retains its shape and position as no migration of neither the peak nor the footprint occurs, as is shown in Figure 4.18. Under non-oscillatory flow the mound footprint migrates with a rate of 0.15 cm/s, while the peak migrates with cm/s. The largest migration rates of both the mound footprint, and the peak are measured under combined flow, where the first moves with a rate of about 1 cm/s, and the second with 2 cm/s, respectively.

When the wave - current contributions are equal the mound peak migrates the least (among the combined flow scenarios), while the footprint migrates the most. The opposite is noticed in the case of stronger current contribution.

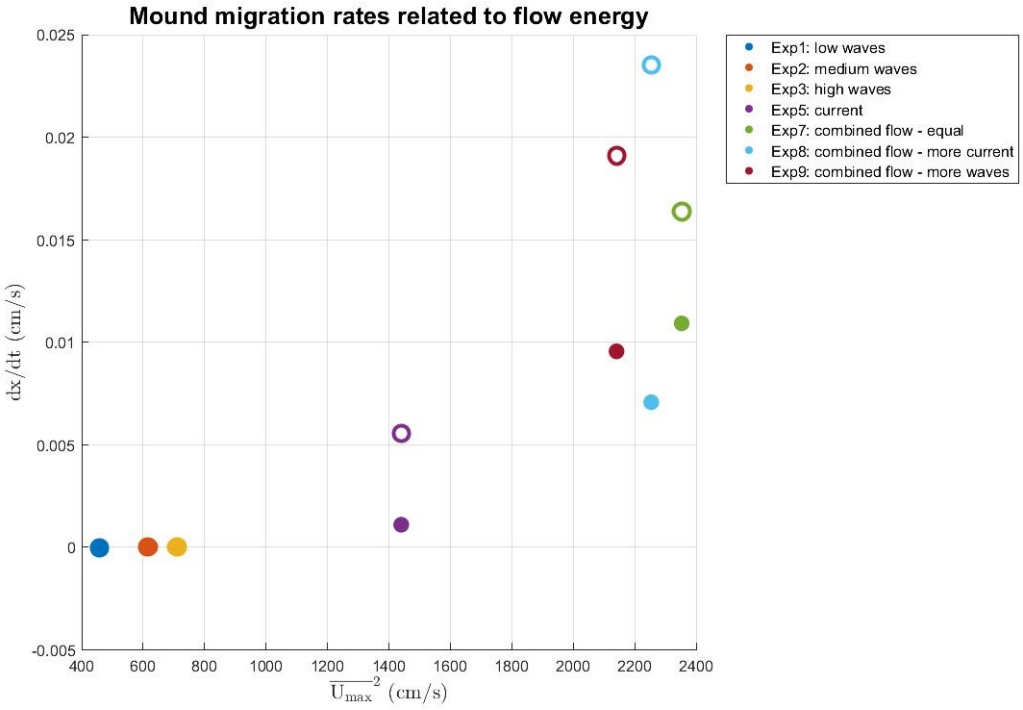

Figure 4.18: Mound migration rate (dx/dt) plotted against the second power of the average maximum free stream velocity ($\overline{U_{max}}^2$) for all scenarios. The hollow markers represent the mound peak, and the filled markers the mound footprint, respectively. The footprint and peak locations are based on the laser scanner data.

5

Discussion

The analysis of the theoretical processes taking place in the mound vicinity and their effect on the velocity field established the main lines and expectations for the sediment pathways, while a developed conceptual model set the basis for their construction. The observations and derived results provided insight on the mound evolution under various flow conditions, and the relation between hydrodynamic forcing and morphodynamic response. This chapter is devoted to the interpretation of the previously presented results to provide answers to the suggested hypotheses, and the critical reflection on the approach, strengths and limitations of this thesis.

Section 5.1 discusses the derivation of sediment pathways from the observed morphological evolution of the mound. The scenarios are divided into subgroups based on the imposed flow conditions, waves only, current only, and combined flow. For each subgroup the main findings are discussed and interpreted. The drawn conclusions are summarised in a bed map where the sediment pathways are depicted. Section 5.2 reflects on the connection between morphodynamic response and hydrodynamic forcing demonstrated in the results. Section 5.3 discusses the strengths and limitations of this study. Finally, section 5.4 reviews the findings of this thesis under a wider perspective.

5.1. Sediment pathways

As was mentioned in chapter 2, the available dataset doesn't cover the full spectrum of acting processes at the mound. However, evidence of the action of these processes lies in the observed morphodynamic response. Although it doesn't qualify as a hard fact, the effect of the mechanisms can be identified based on reasoning.

Valuable information about sediment movement and the mechanisms it owes to can be inferred from the spacial pattern, and geometry of morphological features (bedforms, mound shape). In the following sections the morphological evolution of the mound is analysed, leading to our interpretation of the sediment transport pathways per case group.

5.1.1. Oscillatory flow cases

Based on the direction of the estimated sediment transport rates the sediment that is eroded from the mound top is transported downstream the flume. However, the mound also shows diffusion in all directions, as the slope of its sides decreases, sand settles at the back and front toe, and the footprint expands. This leads us to believe that only part of the eroded sediment is transported

downstream while the rest redistributes in the mound area and feeds the bedforms. This is also supported by the relative angle, and magnitude changes of the sediment transport direction at the mound. The gradual turning and decreasing from the peak to the side of the mound signifies a growing lateral velocity component. Lastly, around the mound base the bedforms show changes in crest angle signifying a near-bed current towards the back toe, while sediment is also deposited at the arms extending downstream the mound. Based on the above response, our interpretation of sediment movement across the flume under oscillatory flow is presented in Figure 5.1.

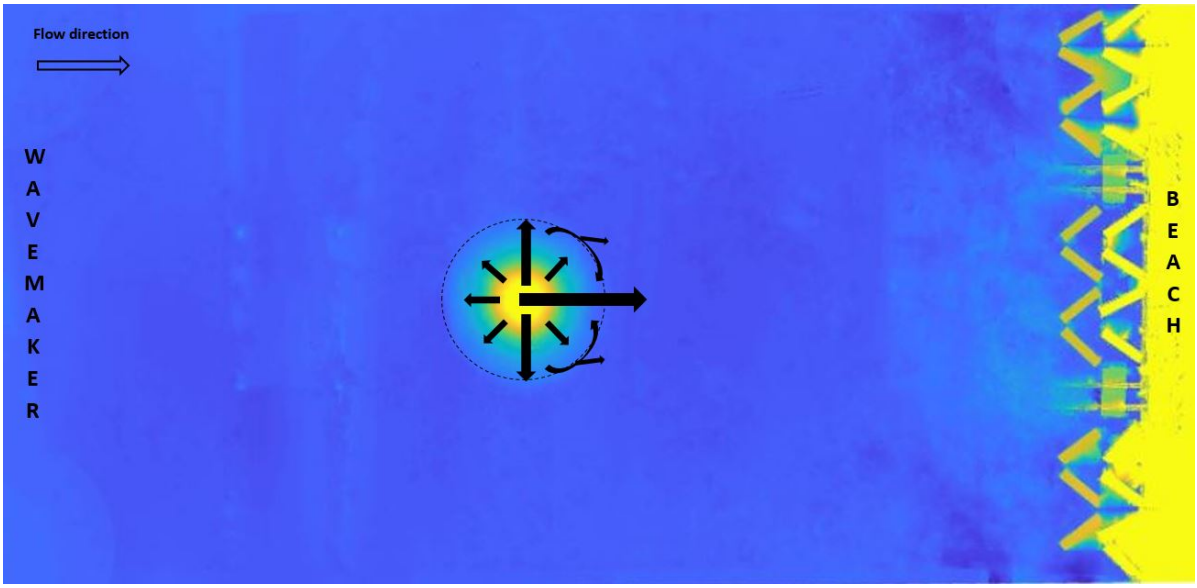

Figure 5.1: Generalised sediment pathways under oscillatory flow. The focus is on the mound area. The sediment movement is depicted with arrows reflecting the direction and (coarse relative) magnitude of sediment transport.

The aim of the sediment pathways is not only to recreate sediment movement, but to also understand the driving mechanisms behind it. Although the measured velocities are more or less constant in time (fluctuations within instrument error), the sediment transport rate gradually increases in time in some scenarios, especially over the side and back of the mound. It is believed that as ripples form, the sediment redistributes locally and becomes more loosely packed, hence its mobilisation by the flow becomes easier.

The accretion at the back toe is in contradiction to the highest velocity occurring at the back of the mound, which should erode owing to shoaling. Therefore additional mechanisms act at this location. One possible explanation is that the shoaling skewed waves mobilise sediment that rolls downslope due to slope effects. Another alternative is the formulation of a vertical flow separation zone owing to the incoming lateral flow from the sides, and free flow from above the mound. The deposition at the front toe is attributed to slope effects due to the loose packing of the sediment after the ripple formation. This claim is supported by the absence of this behaviour from the laser scanner data, signifying a small accretion height.

The appearance of the largest relative angle in velocity at the back of the mound may be the effect of refraction during de-shoaling, which would also explain the formation of the extending arms downstream the mound.However, the variation of flow velocity among the various positions in the flume is in many cases within instrument error margin, thus the effect of shoaling and refraction may be too small to be captured by the data.

5.1.2. Non-oscillatory flow case

Also in this flow type sediment is redistributed in the mound area, with the difference that the diffusion is not uniform. By the end of the experiment the mound has evolved into a pitched forward triangle while has slightly migrated downstream from the original position. The general angle in the measured velocities pertains, thus strengthening the claim that it relates to flume operation. No change in the relative angle is observed, signifying the absence of lateral transport component. The changes in ripple direction at the back of the mound indicate a turning of the flow as the streamlines re-align with the current, while the smoother pattern indicates either locally weaker flow or sediment deposition. Based on the above response, our interpretation of sediment movement across the flume under non-oscillatory flow is presented in Figure 5.2.

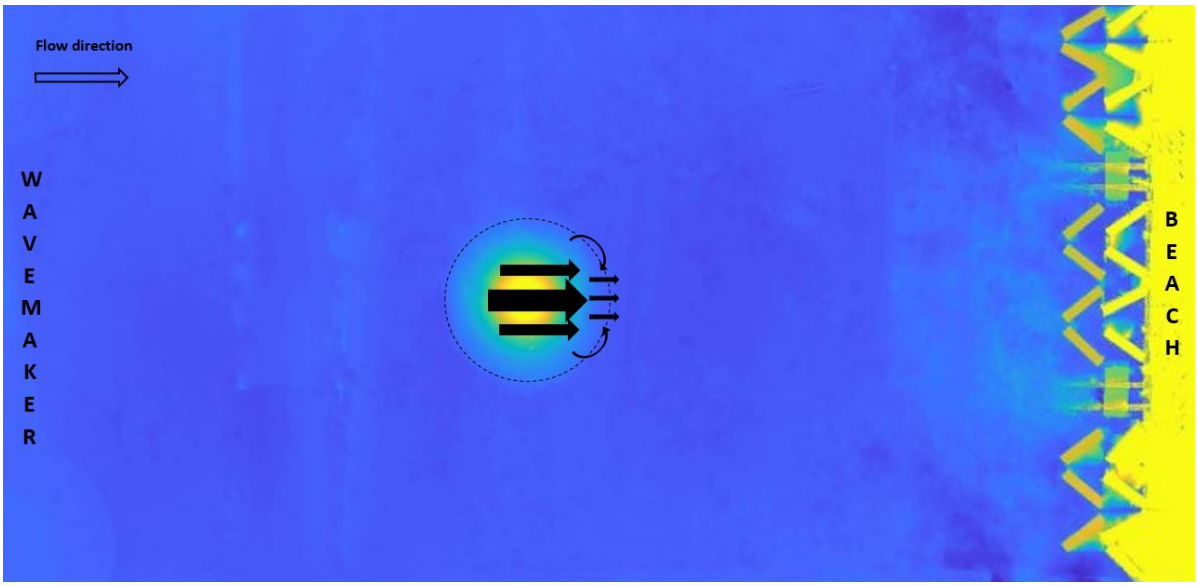

Figure 5.2: Generalised sediment pathways under non-oscillatory flow. The focus is on the mound area. The sediment movement is depicted with arrows reflecting the direction and (coarse relative) magnitude of sediment transport.

The loosely packed sand and smooth area at the back toe of the mound owes to recirculation flow forming between the peak and the reattachment point of the streamlines, sloping effects, or a combination of the two. In the first situation, the velocity decreases as soon as it passes the highest point resulting in entrained sediment deposition. In the second situation, sand at the edge of the mound lee side is mobilised just enough to become loose, and then rolls down the slope due to gravity.

No sediment deposition at the front toe of the mound is captured by the laser scanner data, although the compaction measurements showed some relaxation of the sand. This is most probably a consequence of ripple formation and migration at the area.

It is not certain whether the Vectrino measurements are affected by the boundary layer. Several levels above the bed were examined in order to reach the free stream velocity level. However, at distances greater than 2 cm the signals became very intermittent, as the designated levels were more and more out of the instrument range.

5.1.3. Combined flow cases

Under combined flow the mound response combines elements from the response under both waves, and current. It diffuses forming a pitched forward triangle, migrates downstream but retains a circular footprint. The situation regarding the measured velocities, and their relative angle evolution, as well as the ripple pattern at the back toe is the same as in non-oscillatory flow. However, the ripples on the mound indicate a faster migration rate at the top with reference to the sideslopes. Based on the above response, our interpretation of sediment movement across the flume under combined flow is presented in Figure 5.3.

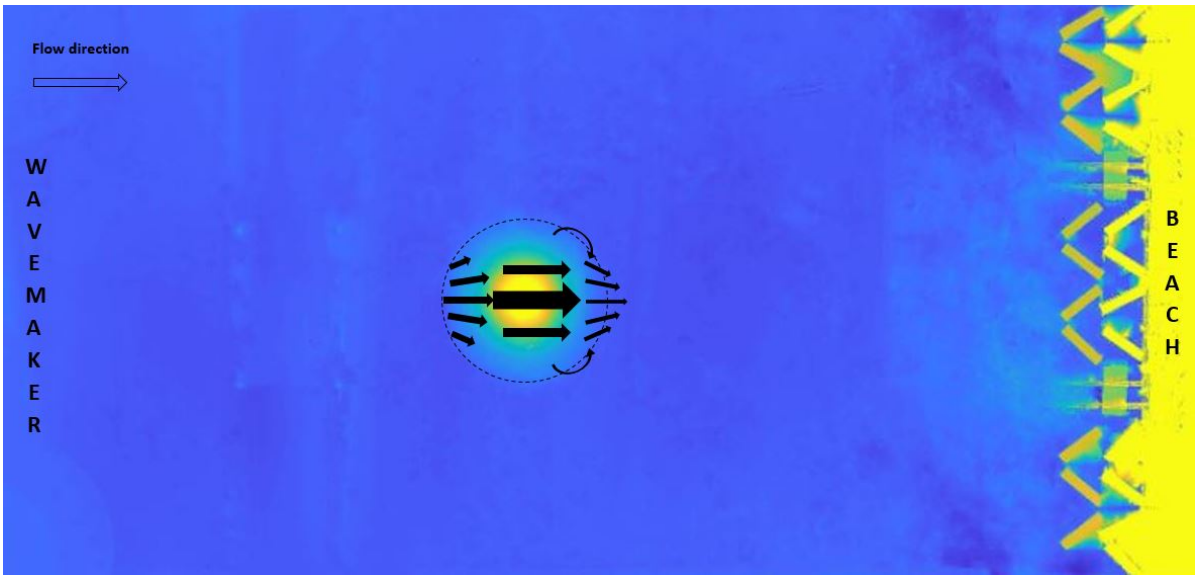

Figure 5.3: Generalised sediment pathways under combined flow. The focus is on the mound area. The sediment movement is depicted with arrows reflecting the direction and (coarse relative) magnitude of sediment transport.

Despite the wave presence, no lateral transport component appears to occur based on the sediment transport rate relative angles. Therefore, any redistribution of sediment on the sideslopes owes to ripple formation, and slope effects. However, the effect of the waves is apparent in the ripple direction.

Also here it is not certain whether the Vectrino measurements are affected by the boundary layer.

5.2. Link between morphodynamics and hydrodynamics

In this section the suggested hypotheses are tested based on the results presented in chapter 4.

Hypothesis 1: The observed sedimentation - erosion pattern can be explained using mean and orbital velocities.

In order to test this hypothesis sedimentation - erosion patterns were created, and compared to the observed ones as shown in the laser scanner data. The constructed patterns are based on gradients in the sediment transport rate, which in turn is estimated using mean, and orbital velocities. It should be kept in mind that the inferred patterns reflect crudely the transport gradient between two locations, by considering the effect of this gradient uniform in the in-between area.

In all scenarios the velocity based patterns capture the main erosion and deposition areas, but also display differences at the lower half of the mound sideslope, and the front upslope. At these areas the constructed patterns reveal opposite response than the laser scanner data. The greatest deviations between the patterns are noticed at the wave flow scenarios, where the velocity pattern lead to a very different response than the observed. They show some erosion and deposition at the locations of the laser scanner main erosion-deposition areas, however different location appear as main.

This general disagreement in all oscillatory flow scenarios is attributed to the estimation method of sediment transport rate. The model proposed by Hsu et al. (2006) depends on higher powers of the orbital velocity. When estimating the gradient of sediment transport rate, $U^2_{orbital}$ and $U^3_{orbital}$ are used for the calculation, which relate to acceleration and skewness of the wave. From the front toe to the mound top the shoaling waves experience greater changes in acceleration and skewness than when moving from the mound top to the middle of the downslope, which explains the difference in the erosion magnitude in the inferred sedimentation -erosion patterns. This does not hold for the combined flow scenarios, signifying that when both mean and orbital velocities are used, the model estimate of sediment transport is less sensitive to high powers of velocity.

Regarding the differences at the mound sideslope, on one hand they may find their cause at the used method for the pattern construction, since the estimation of the cross-flume gradients is based only on the cross-flume transport component. This choice was made to account for the difference in transport direction during mound spreading. On the other hand, it is possible that they owe to processes that do not affect flow velocity or are not captured by the free stream velocity measurements, such as slope effects, sediment transport via ripple spreading, flow separation over ripples, or boundary layer processes.

The differences between the observed and inferred sedimentation - erosion patterns show that basic hydrodynamics can not fully explain the mound response. Although the main lines are captured, there are more mechanisms that act and should be taken into account for a detailed response investigation and prediction.

Hypothesis 2: The morphodynamic response under all flow condition types scales with flow energy.

From the possible hydrodynamic aspects to be examined flow energy poses a physically meaningful and comparable measure between different flow types. As a measure of flow energy $\overline{U_{max}}^2$ was used. Maximum velocity has the following advantages:

- it is a pure value that is extracted straight from the signal
- it has gone through minimum processing (noise reduction and time averaging)
- it relates to storm impact

Most of the investigated aspects revealed a relation with flow energy. In particular, as $\overline{U_{max}}^2$ increases the mound erodes more, migrates further (if migration occurs), and obtains a less elongated footprint. The linear relations of mound height reduction, and migration rate show that the mound respond intensifies with stronger flow as velocity affects sediment at greater depths. The inverse linear relation of footprint shape evolution indicates that as flow energy increases the width of the footprint grows more than the length.

The aspect that does not scale uniformly with flow energy is footprint area change. There flow type seems to be of importance as two different relations with flow energy are observed. On one hand, under oscillatory flow the mound footprint expands parabolically with increasing wave height. On

the other hand, the mound footprint area grows linearly with flow velocity under non-oscillatory, and (all types of) combined flow.

Overall, the morphodynamic response does scale with flow energy, with some dependence on flow type for certain morphodynamic aspects.

5.3. Strengths and limitations

As every research project, this study has its strengths and limitations.

The strongest point of this research is the combination of many different flow types which allowed the monitoring of the mound response in flows that are also encountered in the field. In addition, the large number of instruments used provided a diverse reference dataset, a large part of which is used in this study.

However, the lack of repetition of the scenarios makes the results susceptible to flume operation, and instrument errors. The small number of experiments gives some uncertainty to the derived relations, which need to be verified in the future over a larger sample. Finally, the effect on the mound of the processes that are not captured by the data introduces additional uncertainty and unexplored angles.

5.4. Value of study

This thesis constitutes the first step towards the investigation and analysis of a wide and multiply angled topic. It provides insight on the evolution of submerged sand mounds under various flow conditions, and attempts to identify the driving processes behind this response. The finding relate the observed morphodynamic response to storm impact, which in the light of climate change is crucial for the better design of nourishments and other protection measures against coastal erosion.

6

Conclusions & Recommendations

The objective of this study was to investigate the effect of different hydrodynamic conditions on the morphology of a submerged sand mound, and link the observed response to hydrodynamic aspects. This was fulfilled by means of a literature study, a large-scale physical experiment, the development of a conceptual model, and extensive data analysis of the obtained measurements. In this chapter the main conclusions of the study and recommendations for further research are discussed.

Section 6.1 provides the answers to the research questions defined in chapter 1. The sub-questions are answered first, followed by the main research question that concludes this thesis.

Section 6.2 provides recommendations for future research. They are directed both on improvements of the method used in this research, and suggestions for expansion of this research and MODEX.

6.1. Conclusions

Which hydrodynamic processes in the mound vicinity are captured by the measurements?

The processes acting under wave and current conditions are well known and extensively documented in literature, thus providing a solid basis for their investigation. However, the types of measurements, and the number and type of available instruments during MODEX resulted in a incomplete coverage of the full spectrum of acting mechanisms in the dataset. Slope effects, ripple influence on velocity, and flow separation were not captured by the measurements, hence they are not explicitly analysed in this thesis.

How do waves, current and combined flow affect the mound geometry and position?

The results showed that the mound peak erodes constantly with a decreasing rate in time, in all scenarios. The largest height reduction (about 8 cm) is observed under combined flow, and high waves. Under non-oscillatory flow, the mound initially behaves similarly as above, although due to ripple grow and migration some accretion occurs, resulting in a total height reduction of 7 cm. As wave height and period decrease the mound erodes with an ever decreasing rate, reaching a total height reduction of 7 and 5.5 cm, for medium and low waves respectively.

The footprint area increases in all scenarios with the largest expansion rate (0.8 cm^2/s) occurring under combined flow, and high waves, and the smallest being observed under low waves (0.11 cm^2/s). The shape of the footprint also alters in all scenarios. It becomes more ellipsoidal in almost

all cases, with the exceptions of pure non-oscillatory flow, and combined flow with equal contributions, where the mound became more circular, and remained unchanged, respectively.

The imposed flow types have different effect on the mound position. No migration is measured under pure oscillatory flow. The mound migrates downstream with a rate of 0.15 cm/s under pure current. The largest migration is observed under combined flow, where the migration rate is about 1 cm/s. Besides the footprint, the mound peak also migrates downstream under non-oscillatory, and combined flow. The peak migration rate is in all cases larger than the footprint migration rate, while it follows the same pattern with regards to the scenarios.

Lastly, the mound shape changes are accompanied by the superposition of bedforms. Depending on the type of flow the formed ripples differ in shape (two- or three- dimensional pattern, symmetric or asymmetric) and size. Nevertheless they persist throughout the duration of all the scenarios, grow and migrate.

How can the morphodynamic response be related to hydrodynamics?

Several hydrodynamic parameters were examined to establish a connection between morphological aspects of the mound and the imposed flow conditions, from which a uniform relation of dH_m/dt, footprint length/width ratio, and dx/dt with $\overline{Umax}^2$ was found. This parameter relates to flow energy, thus posing a comparable between scenarios and physically meaningful measure.

The results show a linear relation of dH_m/dt with increasing flow energy. The scatter of the wave scenarios displays a broad compliance of oscillatory flows with the linear relation. The combined flow scenarios were clustered together, signifying little influence of the flow dominant contribution.

The mound footprint shape change, expressed as the length/width ratio, scales with flow energy following an inverse linear relation. As $\overline{Umax}^2$ increases, the footprint tends to become more circular (length/width ratio closer to 1). No uniform relation for all scenarios could be established for dA/dt.

The migration rate of both the footprint, and the peak of the mound relate linearly to flow energy, with the peak migration rate displaying a steeper inclination. The wave scenarios are excluded from the relation, as the mound remained at its original position under oscillatory flow.

Finally the main research question is answered:
How does the mound evolve under waves, current, and combined flow conditions?

The evolution of the mound is dictated by the acting processes. This study investigated the effect of those processes on the mound morphology via an available dataset, which however did not cover their full spectrum. It was found that the flow type affects the height, footprint shape and area, bedform pattern, and position of the mound. Moreover, the measurements revealed a relation of several morphological aspects with the imposed hydrodynamic forcing.

However, the observed response is not fully explained using mean and orbital free stream velocities. The inferred sedimentation-erosion patterns do capture the main erosion and deposition areas, but show deviations from the measurements around the mound base. This indicates that more processes affect sediment movement at the mound base that were not examined.

Nevertheless, significant insight on the evolution of submerged mounds has been gained through this thesis. It is first step in the direction of the prediction of morphological change, and more efficient design of nourishments.

6.2. Recommendations

MODEX is an experiment with many angles, and this thesis is only a first step towards the investigation of a complex situation with numerous aspects. As a result not all could be covered in the scope of this study.

Regarding the used method, the following improvements are suggested for future studies:

Firstly, the used velocities were considered to be outside the boundary layer and no investigation of the velocities, and sediment movement within the boundary layer was performed. However, an estimation of the boundary layer thickness and a better understanding of the underlying situation would verify with certainty our assumptions and could bridge the gap between observed and recreated sedimentation-erosion pattern around the mound base.

In addition, although the induced waves are in the intermediate water regime, they are considered as shallow water waves in this study. It is suggested that the depth dependency of the velocity is accounted for in future studies, as it will lead to more accurate representation of the situation ans potential changes in the results (e.g. relation with hydrodynamics). Moreover, more hydrodynamic aspects need to be investigated to thoroughly examine the link between the morphodynamic response of the mound and the imposed hydrodynamic forcing.

Lastly, the suggested sediment pathways are recommended to be verified via measurements or another form of solid proof, since this was not possible in this study.

Regarding MODEX and future experimental work, the following are recommended:

For a more detailed investigation of sediment transport pathways the use of coloured sand is highly recommended. In addition, instruments with higher resolution should be used to capture turbulent velocities in detail, as well as a denser instrument layout to enable flow separation measurements both in the horizontal and vertical plane, and detailed near bed velocity measurements.

MODEX investigated a number of different flow conditions. However, due to the limited available time period each scenario was conducted only once. It is suggested to repeat the experiment in the future with each scenario being repeated a few times. That way the sample size will increase thus making the results statistically significant.

Bibliography

Bagnold, R. (1946). Motion of waves in shallow water: Interaction between waves and sand bottom. *Proceedings of Royal Society London A*, 187:1 – 15.

Berkhoff, J., Booy, N., and Radder, R. (1982). Verification of numerical wave propagation models for simple harmonic linear water waves. *Coastal Engineering*, 6:255–279.

Bosboom, J. and Stive, M. (2015). *Coastal Dynamics I*. Delft Academic Press.

Clifton, H. (1976). Wave-formed sedimentary structures: A conceptual model, in beach and nearshore sedimentation. *SEPM Special Publications*, 24:126–148.

Drake, D. and Cacchione, D. (1992). Shear stress and bed roughness estimates for combined wave and current flows over a rippled bed. *Journal of Geophysical Research*, 97:2319 – 2326.

Flanders Marine Institute (VLIZ) (2008). Shore nourishment. Retrieved from: http://www.vliz.be/wiki/Shore_nourishment.

Garcia-Hermoza, M. (2008). *Morphodynamics of sand mounds in shallow flows (Doctoral Dissertation)*. PhD thesis, University of Oxford. Retrieved from Research Gate (Publication No. 266614864).

Garnier, R., Calvete, D., Falques, A., and Dodd, N. (2008). Modelling the formation and the long-term behavior of rip channel systems form the deformation of a longshore bar. *Journal of Geophysical Research*, 113(C7).

Grant, W. and Madsen, O. (1982). Movable bed roughness in unsteady oscillatory flow. *Journal of Geophysical Research*, 87:469 – 481.

Holthuijsen, L. (2007). *Waves in Oceanic and Coastal Waters*. Cambridge University Press.

Hsu, T., Elgar, S., and Guza, R. (2006). Wave-induced sediment transport and onshore sandbar migration. *Coastal Engineering*, 53:817 – 824.

Kovacs, A. and Parker, G. (1994). A new vectorial bedload formulation and its application to the time evolution of straight river channels. *J. Fluid Mech.*, 267:153–183. Cambridge UK.

Lloyd, P. and Stansby, P. (1997). Shallow-water flow around model conical islands of small side slope. ii: Submerged. *Journal of Hydraulic Engineering*, 123(12):1068–1077.

MODEX (2018). Data storage report. Technical report, TU Delft.

Moulton, M., Elgar, S., and Raubenheimer, B. (2014). A surfzone morphological diffusivity estimated from the evolution of excavated holes. *Geophysical Research Letters*.

Munson, B., Young, D. F., Okiishi, T., and Huebsch, W. (2009). *Fundamentals of Fluid Mechanics*. Jon Wiley &Sons, Inc., sixth edition.

Schiereck, G. J. (2012). *Introduction to Bed bank and shore protection*. VSSD, second edition.

Smith, E., D'Alessandro, F., Tomasicchio, G., and Gailani, J. (2017). Nearshore placement of a sand dredged mound. *Coastal Enginereing Journal*, 126:1–10.

van Duin, M., Wiersma, N., Walstra, D., van Rijn, L., and Stive, M. (2004). Nenourishing the shoreface: observations and hindcasting of egmond case, the netherlands. *Coastal Enginereing Journal*, 51:813–837.

van Rijn, L. (2007). Unified view of sediment transport by currents and waves. i: initiation of motion, bed roughness and bed-load transport. *Journal of Hydraulic Engineering*, 133:649 – 667.

Wengrove, M. (2018). *Bedform geometry and bedload sediment flux in coastal wave, current and combined wave-current flows*. PhD thesis, University of New Hampshire.

Wilberg, P. and Harris, C. (1994). Ripple geometry in wave-dominated environments. *Journal of Geophysical Research*, 99:775 – 789.

A

Data processing methods

This appendix is devoted to the data processing performed on three types of instruments, ADVs, Vectrinos and URSs. In section A.1 the main assumptions and the method followed for processing of the velocity data are presented. Section A.2 describes the processing method applied to the URS data. Finally, Section A.3 elaborates on the implementation of the Hsu et al. (2006) model for the estimation of the sediment transport rate.

A.1. Velocity data

The purpose of the velocity data processing was to obtain the free stream velocity for each experiment. This is defined as the flow velocity occurring just outside the bottom boundary layer and is associated with sediment transport as it mobilises and carries the sediment further down the flume.

Assumptions verification

The presented approach is based on the following assumptions:

- Assumption 1: The waves are in the shallow water regime, therefore the horizontal velocity is constant over depth.
- Assumption 2: The bed is rough, meaning that the bedforms (ripples) protrude from the bottom boundary layer.

Regarding assumption 1, it was found that the waves aren't actually in the shallow water regime, but rather in the intermediate water regime with the highest waves at the transition point of the regimes. Table A.1 shows the computed values of the relative depth (h/L) for the conducted experiments, and the wave type as follows from linear wave theory and the shallow and deep water criteria. The presented values refer to two locations in the flume, the mound peak and full depth, and the beginning of each experiment. Since the bed is expected to erode (in the mound area) or remain about the same (plain bed) the water regime at any location remains between the presented values throughout the experiment.

Although the obtained measurements don't cover a full profile of the water column, preliminary model results suggest that the velocity difference (Δu) between mean water level and bed level is Δu = 3cm/s over the mound peak. In addition, for the profiles over flat bed, they show changes in velocity until midwater, lower from which Δu is negligible. Given that the recorded velocities are

in the order of 20cm/s, the assumption of shallow water waves is maintained in the analysis of the velocity signals, as its effect on the results is considered to be small.

Experiment number	**h/L (h = 0.4m)**	**Water regime**	**h/L (h = 0.2 m)**	**Water regime**
1	0.2733	Intermediate	0.165	Intermediate
2	0.2066	Intermediate	0.1313	Intermediate
3	0.1846	Intermediate	0.1194	Intermediate
6	0.4053	Intermediate	0.2252	Intermediate
7	0.2066	Intermediate	0.1313	Intermediate
8	0.2733	Intermediate	0.165	Intermediate
9	0.1846	Intermediate	0.1194	Intermediate

Table A.1: Estimated wave water regime during MODEX. The regime is computed at two locations for each experiment, at the mound top (h=0.2m) and at over plain bed (h=0.4m). The deep water and shallow water regime criteria are h/L>0.5, and h/L<0.05, respectively. Hence anything in between belongs to the intermediate water regime, as is the case with MODEX.

Assumption 2 was verified by looking into the velocity profiles recorded by the Vectrinos, where the thickness of the boundary layer is easily discerned. The situation of Experiment 1 is presented in Figure A.1 where the boundary layer is 3mm thick at the beginning of the experiment (when the mound is at its highest point), whereas the ripple height is 3 cm after a few seconds and generally ripples only get bigger as time advances until they reach equilibrium. Since the assumption is met in the weakest flow case, it is considered that it also holds for the stronger flow cases.

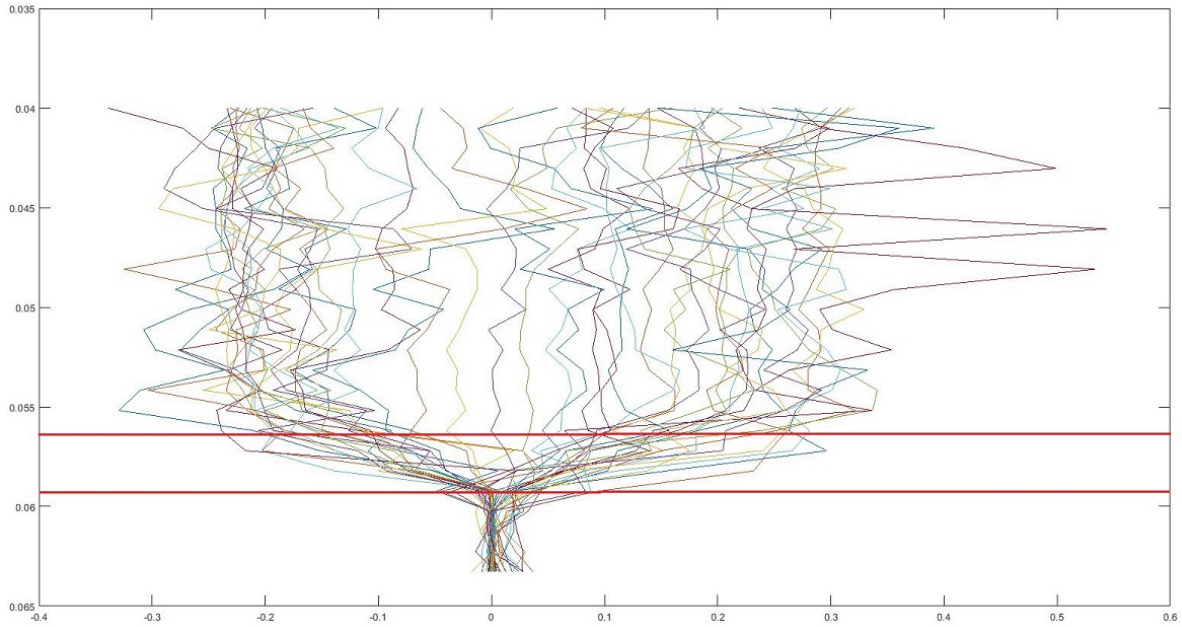

Figure A.1: Boundary layer thickness at the top of the mound during Experiment 1, as captured by the Vectrino profiler. The red lines indicate the boundary layer edges, with the lower line representing the bed level and the upper line showing roughly the threshold of free stream velocity.

Signal processing method

The presented method aims to clean the data. The main steps of the method are:

1. Selecting the part of the record with fully developed flow.
2. Applying a filter to remove noise from the data (only for ADVs).
3. Detecting the bed and locating the signal 1.5cm above the bed (only for Vectrinos).
4. Separating the mean and oscillatory component of the velocity signal.
5. Averaging orbital velocities over a few waves to enable trend detection in signal evolution.
6. Calculating the total free stream velocity U_{total}.
7. Calculating the angle of U_{total} with the along-flume direction (x axis).

Most of the above steps are common for both ADVs and Vectrinos. Vectrinos need more processing because they measure over a profile in the water column, and in order to have comparable results with the ADVs (point measurements) the two signals need to have similar characteristics. The ADVs are all at the same level with reference to the flume bed (10 cm below the still water surface). They are considered to be unaffected by the boundary layer, and thus measure directly the free stream velocity. Vectrinos are much closer to the bed, since the intention was to also measure the velocities in the boundary layer, and the individual instruments are at different levels with reference to the flume bed. Hence, before processing the Vectrino signals, velocities at a constant level above the bed should be considered, and the level should be such that the signal isn't affected by the boundary layer.

1. During the experiments, the ADVs and the Vectrinos were set to measure longer that the flow duration, staring before and finishing after a run. In the processing, those initial and final parts of the records where there is no or developing flow, are disregarded.

2. Data is always a mixture of real measurements and noise. When multiple instruments are employed the noise levels encountered in the signals vary, between devices. To eliminate the noise from the data, multiple commonly applied filters were investigated, such as a moving average filter, AVT statistical filtering, and linear and quadratic regression. However, none of the above satisfied the desired level on noise reduction. Finally, upper and lower threshold values for velocity, tailored to each signal separately, were posed on based on the observed envelope limits. An example of the effectivity of this method is presented in Figure A.2 below.

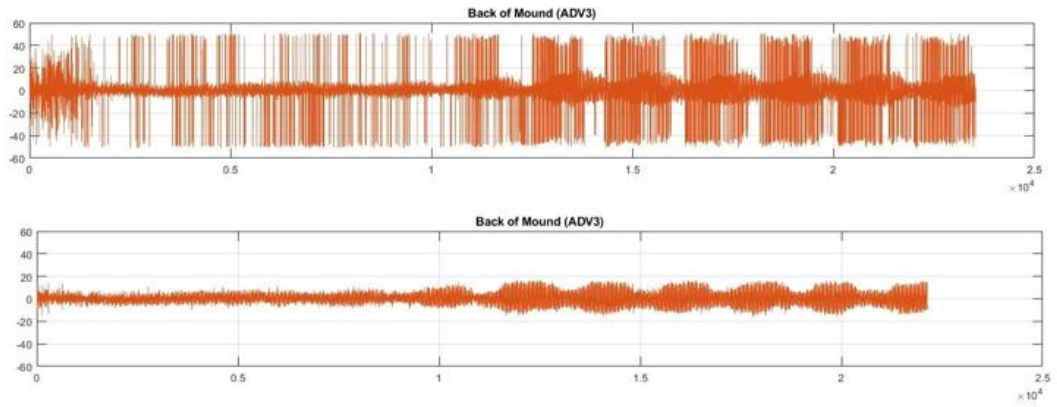

Figure A.2: ADV velocity signal before (top) and after (bottom) the noise filter application.

In the case of Vectrinos, the general processing method (U_{rms} velocity) worked as form of filter averaging out outliers. Therefore, no additional filtering was considered necessary.

3. A bed finding routine that was developed during this thesis locates the bed based on the records of the master Vectrinos, accounting for differences in bed level and instrument height. Since the level where velocities are considered is constant, a simple subtraction gives the bins over the recorded profiles that correspond to the desired level. The choice of the distance from the bed where the velocities should be regarded is derived by literature.

4. As was observed during the experiments, the imposed waves were not entirely symmetric. This became first apparent from the wave rod measurements where the recorded waves appeared skewed with reference to still water level, which was confirmed by the velocity data. As a result, mild mean flows (currents) emerge in wave only flow conditions, especially on top of them mound where the waves are the most skewed. Despite their small magnitude, these flows may have a significant effect on the sediment transport. Therefore, to identify the effect of the orbital component alone, a separation between orbital and mean component is vital.

5. For the analysis of the orbital velocities the most important values are those under the crest and trough of the waves (the envelope). To obtain representative values of the orbital velocity signal maxima and minima, which aren't sensitive to instrument noise, the root mean square of the velocities is used.

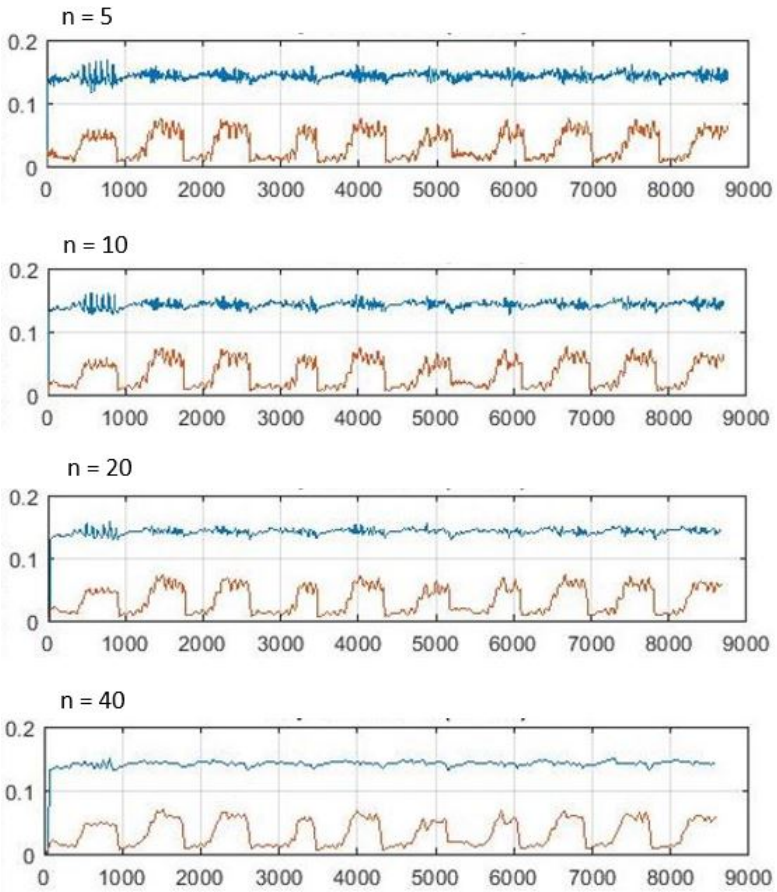

Figure A.3: Effect of number of waves (n) in signal averaging.The signal presented here is part of the orbital velocity component measured by ADV6 during experiment 1.

In order to observe the evolution of velocities throughout an experiment, cumulative graphs with the records from all runs consecutively are plotted. However, a signal with 25 - 50 points per second (points per second for ADVs and Vectrinos, respectively) includes much variation on a fine scale that

is not needed. To simplify things, an averaging cycle over a number of waves (n) is adopted to filter out the finer scale variations and focus on the main trends. To determine the optimum number of waves for the averaging, several options were examined. In Figure A.3 the result is shown for 5,10, 20, and 40 waves. As one can see, the larger n is, the less detailed the signal becomes. Finally, the value of n=20 was chosen to avoid oversmoothing the signal.

6. The records exported from the instruments are separated in along-flume (u), cross-flume (v) and vertical (w) velocity components. All ADV and Vectrino probes are aligned with the flow so that u is in the x-, v is in the y-, and w is in the z-direction (Figure 2.1). However, the flow force as it's "felt" by the grains doesn't distinguish between directions. Thus, the x and y component of the records are combined to compute the total flow velocity (U_{total}), to be able to assess realistically the observed response.

7. Besides the magnitude, the direction of U_{total} is also of importance. This is computed from the individual velocity components and is in reference to the x (along-flume) direction.

8. Finally, the desired result is a single value of velocity magnitude and direction per run. The evolution of U_{total}, magnitude and direction, throughout an experiment is depicted in a quiver plot to enable comparison between different cases.

A.2. Bed level data

The bed level data were extracted from the URSs. The main steps of the processing method are:

1. Calibrating the instruments.
2. Correcting the measurements according to the calibration factor.
3. Applying filters to remove noise from the data.
4. Plotting the data to enable trend detection.

1. Before each experiment, a URS calibration was performed which consisted of a 2 minute period where the instruments collected measurements in still water (no-flow condition). The calibration factors are obtained by comparing the measured bed distance with the actual distance of each instrument from the bed. They differ per device and are considered to be constant throughout the experiment.

2. A calibration factor is basically an offset of the measured bed distance. Thus, they are incorporated in the records, early in the processing phase, by simply adding or subtracting the calibration factor to the corresponding record.

3. It was observed that the URS data are clean during no-flow condition, but rather noisy during running flow (Figure A.4). To remove that noise, an envelope-based filter (similar to that used for the velocity data) was applied. However, the part of the signal corresponding to the actual bed level appears to be only the maxima of this filtered signal, hence a different filter is applied maintaining only the maxima of the record. The final result is shown in Figure A.5.

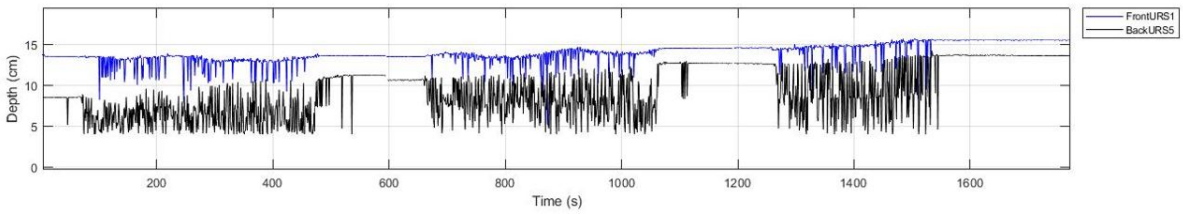

Figure A.4: URS full signal during the first three runs of experiment 3.

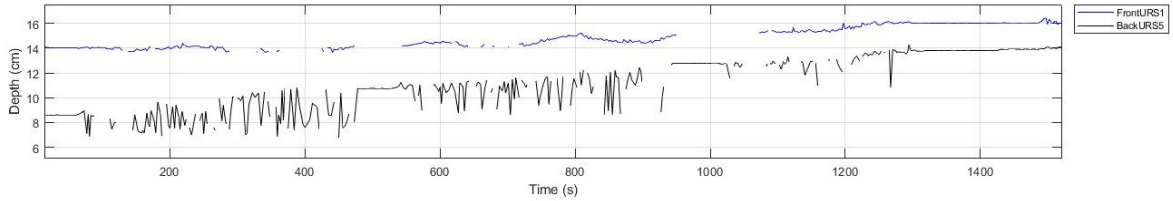

Figure A.5: URS signal of figure A.4 after the maxima filter application.

4. In order to observe the bed level change evolution throughout an experiment, detect trends, and compare the situation in different parts of the mound, cumulative plots are created. Example of such plots is Figure 4.8. They follow the instrument configuration logic and attempt to monitor ripple behaviour, thus are organised as follows:

- in the top panel appears a cluster of five URSs which are deployed just upstream the mound peak, with URS5 being almost on top of it
- in the middle panel appears a second cluster of five URSs which are deployed downstream of the mound peak, over the downslope
- in the bottom panel appear the final two URSs which are deployed downstream of the mound, above the plain bed.

A.3. Sediment transport rate

Following the separation of the oscillatory from the mean velocity component of the records, the implementation of the model of Hsu et al. (2006) is based on equations 3.1 and 3.2, and the values of the various coefficients as presented in Table A.2 below.

Parameter	Value	Unit
ϵ_b	0.135	-
ϵ_s	0.015	-
ϕ	0.63	rad
W_0	0.025	cm/s
s	2.65	-
g	9.81	m/s^2
C_w	0.0018	-
C_c	0.0021	-

Table A.2: Assigned parameter values for the implementation of the sediment transport model. The highlighted parameters receive values adjusted to bedload transport during bedform migration according to Wengrove (2018).

The velocities input in the model are the $U_{rms,orb}$ and $U_{rms,total}$, computed as described in section A.1. The model result is a bedload sediment transport rate averaged over every 20 waves throughout the experiment duration. From this a single representative value needs to be chosen, which is done in the same manner as for the velocities.

B

Results

B.1. Wave cases

B.1.1. Low waves

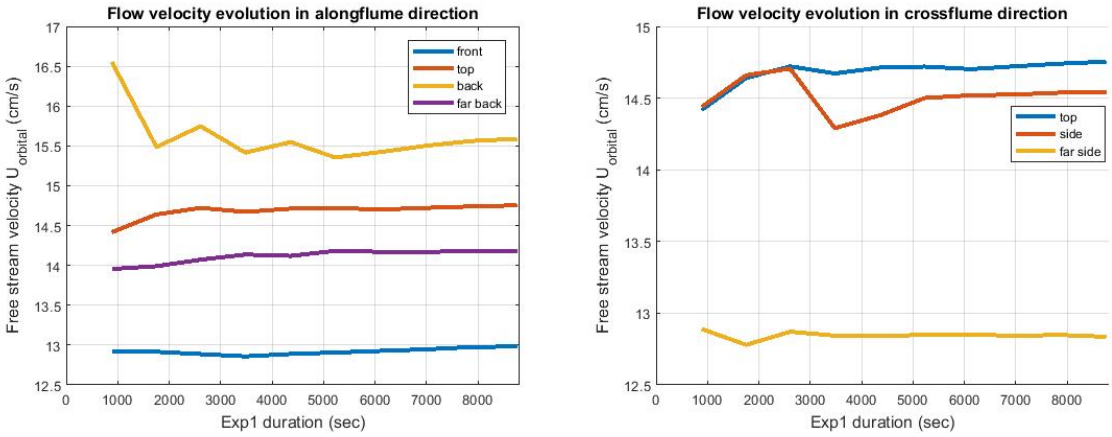

Figure B.1: ADV records of orbital velocity in the along-flume (left) and cross-flume (right) direction during scenario 1 (low waves).

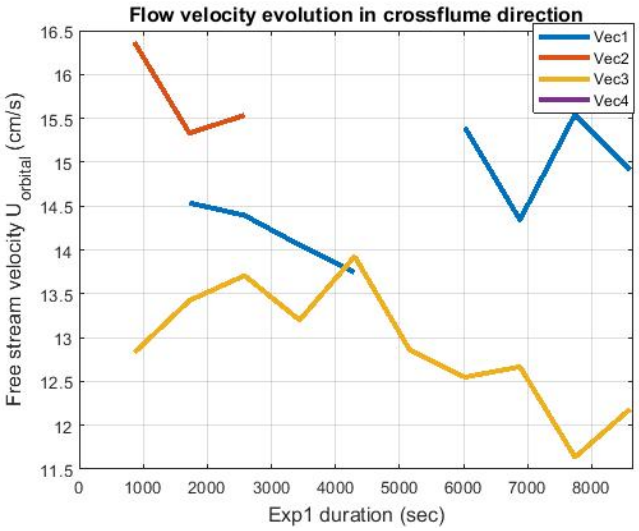

Figure B.2: Vectrino records of orbital velocity in the cross-flume direction during scenario 1 (low waves). The measurements are taken 1.5 cm above the bed.

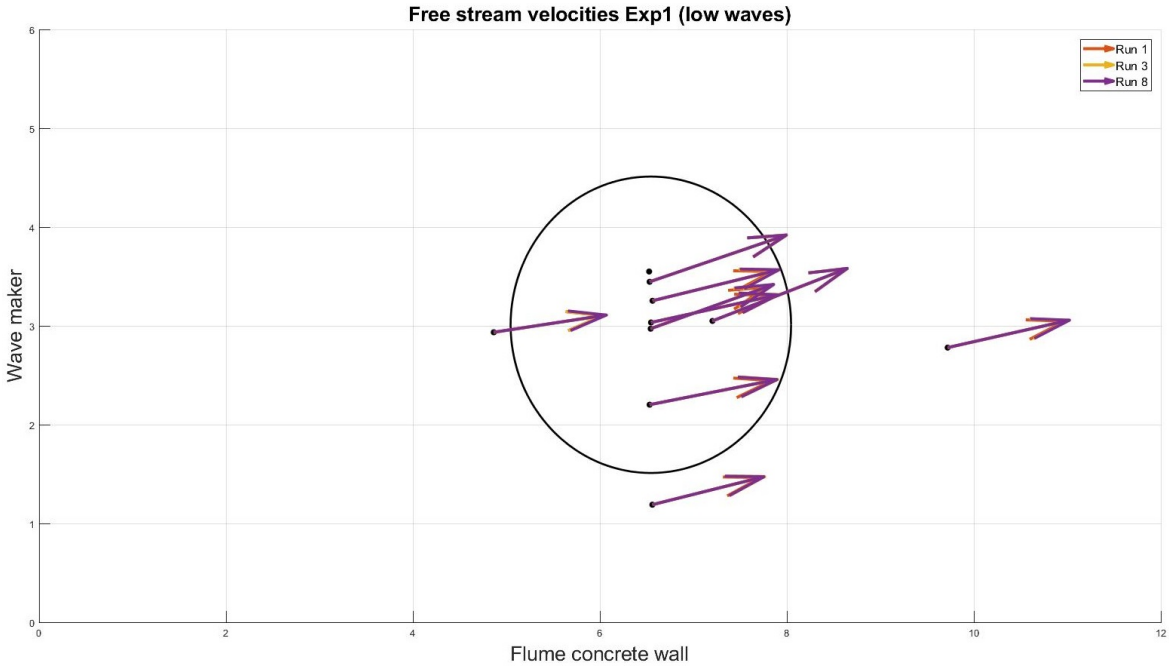

Figure B.3: Flow velocity evolution at the instrument locations across the flume, during scenario 1. The direction and size of the arrows correspond to the measured values.

B.1.2. Medium waves

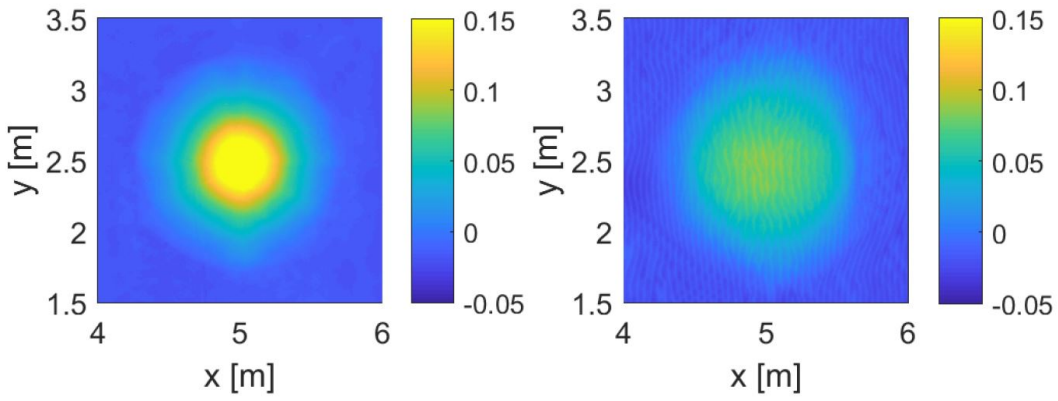

Figure B.4: Mound morphology before (left) and after (right) scenario 2 (medium waves), as captured by the laser scanner. x- and y-axes are in the along-flume and cross-flume direction, respectively. The flow direction is from left to right. The colorbar represents elevation (in m) with regard to flat bed level.

Figure B.5: Top: Mound morphology after the end of scenario 2. The flow direction is from right to left. Bottom: Ripple checkered pattern after scenario 2.

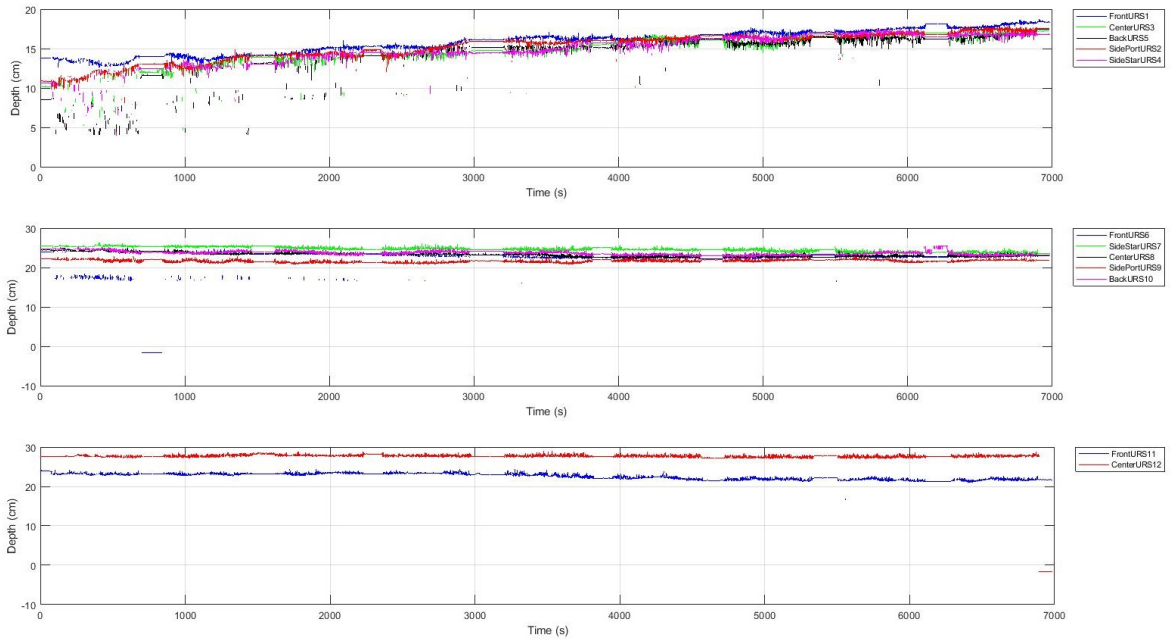

Figure B.6: Cumulative plot of bed level change evolution during scenario 2 (medium waves). The top panel depicts the measurements of the URS cluster located on the side of the peak (URSs 1-5). The middle panel depicts the measurements of the URS cluster just downdrift the mound over the downslope (URSs 6-10). The bottom panel depicts the measurements of the URSs on the back of the mound (URSs 11-12). The horizontal axis is the duration (in seconds) of the measuring period for the depicted scenario, and the vertical axis is the distance (in cm) of the bed from the probe.

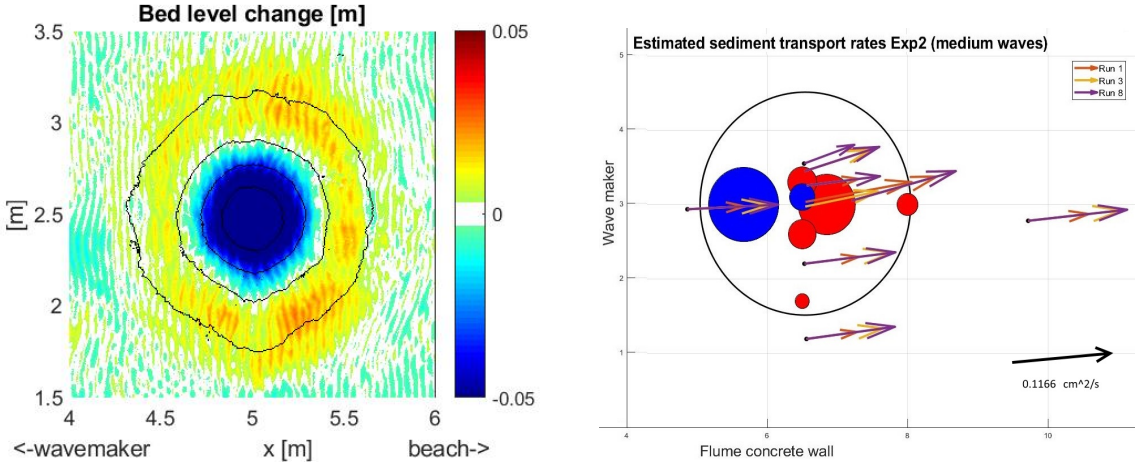

Figure B.7: Left panel: Sedimentation - erosion pattern at the mound at the end of scenario 2 (medium waves) as captured by the laser scanner. The colorbar indicates the height (in m) of accretion (positive values) and erosion (negative values). Right panel: Estimated sediment transport rates at the instrument locations across the flume, and resulting sedimentation - erosion pattern at the mound during scenario 2 (medium waves). The direction and size of the arrows correspond to the model estimated values. At the bottom right corner is a scale for magnitude reference, and is equal in size to the most right purple arrow. The blue circles indicate erosion, while the red circles show accretion. All circles are estimated based on sediment transport gradients and are scaled according to gradient magnitude. In both panels, the flow is from left to right, and x and y axes are in the along-flume and cross-flume direction, respectively.

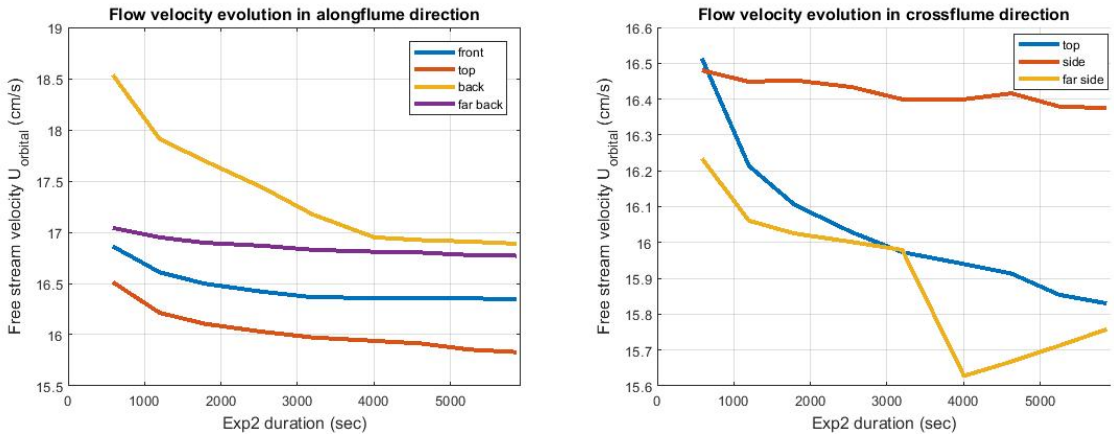

Figure B.8: ADV records of orbital velocity in the along-flume (left) and cross-flume (right) direction during scenario 2 (medium waves).

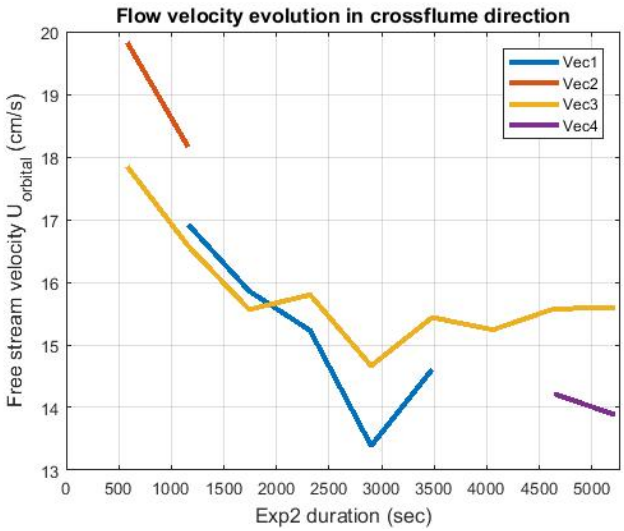

Figure B.9: Vectrino records of orbital velocity in the cross-flume direction during scenario 2 (medium waves). The measurements are taken 1.5 cm above the bed.

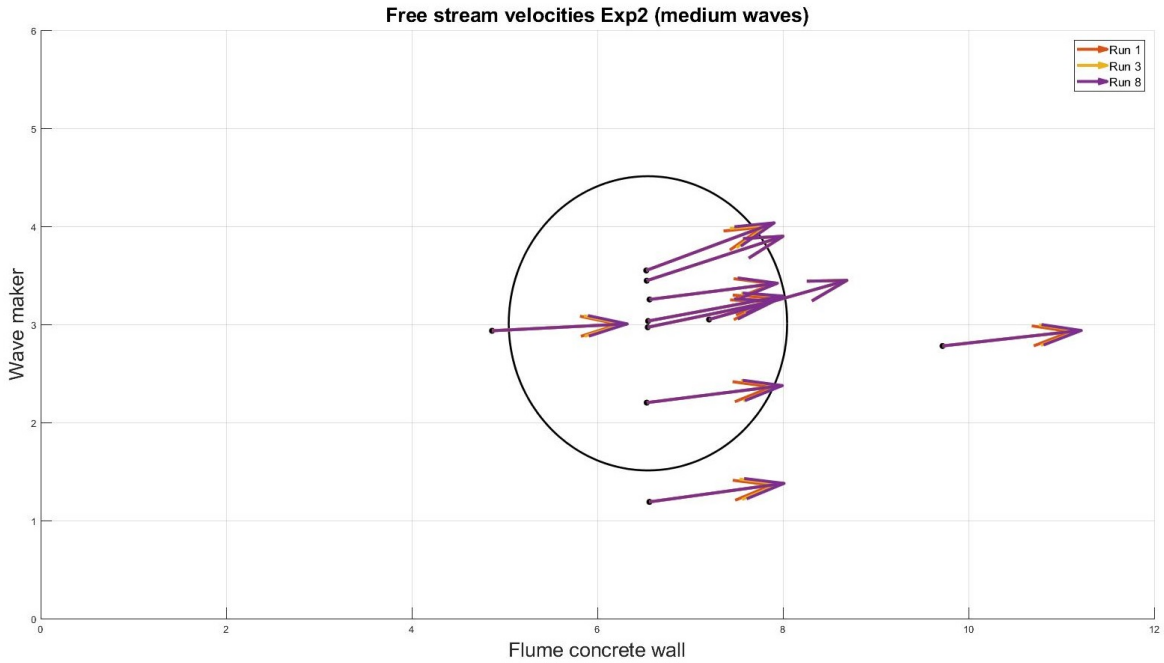

Figure B.10: Flow velocity evolution at the instrument locations across the flume, during scenario 2. The direction and size of the arrows correspond to the measured values.

B.1.3. High waves

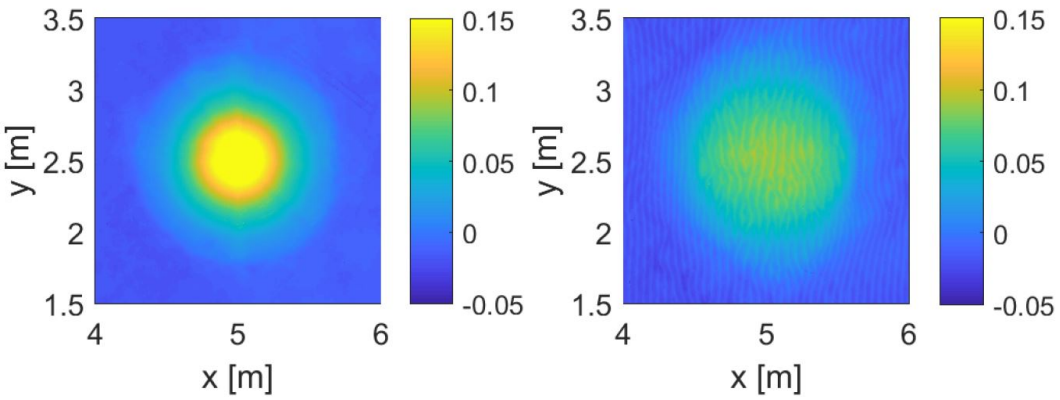

Figure B.11: Mound morphology before (left) and after (right) scenario 3 (high waves), as captured by the laser scanner. x- and y-axes are in the along-flume and cross-flume direction, respectively. The flow direction is from left to right. The colorbar represents elevation (in m) with regard to flat bed level.

Figure B.12: Top: Mound morphology after the end of scenario 3. Top: The focus is at the front of the mound. The flow direction is from left to right. Bottom: The focus is at the back of the mound. The flow direction is from right to left.

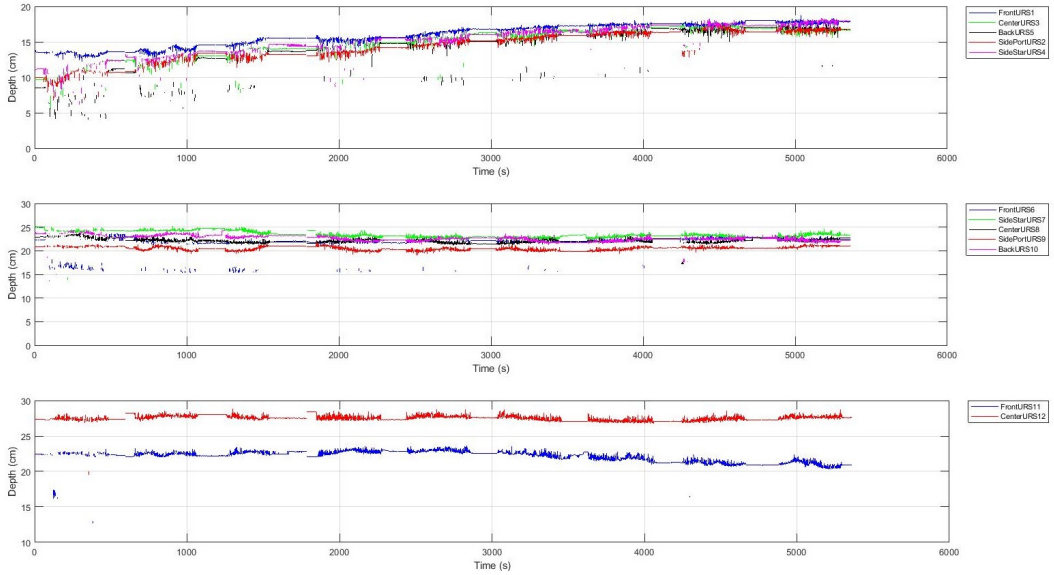

Figure B.13: Cumulative plot of bed level change evolution during scenario 3 (high waves). The top panel depicts the measurements of the URS cluster located on the side of the peak (URSs 1-5). The middle panel depicts the measurements of the URS cluster just downdrift the mound over the downslope (URSs 6-10). The bottom panel depicts the measurements of the URSs on the back of the mound (URSs 11-12). The horizontal axis is the duration (in seconds) of the measuring period for the depicted scenario, and the vertical axis is the distance (in cm) of the bed from the probe.

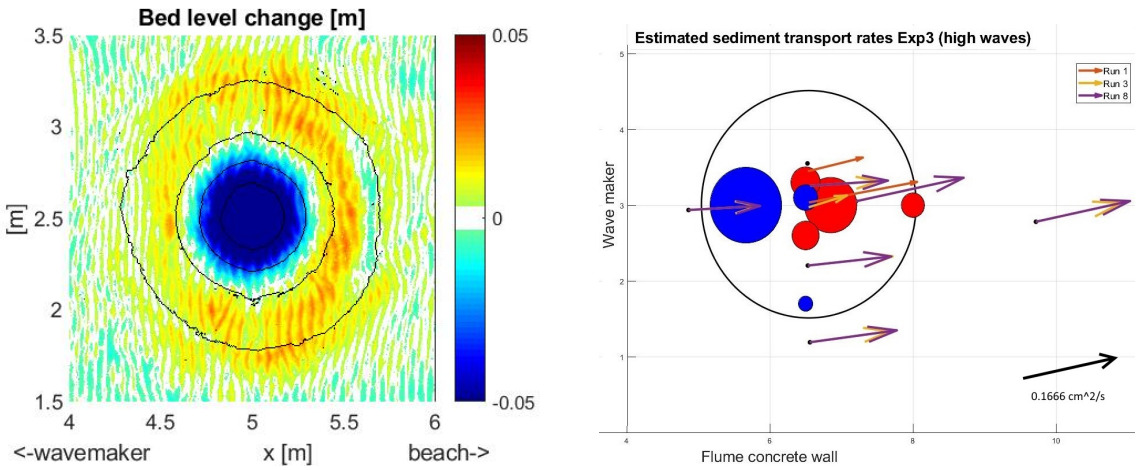

Figure B.14: Left panel: Sedimentation - erosion pattern at the mound at the end of scenario 3 (high waves) as captured by the laser scanner. The colorbar indicates the height (in m) of accretion (positive values) and erosion (negative values). Right panel: Estimated sediment transport rates at the instrument locations across the flume, and resulting sedimentation - erosion pattern at the mound during scenario 3 (high waves). The direction and size of the arrows correspond to the model estimated values. At the bottom right corner is a scale for magnitude reference, and is equal in size to the most right purple arrow. The blue circles indicate erosion, while the red circles show accretion. All circles are estimated based on sediment transport gradients and are scaled according to gradient magnitude. In both panels, the flow is from left to right, and x and y axes are in the along-flume and cross-flume direction, respectively.

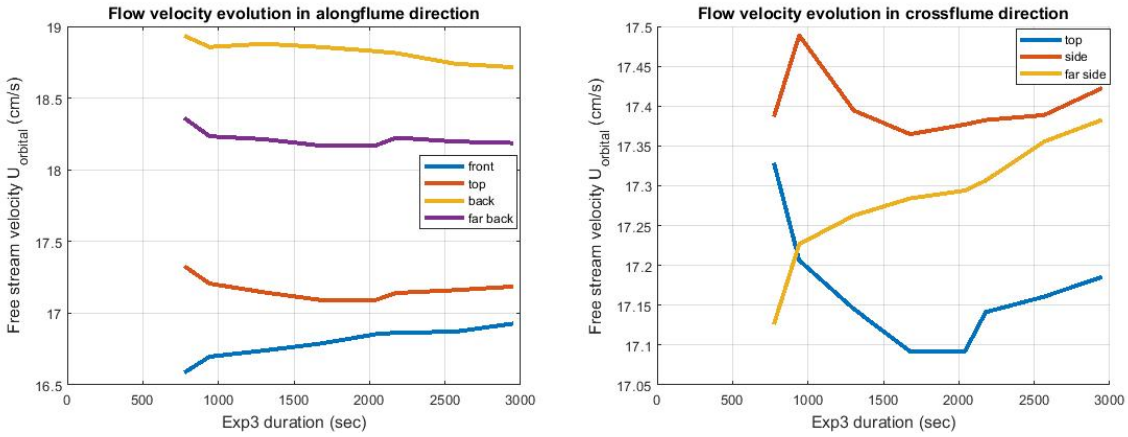

Figure B.15: ADV records of orbital velocity in the along-flume (left) and cross-flume (right) direction during scenario 3 (high waves).

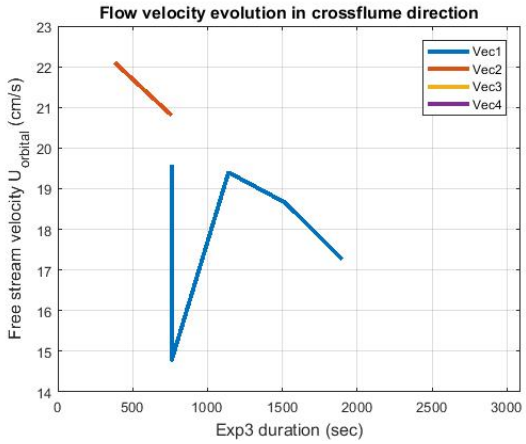

Figure B.16: Vectrino records of orbital velocity in the cross-flume direction during scenario 3 (high waves). The measurements are taken 1.5 cm above the bed.

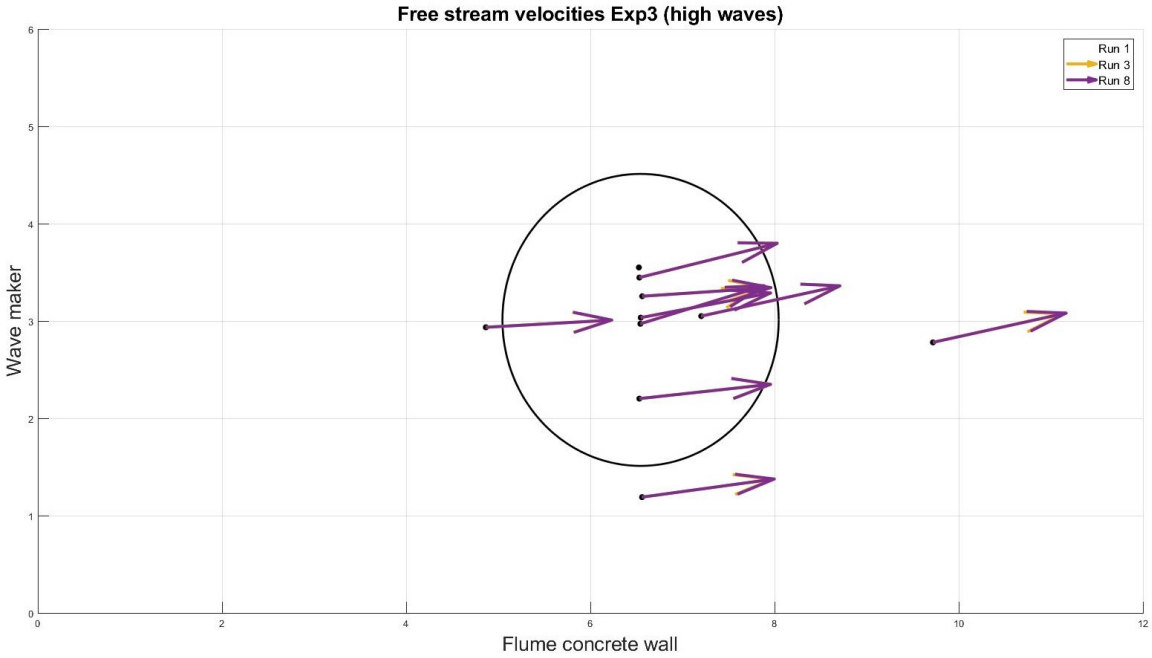

Figure B.17: Flow velocity evolution at the instrument locations across the flume, during scenario 3 (high waves). The direction and size of the arrows correspond to the measured values.

B.2. Current only

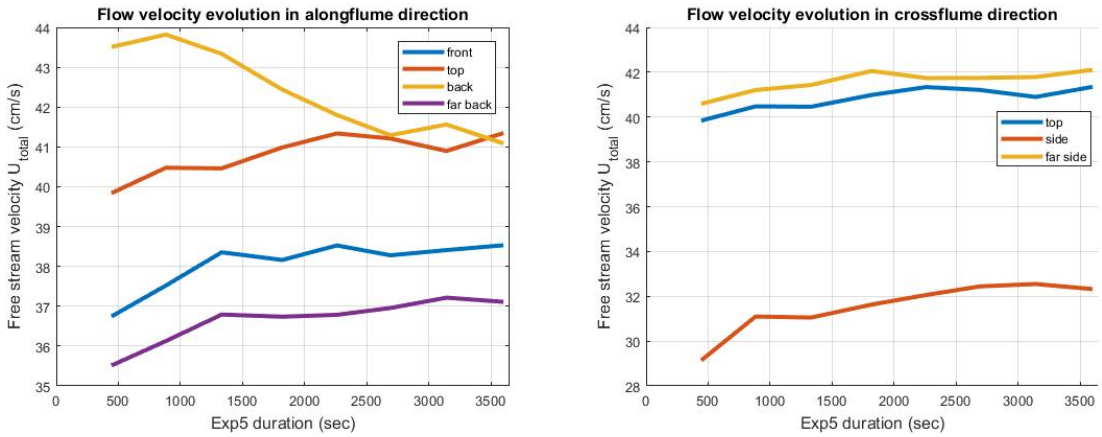

Figure B.18: ADV records of orbital velocity in the along-flume (left) and cross-flume (right) direction during scenario 5 (current only).

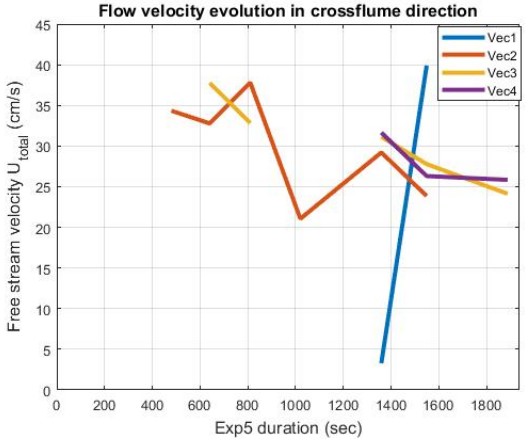

Figure B.19: Vectrino records of orbital velocity in the cross-flume direction during scenario 5 (current only). The measurements are taken 1.5 cm above the bed.

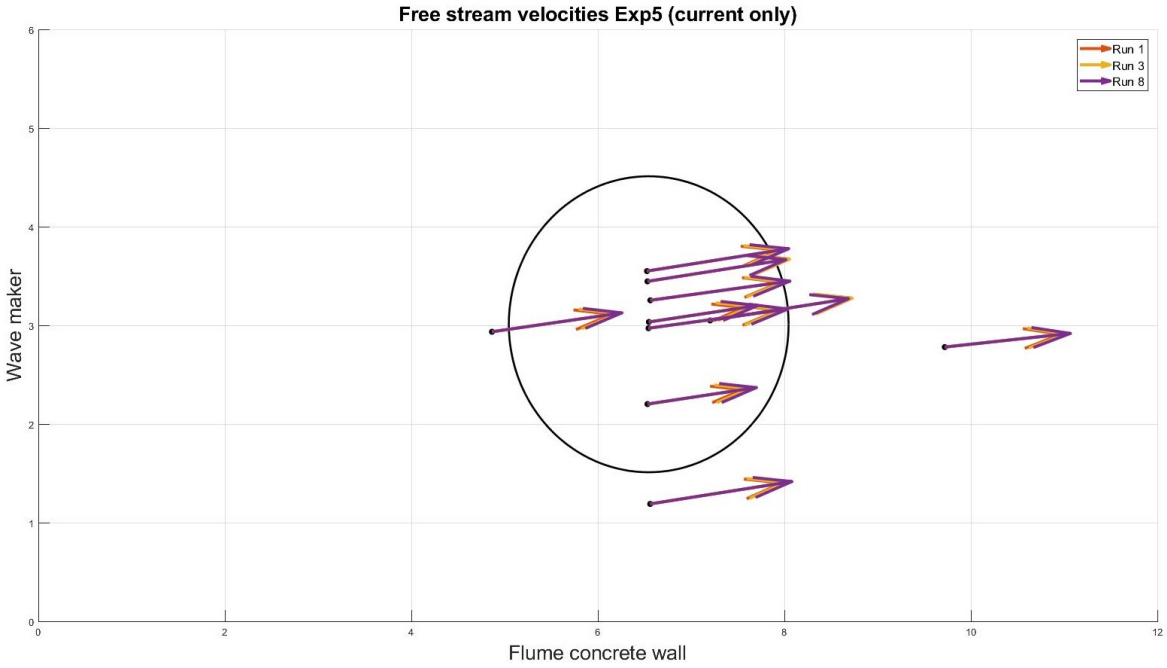

Figure B.20: Flow velocity evolution at the instrument locations across the flume, during scenario 5 (current only). The direction and size of the arrows correspond to the measured values.

B.3. Combined flow cases

B.3.1. Equal wave-current contributions

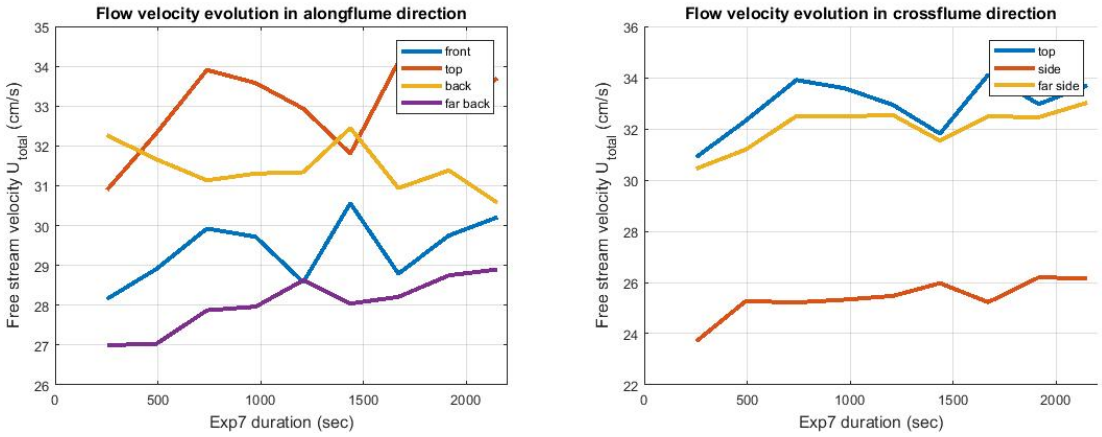

Figure B.21: ADV records of orbital velocity in the along-flume (left) and cross-flume (right) direction during scenario 7 (combined, equal contributions).

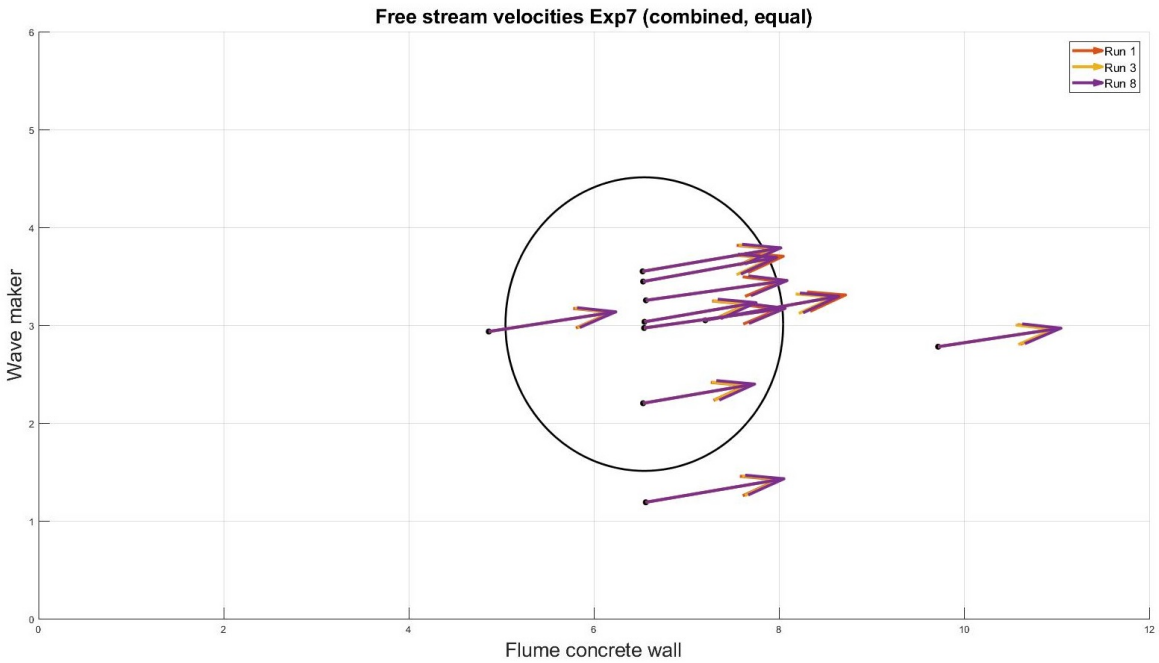

Figure B.22: Flow velocity evolution at the instrument locations across the flume, during scenario 7 (combined, equal contributions). The direction and size of the arrows correspond to the measured values.

B.3.2. Greater current contribution

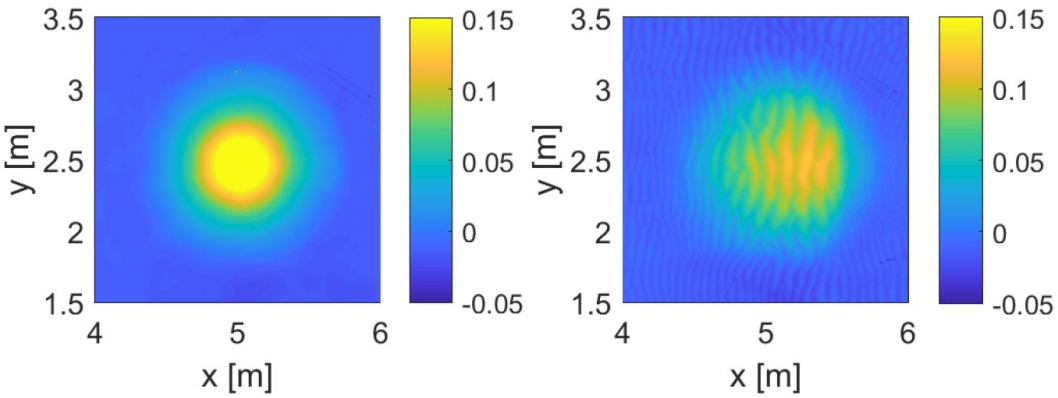

Figure B.23: Mound morphology before (left) and after (right) scenario 8 (combined, more current), as captured by the laser scanner. x- and y-axes are in the along-flume and cross-flume direction, respectively. The flow direction is from left to right. The colorbar represents elevation (in m) with regard to flat bed level.

Figure B.24: Top: Mound morphology after the end of scenario 8 (combined, more current). The flow direction is from left to right.

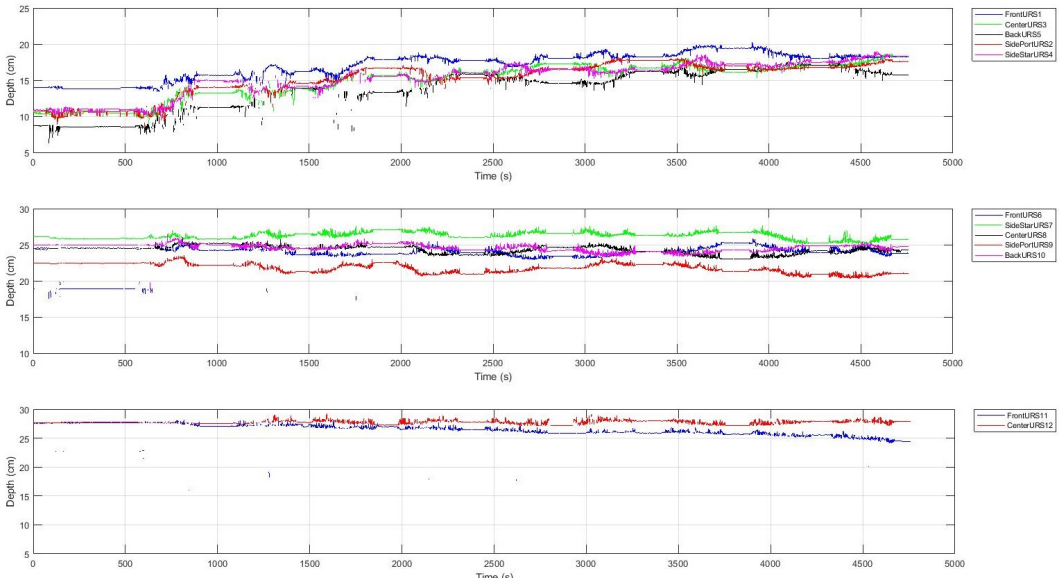

Figure B.25: Cumulative plot of bed level change evolution during scenario 8 (combined, more current). The top panel depicts the measurements of the URS cluster located on the side of the peak (URSs 1-5). The middle panel depicts the measurements of the URS cluster just downdrift the mound over the downslope (URSs 6-10). The bottom panel depicts the measurements of the URSs on the back of the mound (URSs 11-12). The horizontal axis is the duration (in seconds) of the measuring period for the depicted scenario, and the vertical axis is the distance (in cm) of the bed from the probe.

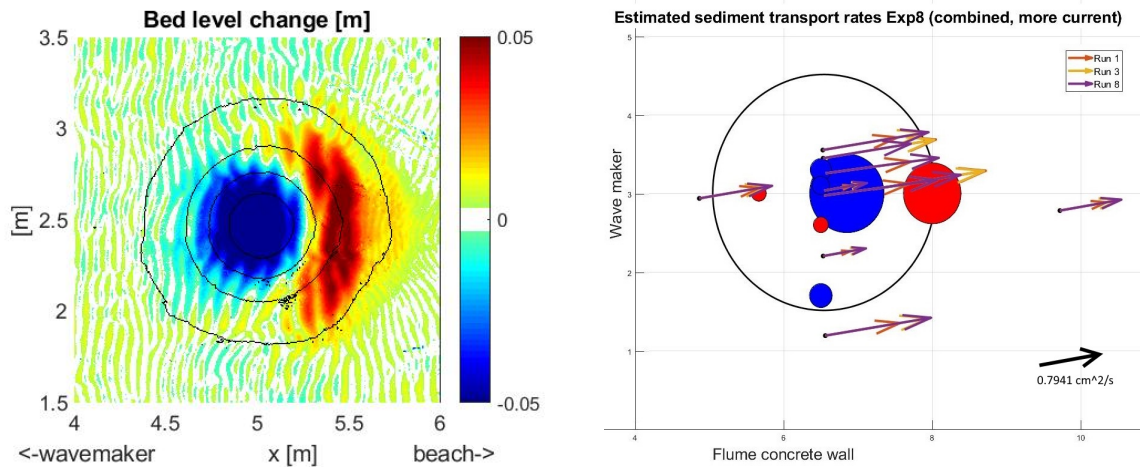

Figure B.26: Left panel: Sedimentation - erosion pattern at the mound at the end of scenario 8 (combined, more current) as captured by the laser scanner. The colorbar indicates the height (in m) of accretion (positive values) and erosion (negative values). Right panel: Estimated sediment transport rates at the instrument locations across the flume, and resulting sedimentation - erosion pattern at the mound during scenario 8 (combined, more current). The direction and size of the arrows correspond to the model estimated values. At the bottom right corner is a scale for magnitude reference, and is equal in size to the most right purple arrow. The blue circles indicate erosion, while the red circles show accretion. All circles are estimated based on sediment transport gradients and are scaled according to gradient magnitude. In both panels, the flow is from left to right, and x and y axes are in the along-flume and cross-flume direction, respectively.

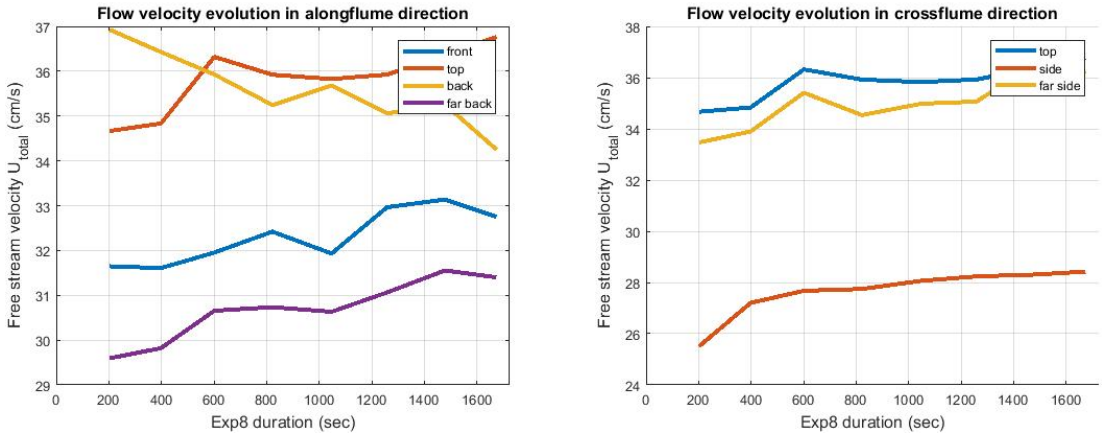

Figure B.27: ADV records of orbital velocity in the along-flume (left) and cross-flume (right) direction during scenario 8 (combined, more current).

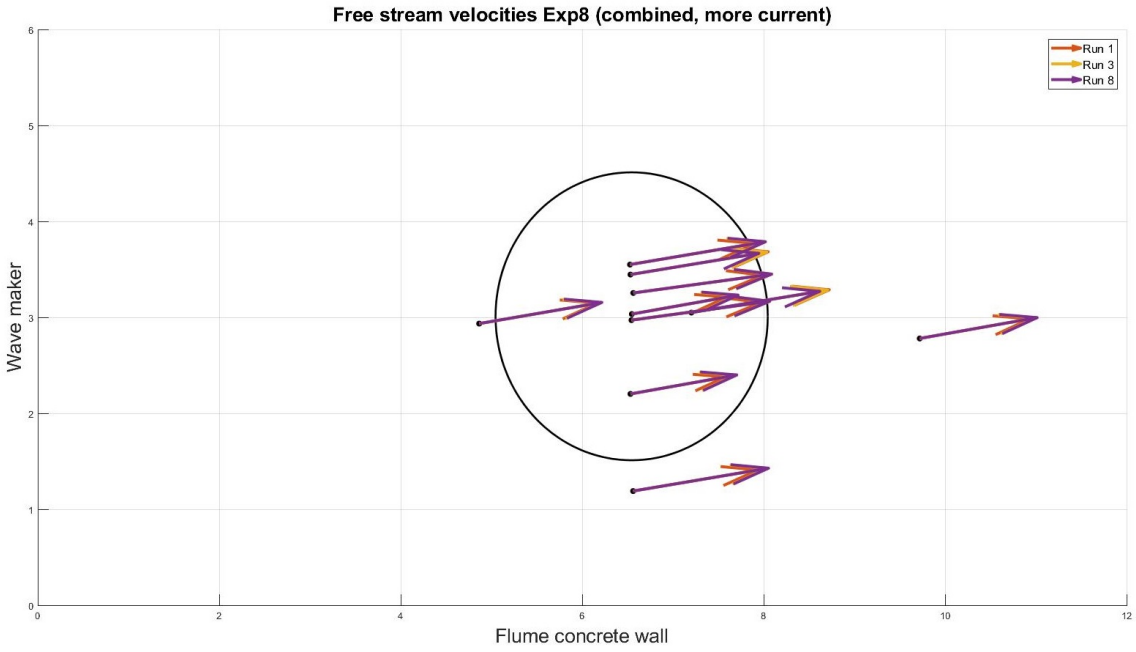

Figure B.28: Flow velocity evolution at the instrument locations across the flume, during scenario 8 (combined, more current). The direction and size of the arrows correspond to the measured values.

B.3.3. Greater wave contribution

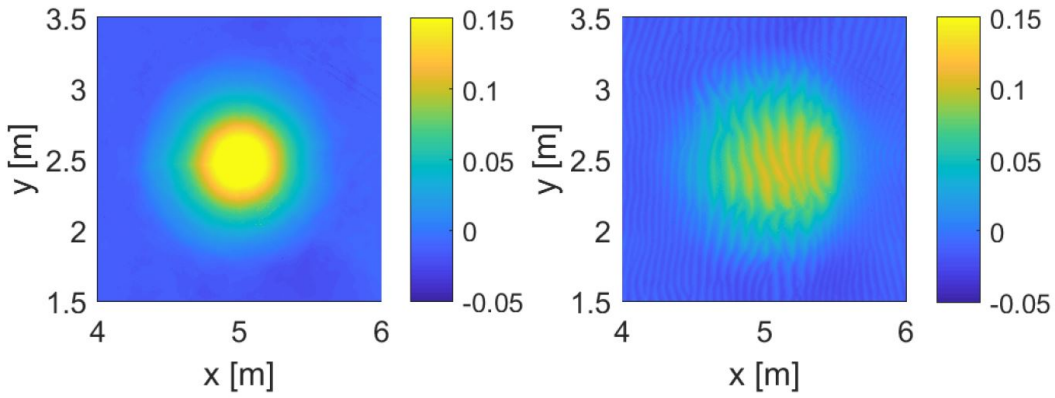

Figure B.29: Mound morphology before (left) and after (right) scenario 9 (combined, more waves), as captured by the laser scanner. x- and y-axes are in the along-flume and cross-flume direction, respectively. The flow direction is from left to right. The colorbar represents elevation (in m) with regard to flat bed level.

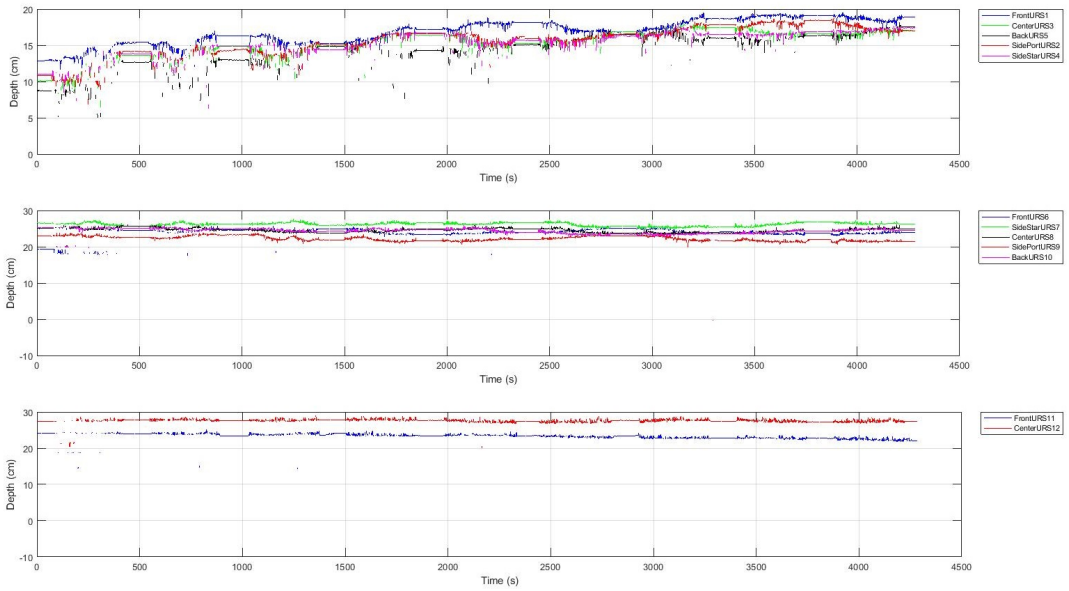

Figure B.30: Cumulative plot of bed level change evolution during scenario 9 (combined, more waves). The top panel depicts the measurements of the URS cluster located on the side of the peak (URSs 1-5). The middle panel depicts the measurements of the URS cluster just downdrift the mound over the downslope (URSs 6-10). The bottom panel depicts the measurements of the URSs on the back of the mound (URSs 11-12). The horizontal axis is the duration (in seconds) of the measuring period for the depicted scenario, and the vertical axis is the distance (in cm) of the bed from the probe.

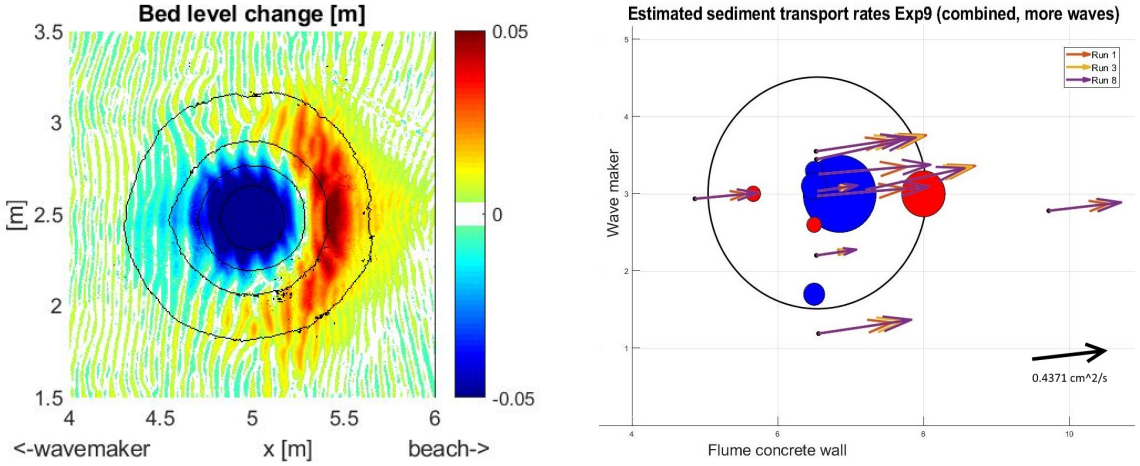

Figure B.31: Left panel: Sedimentation - erosion pattern at the mound at the end of scenario 9 (combined, more waves) as captured by the laser scanner. The colorbar indicates the height (in m) of accretion (positive values) and erosion (negative values). Right panel: Estimated sediment transport rates at the instrument locations across the flume, and resulting sedimentation - erosion pattern at the mound during scenario 9 (combined, more waves). The direction and size of the arrows correspond to the model estimated values. At the bottom right corner is a scale for magnitude reference, and is equal in size to the most right purple arrow. The blue circles indicate erosion, while the red circles show accretion. All circles are estimated based on sediment transport gradients and are scaled according to gradient magnitude. In both panels, the flow is from left to right, and x and y axes are in the along-flume and cross-flume direction, respectively.

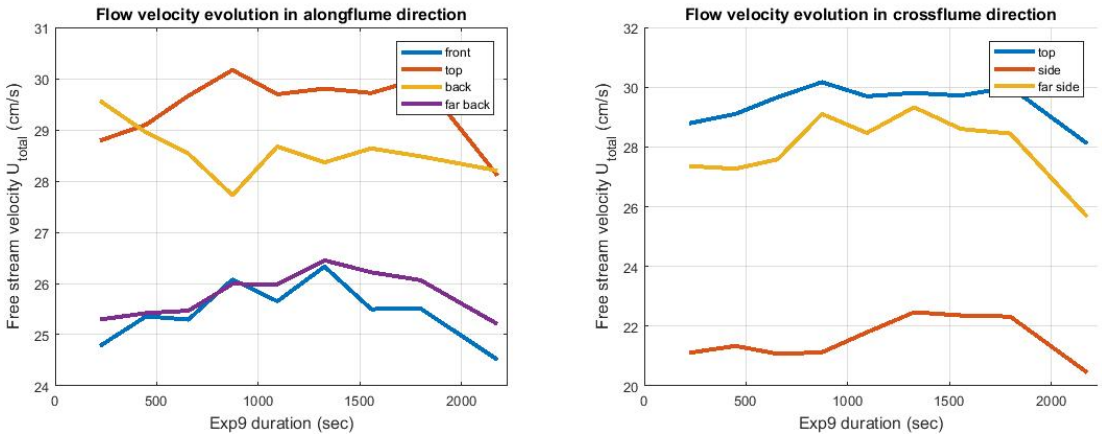

Figure B.32: ADV records of orbital velocity in the along-flume (left) and cross-flume (right) direction during scenario 9 (combined, more waves).

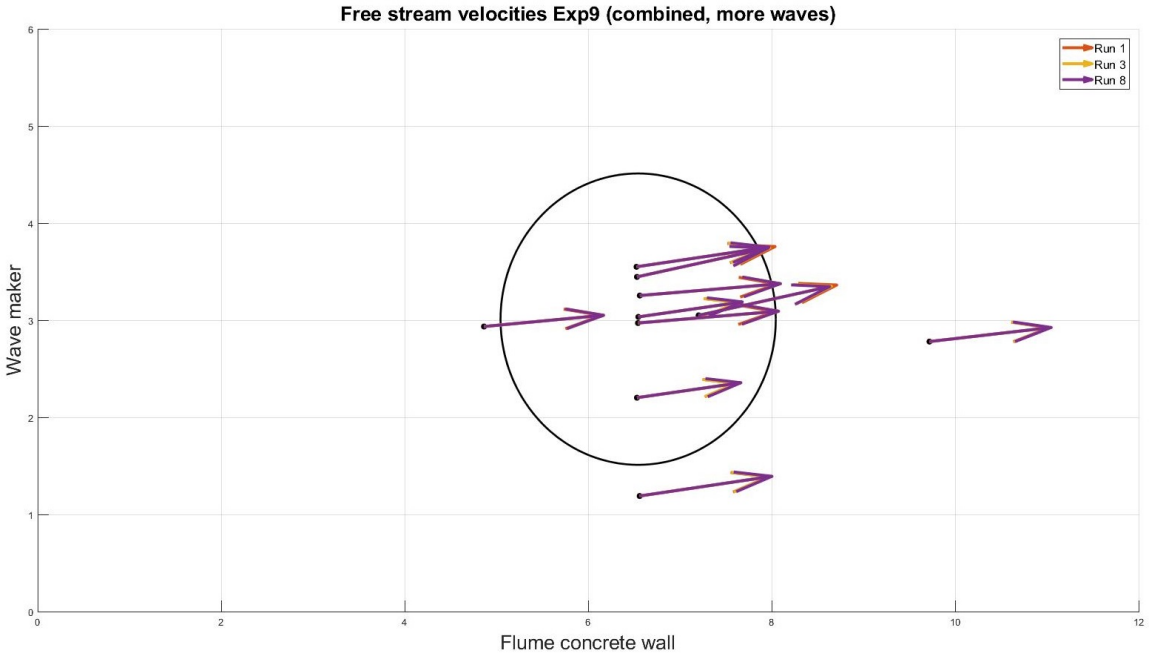

Figure B.33: Flow velocity evolution at the instrument locations across the flume, during scenario 9 (combined, more waves). The direction and size of the arrows correspond to the measured values.